Development and testing of the new design for a single-stage solar still

By

Nandipha Pangwa

Thesis submitted in fulfilment of the requirements for the degree Master of Engineering: Mechanical Engineering

In the faculty of
Engineering and the Built Environment

At the
Cape Peninsula University of Technology

Supervisor: Prof V. Msomi

Bellville

January 2025

DECLARATION

I, Nandipha Pangwa, declare that the contents of this thesis represent my own unaided work and that the thesis has not been previously submitted for academic examination towards any qualification. Furthermore, it represents my own opinions and not necessarily those of the Cape Peninsula University of Technology.

Signed: ____________________

Date: ______10/01/ 2025______

ABSTRACT

The global water demand is increasing alongside the growing world population. Adequate access to clean drinking water is essential for the well-being of all living organisms, and the scarcity of this resource is a significant worldwide issue. In addressing this challenge solar desalination systems, particularly solar stills, have proven to be effective solutions, generating fresh drinking water from saline or contaminated water. A solar still is a device used to produce fresh water from contaminated water using heat from the sun. Solar stills mainly consist of a water basin, a glass cover positioned at an angle facing the sun, a collecting tray, a collecting tank and a feeding tank. The basic operation of the device is that the contaminated water inside the water basin is heated and evaporated using the heat from the sun. This water vapor then is condensed on the inner surfaces of the solar still cover and from there potable water is accumulated.

This study comprises a design, fabrication and testing of a new design of a double slope single-stage solar still (D5S). The system was constructed at the Mechanical Engineering workshop at Cape Peninsula University of Technology (CPUT), Bellville Campus. The tests were conducted on the roof of the Mechanical Engineering workshop over twelve days during October and November 2023 (spring season in South Africa). Out of the four seasons, spring is the second warmest after summer, thus, testing during this season was deemed feasible, given that sun irradiation is one of the most important elements influencing the productivity of solar stills.

The D5S was incorporated with a 16-tube evacuated tube solar collector. The solar still was tested during the day (7 am to 7 pm) and night (7 pm to 7 am). The system consisted of a saline tank that was elevated and positioned to allow a gravitational flow of seawater to the basin. A water circulation pump was used to hasten the flow from the basin to the solar collector and back to the basin where the evaporation and condensation processes took place, thus, leading to the production of the distillate.

During the experiment test, the highest production obtained per day was 513ml, being the total production for day and night achieved on a day when the maximum outdoor temperature was 30°C. The minimum distillate produced was 140ml on a day that had a maximum temperature of 22°C that was one of the coldest days during the testing period. The total distillate produced by the solar still system during the testing cycle was 3821 ml.

The knowledge produced from this research will assist the industries dealing with water distribution and management in enhancing the water resources. The knowledge will also serve as the guide in cases where such systems are taken for commercialization. The knowledge from this study can be useful in remote areas that are faced with the water crisis and all sectors that are water depended for their operations and for remote areas.

PUBLICATIONS

Part of this thesis is published as: Nandipha Pangwa and Velaphi Msomi, “Materials Today : Proceedings Progress made in eliminating factors affecting solar stills productivity,” *Mater. Today Proc.*, no. xxxx, 2022, doi: 10.1016/j.matpr.2022.03.300.
3rd International Conference on Aspects of Materials Science and Engineering 2022, Volume 57, Part 2, 2022, Pages 969-974, https://doi.org/10.1016/j.matpr.2022.03.300

ACKNOWLEDGEMENTS

Firstly, I would like to thank my heavenly father, God, for carrying me through this journey. I would also like to deeply acknowledge and thank Professor Velaphi Msomi for believing in me from the day I walked into his office requesting supervision. *Ndibulela Ngazo-Zozibini Phingoshe, Nomndayi,* for your continuous support, guidance, and patience throughout these years. Thank You!

I would further like to thank the Mechanical Engineering workshop staff for assisting me with the construction process. A special thank you to Mr. Jenkins for his tireless support and motivation on days when giving up seemed to be an option because things weren't working out. Thank you for all the technical and life lessons.

I would like to further thank Tebogo Mosohli and Dr. Ncediwe Ndube-Tsolekile from the Department of Chemistry for their assistance with conducting conductivity and salinity tests on the water.

Not forgetting to thank my dearest family and friends who carried me throughout this journey. Mostly my sister who made sure that I kept going no matter what and my son who had to understand that on some days I had to also go to school (at my big age).

I would also like to thank the National Research Foundation (NRF) for their financial support. The opinions expressed in this thesis and the conclusions arrived at, are those of the author, not to be attributed to the funders.

DEDICATIONS

I would like to dedicate this work to my family. My father (Bongani Goodwill Pangwa) my mother (Nomonde Pangwa), my sister (Sipokazi Pangwa), my brothers (Sandiso & Paulomzi Pangwa), my little twin sisters (Izibele & Zizibele Pangwa), and lastly my son (Alunamda Pangwa). Thank you to all of you for carrying me throughout this journey.

TABLE OF CONTENTS

LIST OF FIGURES

LIST OF TABLES

CLARIFICATION OF TERMS

Definitions:

Condensation – is the process by which gas/vapor changes to a liquid form. This generally happens when vapor in warm air encounters a cool surface.

Desalination - is a process of removing minerals and salts from saline water to produce fresh drinking water for humans.

Evaporation – is the process by which liquid changes to gas or vapor. This happens when a liquid is heated.

Phase change materials (PCM) - organic or mineral compounds capable of absorbing and storing large amounts of latent thermal energy.

PV/T collector - is a kind of heat exchanger that receives solar radiation and converts it into electrical and thermal energies.

Solar Collector - is a device that collects solar radiation from the sun for future use.

Solar still - A solar still is a device that yields drinkable and potable water from contaminated and saline water utilizing the energy from the sun.

NOMENCLATURE

Abbreviations:

CSS – Conventional Solar Still

D5S – Double slope single-stage solar still

DC – Direct current

EC – Electrical conductivity

ED – Electrodialysis

ETSC – Evacuated tube solar collector

FPSC – Flat plate solar collector

MD - membrane distillation

MED - multi-effect distillation

MSF - multi-stage flash

MVC/TVC - mechanical/thermal vapor compression

PCM – Phase change material

PSU – Practical salinity unit

PV/T – Photovoltaic thermal

RES – Renewable energy sources

RO – Reverse osmosis

SD - solar distillation

TDS – Total dissolved solids

TSS – Tray Solar Still

TSSIBM - Tray Solar Still with Internal and Bottom Mirrors

TSSIBTM - Tray Solar Still with Internal and Bottom & Top Mirror

TSSIM - Tray Solar Still with Internal Mirrors

Equation Symbols:

Symbol	Description
a	accuracy of the measuring instrument
U	Standard uncertainty
i	Annual interest rate
AC	Annual cost
AMC	Annual maintenance cost

ASC	Annual salvage Cost
CPL	Cost per litre
CRF	Capital recovery factor
FAC	Fixed annual cost
n	Number of operational days per year
N	Number of operational years
P	Present capital cost
S	Salvage value

CHAPTER 1- INTRODUCTION

1.1 RENEWABLE ENERGY SOURCES

Non-renewable energy sources are scarce and depreciating, facts that will lead to their depletion in the next years. This situation entails that the world must look at alternative sources of energy and, therefore, leads directly to the need for renewable energy which complies with the present energy demand. Renewable energy sources are utilized to address the energy challenges the world is experiencing since they are environmentally beneficial and nearly inexhaustible. Solar photovoltaic and solar thermal collectors transform solar radiation energy into usable heat and electrical energy. Solar energy is one of the largest, most efficient and cleanest renewable energy sources utilized for thermal heat and power generation [1] .

Wind, solar thermal, photovoltaic and geothermal are examples of renewable energy that can be used in desalination operations. The utilization of direct sunbeams to create fresh water using solar stills is the most researched way of creating a linkage between renewable energy sources (RES) and desalination processes [2]. Desalination systems powered by renewable energy are often divided into two categories. The first group includes distillation technologies powered by the heat supplied by RES. Meanwhile, the second group includes membrane and distillation processes that use electrical or mechanical energy generated by RES [3].

Solar power is the best type of renewable energy for integrating with desalination technology since it can provide all the heat and electricity required for desalination[4]. The most common sun harvesting methods include photovoltaic (PV), linear Fresnel, parabolic trough and central receiver [4]. Several studies have been conducted on solar stills and some of these studies are discussed in the literature review in Chapter two.

According to Abdelkareem et al. [5], desalination facilities that use wind power are widely accepted as a type of renewable energy, particularly in coastal areas with substantial wind energy supplies. These wind-driven desalination plants have been shown to have the lowest environmental impact among RES, with a remarkable 75% decrease in environmental consequences. Wind energy is primarily integrated with reverse osmosis (RO) and electrodialysis (ED) desalination systems due to their reliance on electricity rather than heat [6].

Geothermal energy harnesses the elevated temperature found beneath the Earth's surface to generate steam or store heat energy. This energy source necessitates drilling into the ground, with depths reaching up to 5000 meters. However, for the excavation efforts to be cost-effective, the underground temperature must exceed 180°C [7]. Wave and tidal energy are well-suited for coastal regions [8]. In 1990, it was proposed to use an oscillating water column (OWC) to convert ocean wave energy into electricity, which would then be used to power RO desalination processes [9],[10]. Figure 1.1 below shows the different types of renewable energy sources and the desalination techniques for which they are suitable.

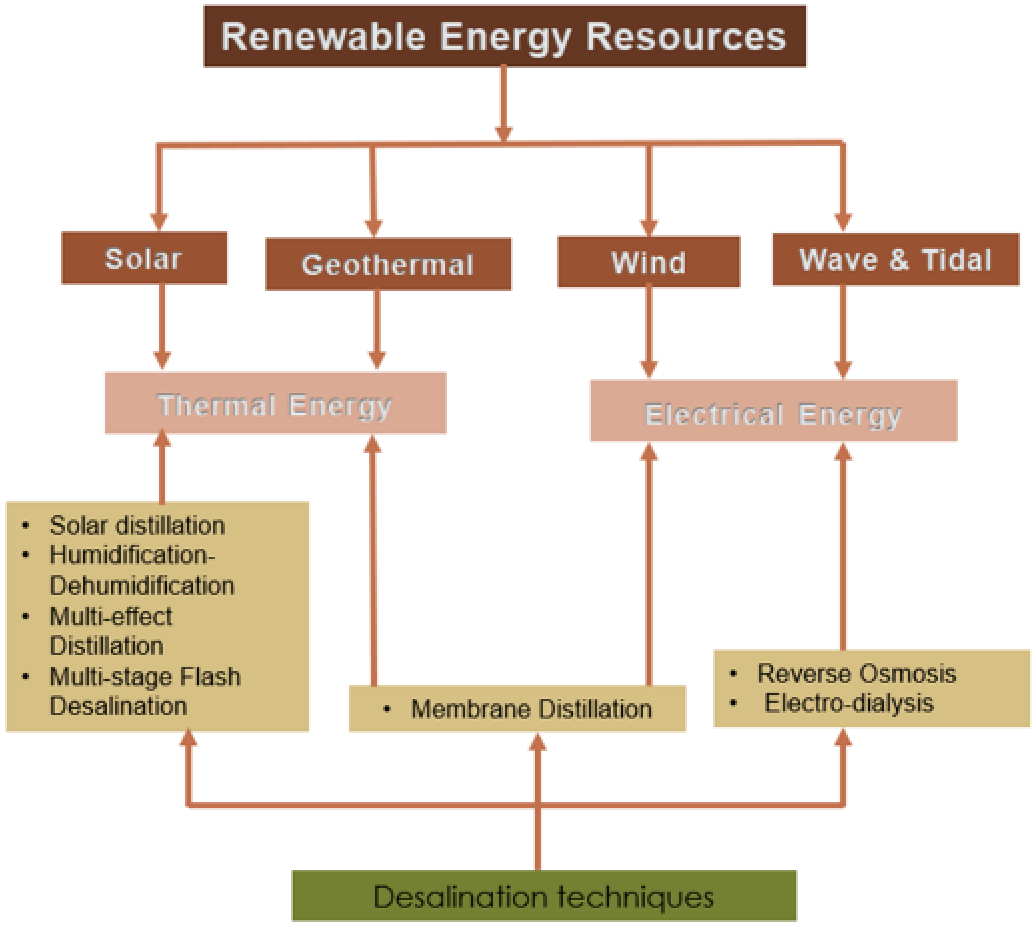

Figure 1.1: Renewable energy resources

1.1.1 Desalination Systems

With an ever-growing population and demand for freshwater, the need for desalination is expanding. Worldwide desalination demands have risen steadily since the 1960s. Countries such as the United Arab Emirates and Saudi Arabia have the most desalination capacity compared to other countries. Saudi Arabia was reported to be using desalination systems to fulfil 60% of its water demands and is the leading producer of desalinated water [11]. According to Jones et al. [12]. Countries such as Kuwait and Qatar rely totally on desalination plants for freshwater. The overall worldwide installed desalination capacity was predicted to be 95.37 million m^3/day[13].

Desalination systems have become essential to meet the growing demand for freshwater. Two main solar desalination approaches are photovoltaic-reverse osmosis (PV-RO) and solar-thermal desalination. Integrating desalination systems with solar energy technologies is one of the solutions for eliminating the need for fossil fuel energy sources [14]. Desalination technologies are used to produce fresh water from seawater utilizing either membranes or thermal processes [15]. Thermal desalination, a phase change process, entails elevating the temperature of the input (seawater, brackish water, or other impaired water) to the "boiling point" at the operational pressure to generate "steam". The steam is then condensed in a condenser unit to yield freshwater. Various methods fall under the thermal desalination process, including multi-stage flash (MSF), multi-effect distillation (MED), mechanical/thermal vapor compression (MVC/TVC), membrane distillation (MD) and solar distillation (SD) [6]. These technologies require complex supporting infrastructure and large installations and such processes become a challenge for poor areas. Due to the high-energy consumption of these technologies, solar-driven desalination systems are a promising approach to producing freshwater [16]. According to Shatat et al. [17], solar energy is the most extensively utilized renewable source.

On the other hand, membrane desalination, characterized by a non-phase change process, involves the separation of dissolved salts from the input waters through mechanical or chemical/electrical means, using a membrane barrier between the feed (seawater or brackish water) and the product (potable water). Commonly employed technologies in membrane desalination include reverse osmosis (RO) and electro-dialysis (ED) [6].

According to Alkaisi et al. [7] the solar still distillation (SD) system, operating as a natural evaporation-condensation process, stands out as the most viable renewable desalination method for application in isolated arid regions. Nevertheless, additional research is necessary to improve the efficiency and freshwater yield of these systems. Figure 1.2 below shows the different types of desalination technologies available.

The focus of this research is mainly on solar distillation, a double slope single stage solar still (D5S) incorporated with an evacuated tube solar collector was designed, constructed and tested in Cape Town, South Africa.

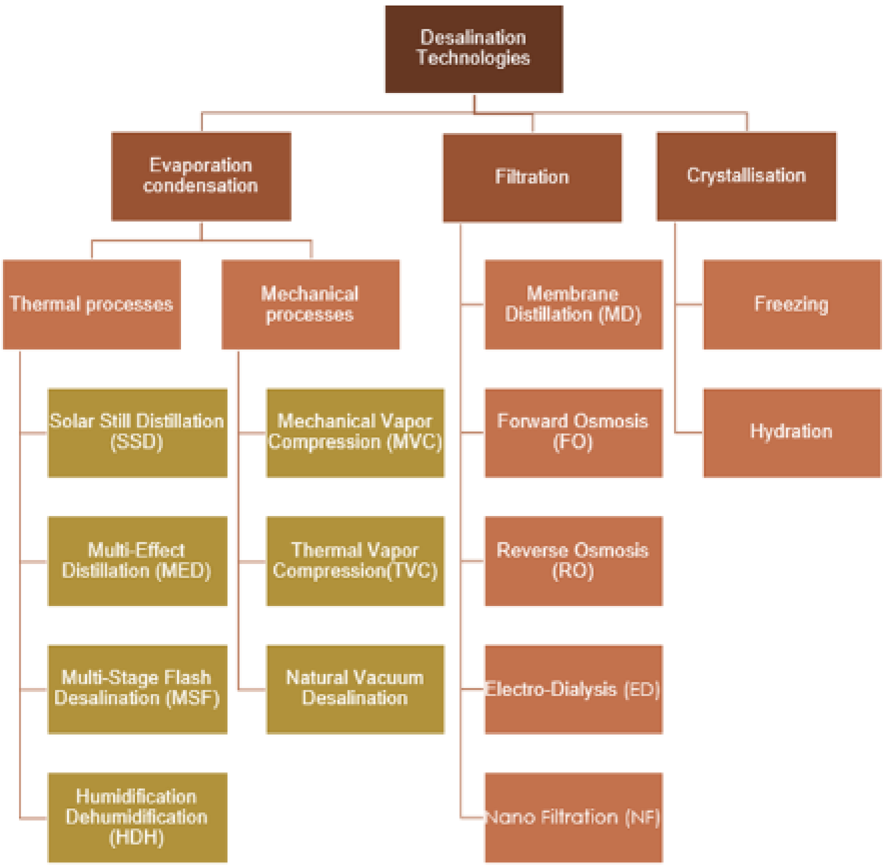

Figure 1.2: Desalination techniques

1.2 PROBLEM STATEMENT

The availability of fresh drinking water has become a challenge all over the world with the increase in population. This is even more serious in remote areas. All living creatures need clean water to survive. Most of the Earth surface is covered by the oceans which covers approximately 97% of the Earth's water and less than 1% of this water is fresh water. Oceans contain saltwater and this requires water purification to qualify as fresh drinking water. Over the year's seawater desalination has been carried out using several techniques such as membrane distillation, multiple effect distillation, multistage desalination and reverse osmosis. However, recent studies report that existing systems have worked well but with challenges such as the low production of potable water, efficiency etc. These are affected by several factors.

This project is looking at redesigning the D5S that will be tested using real environmental conditions. The proposed design will incorporate the mechanism that will be used to store thermal energy for the night-time operation since there is no solar radiation during this time. The performance of the newly designed solar still will be compared with those that are available in the literature.

1.3 DETAILED BACKGROUND TO RESEARCH

Solar stills have become quite popular globally, due to the challenge of accessing freshwater. There are different types of solar stills with different configurations and designs [22]. Efficiency and freshwater yield play a huge role in these systems. Studies have been conducted to improve the efficiency and freshwater yield of solar stills [23]. Solar stills are categorized into active and passive solar stills. Active solar stills make use of additional devices to convert energy from the sun into a more usable form. Passive solar stills only use heat energy directly from the sun [19]. Previous studies have reported that active solar stills are more expensive than passive solar stills [24].

Solar stills mainly consist of a water basin, a glass cover positioned at an angle facing the sun, a collecting tray, a collecting tank and a feeding tank, as depicted in Figure 1.3 below. The sun is directed onto the glass cover, the heat penetrates, and the evaporation process takes place. The water vapour condenses to water droplets on the glass cover and, due to gravity, the water droplets slide down to be collected as potable water. This process does not mean that potable water is ready for consumption. The water quality must be tested before use or consumption for health reasons.

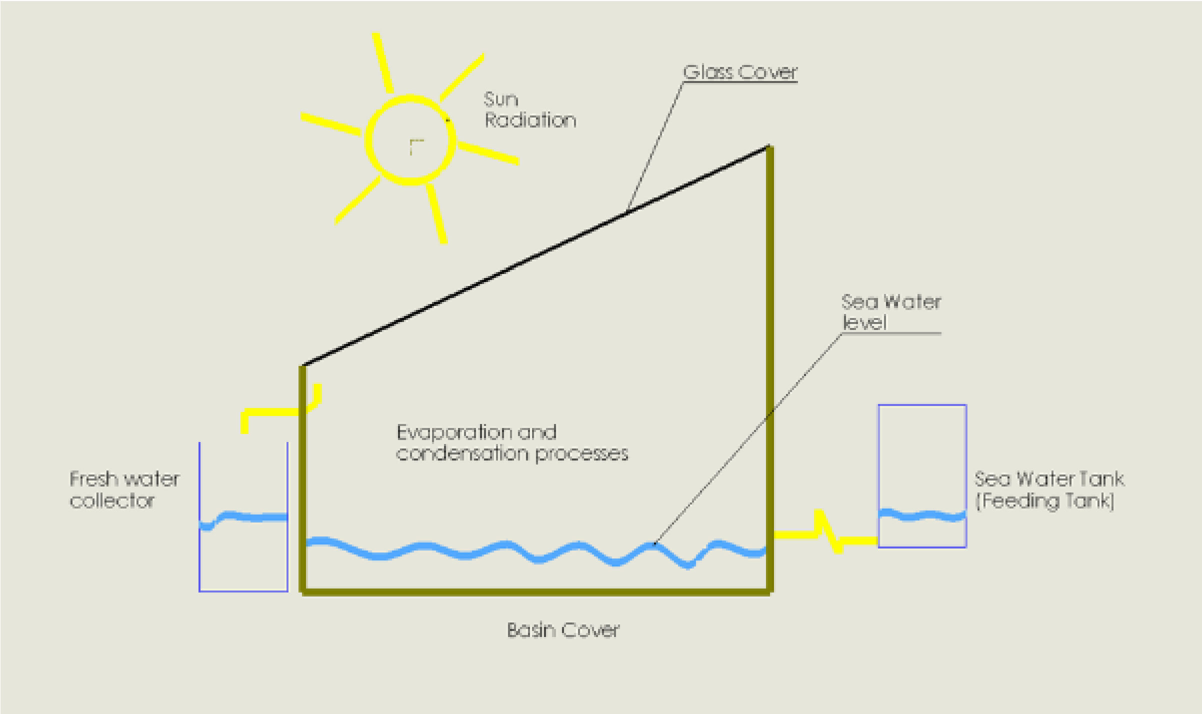

Figure 1.3: Single slope solar still [25]

Single slope solar stills have become more popular for producing freshwater globally. However, the challenge with this design is the low production of distillate [26]. Previous studies have reported that increasing the evaporation surface area of the solar still increases the production of freshwater [27]. One of many ways to achieve this escalation is to incorporate two covers on the system, as shown in Figure 1.4 below.

Recent studies have reported that integrating solar stills with solar collectors increases the yield of fresh water by 36% [28]. This system has been incorporated with thermal storage to increase the efficiency of the system mainly at night-time. This study focused on redesigning a single-stage solar still and focusing mainly on improving the freshwater yield of the existing designs. The system has been designed to be cost-effective to enable people from the poorest backgrounds to access it.

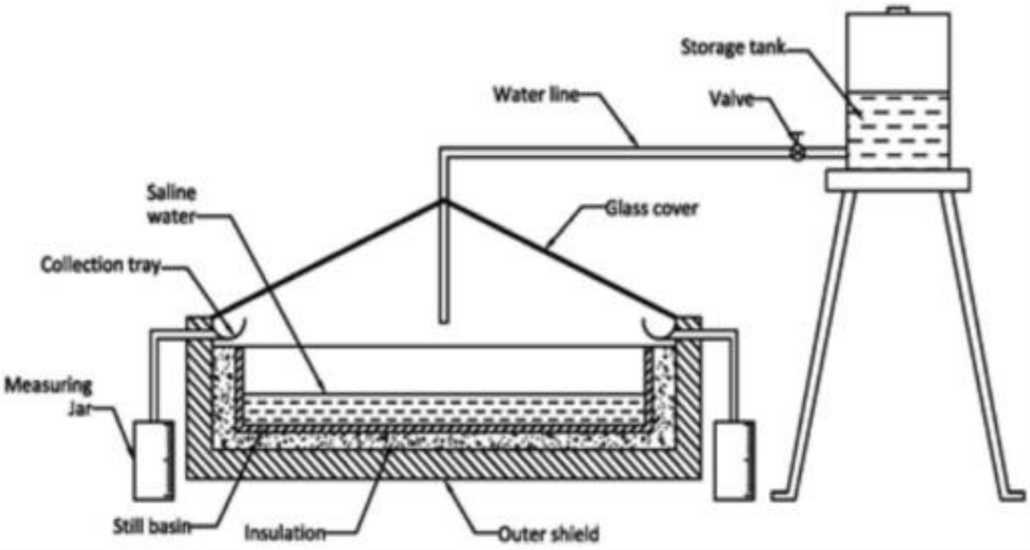

Figure 1.4: Double slope single-stage solar still [20]

1.4 RESEARCH AIMS AND OBJECTIVES

The main aim of this research was to enhance the production of freshwater on a double slope single-stage solar still. This aim was achieved through the following activities:

- Designing and constructing a new design of a single-stage solar still.
- Testing the newly designed single-stage solar still.
- Performing the tests using real environmental conditions.
- Studying the daily output in reference to weather conditions.
- Testing the system during the day and at night.

1.5 ORGANIZATION OF THESIS

Chapter 1 – Introduction

This section consists of the problem statement, a detailed background to the study, research aims and objectives and organization of the thesis respectively.

Chapter 2 – Literature Review

This chapter includes reference to all the literature that was consulted relating to this research. It further discusses single-stage solar stills mainly focusing on double sloped stills. The factors affecting the production and efficiency of solar stills have also been discussed and lastly the summary of the literature.

Chapter 3 – Detailed Construction (Methodology) and Testing

This chapter discusses the components of the system and lists all the materials, tools, and machinery used for construction. It details the construction process of the prototype and all the methods used to achieve the final design. It further discusses the testing process and measuring instruments used. It also briefly discusses challenges that were encountered during the testing phase.

Chapter 4 – Experimental Results

This chapter deliberates the results obtained from the experiments and the data analysis.

Chapter 5 – Conclusions and Recommendations

This chapter discusses the conclusions drawn from the results obtained and further suggests recommendations to resolve challenges encountered for the improvement of future designs.

CHAPTER 2: LITERATURE REVIEW

This chapter presents findings from the reviewed related literature. It focuses on the literature concerning single-stage solar stills. It also describes the factors influencing the efficiency and freshwater yield of these solar stills.

The two main classes of solar stills are passive and active solar stills. In passive stills evaporation and condensation occur naturally mainly utilizing energy from the sun [29]. There are various ways that can be implemented to increase the efficiency of passive stills that will be mentioned in this section.

Active solar stills use extra devices to concert solar radiation into a functional form. The two classes are dependent on meteorological, design and operational conditions to function. Meteorological conditions are out of human control while design and operational conditions can be regulated to a certain extent [30].

Researchers are continuously working on ways to improve the production of active and passive skills. Siva and Sundaram [30] conducted a review of old methods used to improve the performance of these stills. The techniques looked at were energy storage materials that included different types of material, the angle of the glass cover, the vacuum technique, incorporating wick material in the basin, using external reflectors on stills, making use of solar tracking systems to ensure that maximum utilization of solar energy is achieved throughout the day, using liner material in the basin for the maximum absorption of solar radiation, incorporating a solar collector, humidification – dehumidification principle, Multi-effect Distillation(MED)/Multi-stage flash distillation (MSF) desalination systems. All the above-mentioned techniques greatly improved the production of both active and passive solar stills based on all the literature reviewed for this investigation.

Mohsenzadeh et al. [31] studied and reviewed different designs for performance enhancement on passive solar stills for isolated areas. The focus was on the design enhancement and modifications, improving the collection and receiving of solar radiation using mainly internal and external reflectors, enhancement of solar absorption focusing on the modification of the basin design, surface area, inclination angle of the cover, etc., improvements to the heat storage and vapour condensation enhancement.

The literature revealed that the best design enhancement for isolated areas was adding internal and external reflectors positioned near the passive solar still (PSS) in an ideal position for the improvement of insolation collection. It was also established that a concave basin covered by a wick cloth at a predetermined level of wetness can be used to improve heat absorption. To enhance the water vapour condensation process, a hemispherical cover made with recyclable plastic material placed on top of the PSS would be beneficial. Lastly, for the improvement of heat storage, nano composite phase change material placed under the basin and combined with fins greatly boosts the efficiency of the PSS.

2.1 Single Slope Solar Stills

In a study by Arunkumar et al. [32], seven different types of solar stills were constructed and tested under the same weather conditions in Coimbatore, India. The units were a spherical (SSS), pyramid (PSS), hemispherical (HSS), double basin glass (DGBSS), concentrator coupled single slope (CCSSS), tubular and tubular solar still coupled with pyramid solar still. All the stills' internal basin walls were painted black to enhance the solar absorption and insulated with sawdust to minimize heat losses. This material was used due to its affordability. The stills were all tested at the same time between 01 January 2011 and 30 May 2011. The data was recorded at half hour intervals.

The saline water level on six basins was maintained at the same level. The distillate produced by the SSS was 2300 ml/m^2/d. The DGBSS produced an average of 2900 ml/m^2/d. The PSS still produced 3300 ml/m^2/d, the HSS produced 3659 ml/m^2/d. The production of the HSS was higher compared to that of the PSS due to the larger surface area of the HSS. The CCSSS gave 2600 ml/m^2/d and the tubular solar still produced 4500 ml/m^2/d. The tubular solar still coupled with a PSS produced 6928 ml/m^2/d .

The DBGSS produced an average of 2900 ml/m^2/d. The condensation at the bottom glass resulted in the evaporation of the top glass. Due to this, the top basin continued to produce distillate during the nighttime. This practice proves that single basin solar stills are less effective than double basin stills. The temperature difference is one of the key parameters that affect the freshwater yield of solar stills. This study was undertaken to investigate the different types of stills constructed. It was concluded that the tubular solar still coupled with PSS produced more freshwater than the other units due to the concentrator effect.

Jamil and Akhtar [33] have investigated the effect of specific height on the solar still. The basin-type solar still was used in conducting this study. The heat loss was prevented through the incorporation of 1-inch-thick glass and the plain glass was kept at 28^o. The data that was collected included solar radiation, atmospheric temperature, wind velocity and temperatures in the solar still and distillate. The experiment was performed from 8 am to 5 pm from March to June and these months were assumed to be clear sky days. The experiment was conducted on a constant feed water depth of 0.01m. Feedwater was supplied hourly to the solar still basin and it was found to be equal to the amount of distillate collected. It was discovered that daily the freshwater yield improved from 1.341 to 4.186 l/m^2 per day. The daily efficiency also increased from 11.25 to 39.59%. This increment was found to be inversely proportional to the specific height. It was also observed that the quality of water produced from the system improved and was suitable for drinking.

Alwan et al. [34] conducted a study to investigate the effect of modifying a solar still with a solar collector and the focus was to improve the freshwater yield of a traditional solar still. A rotating hollow cylinder made with a galvanized iron sheet was incorporated into the system to increase the surface area of evaporation and reduce the boundary layer thickness of untreated water film. A solar collector was incorporated to increase the temperature of saltwater in the basin. The performance of the system was tested with three rotational speeds (0.5, 1, and 3 rpm).

Two types of solar still were tested, the traditional solar still and the new modified solar still (MSS). The water basin surface area of both systems was 0.5m^2. The covers were made of transparent Plexiglas with a single slope of 35^o on the frame. A DC motor of 12 V and 0.1 A was used to rotate the cylinder. The motor drew power from the photocell panel in the daytime and was connected to a battery at night. The solar collector incorporated on MSS was made of the galvanized steel plate and coated with black colour to increase the absorption of solar energy which was fixed at 35^o. The water circulation between MSS and solar collector was through a water pump with a power consumption of 10 W and a maximum flow rate of approximately 1.2 l/min.

The experiment was performed between 8 am and 8 pm on different days from June to September. The data collection included recording the temperatures of Plexiglas cover, metal basin, brine water, relative humidity within solar stills, solar radiation intensity, wind speed, temperature and relative humidity of ambient air. Data was collected every 30 minutes continuously throughout the day. It was observed that the freshwater yield of the solar still was inversely proportional to the speed of the hollow cylinder. Furthermore, the incorporation of the solar collector increased the freshwater yield of freshwater by 5.5 l/m^2 for MSS compared to 1.4 l/m^2 from traditional solar still.

In a study conducted by Abdullah et al. [35] a new single basin solar still design was studied theoretically and experimentally. Two systems were constructed, conventional solar still (CSS) and tray solar still (TSS) to investigate the efficacy of adding trays on solar still sides. The CSS was made of a galvanized steel sheet with a 3mm thick glass cover at an angle of 24^o and was painted black. The thermal loss was prevented through the incorporation of thermal insulation.

The TSS was also designed the same way as CSS with three additional improvements. Three trays with different colours were attached to the internal sidewalls of the system. Internal mirrors (reflectors) were incorporated between the side trays and mirrors were installed at the top and bottom of the glass cover. The top and bottom mirrors were designed so that they can be inclined according to seasons. The two designs were tested in May and June 2019. Solar radiation, temperature, airspeed and distillate quantity were measured. The basin water depth for both CSS and TSS were kept at 1 cm. The water depth on the trays varied between 0,5, 1, 1,5, and 2 cm. The level of saline water was kept at the same level by the refill that was performed every half an hour.

The results of the experiment showed that TSS with no reflectors was 1.5 times more productive at 1cm basin water level and 0.5cm tray height. TSS with internal mirrors (TSSIM) showed a 58% increase in freshwater yield over that of CSS. The addition of exterior bottom mirrors (TSSIBM) and top mirrors (TSSITM) increased TSSIM freshwater yield by 84% and 75% respectively, as compared to CSS freshwater yield. The use of both the exterior bottom and top mirrors (TSSIBTM) with TSSIM resulted in 95 percent greater freshwater yield than CSS. CSS, TSS, TSSIM, TSSIBM, and TSSIBTM had thermal efficiencies of 34, 41, 42, 44 and 50% respectively, at 1 cm basin water depth and 0.5 cm tray height.

2.2 Double Slope Solar Stills

Gnanaraj and Velmurugan [36] conducted an experimental study to investigate the effectiveness of a double slope single basin solar still with internal and external alterations. The study was conducted to improve the production of distillate. Several solar stills were fabricated and tested, one conventional solar still (CSS) with no modifications, three with internal alterations (one still with finned corrugated basin, one with black granite, and a still with wick), one with external alterations (reflectors), and a combination of the four designs.

Both the basin covers were made from 4 mm thick glass placed at an angle of 30^o. The internal surface of the basin was painted black to better absorb solar radiation. A corrugated basin with fins was incorporated and structured in a wave-like manner using a 2 mm thick iron plate. The corrugated plate was placed at the base with 70 fins (made of 2 mm thick hollow square iron pipe and wrapped with black cotton cloth). A 10-15 mm black granite gravel was laid out at the bottom and 100 fins were placed at the bottom to make a still with a wick. Two external mirrors were incorporated on both sides of the CSS. The angles of these reflectors were flexible according to season. Calibrated K – thermocouples and a digital temperature indicator were used to record basin water and glass cover temperatures. A mercury thermometer was used to measure ambient temperature.

The experiment was performed between 7 am and 6 am from March to May 2018. The basin water level was kept at 200 ml and it was filled every hour to compensate for the distillate collected. Ambient temperature, basin water temperature, glass cover temperature, and distilled water collected were recorded every hour from 7 am to 6 pm. The quantity of distillate collected was recorded for the night period (6 pm to 6 am). The experiment in each modified still was repeated for 5 days. A rapid increase in water temperature was observed in the still with a finned corrugated basin and the still with external reflectors during the daytime. The still with black granite kept high water temperature for a longer period during nighttime. Morning production of distillate was observed to be more on the still with external reflectors. The distillate collected from the CSS was 1880ml/m^2. The distillate production of the still with finned corrugated basin, still with black granite, still with wick, still with reflector and still with all internal and external modifications was 2995, 3210, 2690, 3655 and 5130 ml/m^2 respectively and it was 58.47, 69.84, 42.33, 93.39 and 171.43% respectively higher than the production of the CSS.

Hedayati-Mehdiabadi et al. [37] conducted a study to investigate basin-type double slope solar still equipped with phase change material (PCM) and PV/T collector. A PV/T collector and PCM were incorporated on the still. Paraffin wax was used as the PCM for this study. The production of potable water was studied at day and night times to determine the effect of incorporating PCM on solar stills. The system was tested in winter and summer. The results of the experiment showed that the production of freshwater increased by 10.6% between 06 July and 23 December. Increasing the mass of saline water in the basin reduced freshwater production during the daytime and increased production at night-time.

Rajamanickam et al. [38] conducted a study to compare the effect of water depth, single slope and double slope, and charcoal as an energy storage material. The double slope still had two 4 mm thick adjacent glass covers both positioned at an angle of 20 degrees to the horizontal axis. The saline water tank was placed next to the still at a height of 0,5 m above ground level. The still had a single basin made from galvanized iron in the inner wall. The bottom surface and outer wall of the basin were coated with black paint to better absorb heat. The system was incorporated with thermocouples to measure temperature.

A digital temperature indicator was used to obtain all temperatures and an Eppley Pyranometer was used to measure solar radiation. An anemometer was used to measure the wind speed and a measuring jar was used to measure the condensate water. The experiment was conducted from 9 am to 5 pm in April 2017 on the double solar still. The water level was maintained throughout the experiment. The results showed that the maximum amount of freshwater produced was 3025 ml/day at 0.01 m water depth. The freshwater production increased by 30,57% on double slope solar compared with single slope solar still with the same basin area.

2.3 Factors Influencing the Efficiency and Freshwater Yield of Solar Stills.

The performance of solar stills can be influenced by several factors. These factors can be divided into two categories: ambient and operating conditions, and design conditions. The ambient and operating conditions include factors such as the ambient temperature, wind speed, basin water depth and inlet temperature of the water. On the other hand, design conditions refer to controllable factors that are critical for the overall system performance. These design conditions include the type of still, the slope of the cover, the material used for construction and insulation, modifications and sun-tracking systems.

According to Selvaraj and Natarajan [39], there are four key characteristics that significantly impact the performance of solar stills. These include the collector area, basin water depth, solar radiation intensity and the temperature difference between the glass cover plate and the water.

In a review by Manokar et al. [40], various factors that influence the evaporation and condensation rate of passive solar stills were studied. Several factors influence the evaporation and condensation rates in stills, including, but not limited to, the construction material used on the still, the level of saline water in the basin, the rate of absorption of the saline water in the basin, the temperature of the water entering the basin, the temperature of the basin cover and the wind speed.

2.3.1 Solar radiation intensity

Solar stills are solely dependent on the sun, hence, the solar radiation intensity is an important parameter for the efficiency of the systems. In the year 2000, Boukar and Harmim [41] conducted a study on a simple basin solar still with a solar collector and one without it to investigate the influence of climatic conditions of Adran (a Saharan site in Algeria) on solar stills. The systems were tested for three months between January and March. The stills were tested at varying water depths from 2.5 cm to 3.5 cm.

The production on the still with no collector came at about 4.01 – 4.34 kg/m^2/d and the solar collector incorporated still produced between 8.02 to 8.07 kg/m^2/d that is approximately double to that of the traditional solar still. It was then concluded that incorporating a solar collector on a solar still enhances the production of the still. This study also showed that as the solar radiation increased from January to March, the production of the distillate on both stills increased – a fact that was to be expected since solar irradiance is the main contributing factor to solar desalination systems. This increase, therefore, indicated a direct proportionality relation between the irradiance and production of solar stills.

Badran and Abu-Khader [42] conducted an investigation on a single slope solar still, examining its freshwater yield and efficiency based on solar radiation intensity. The study involved both practical and theoretical analysis, with the MATLAB software used for the latter. The experiment was conducted from 8 am to 5 pm using a passive solar still. The researchers concluded that the freshwater yield and efficiency of the solar still increased with the intensity of solar radiation. They found that the highest efficiency was achieved during the early afternoon, when the sun's radiation intensity was at its highest.

In a study by Badran and Al-Tahaineh [43], the influence of solar radiation and the addition of a flat plate collector on the performance of a solar still was investigated. The experiment was conducted in two scenarios: one with a solar collector (active) and one without (passive). It was carried out over the course of a few months, from October to December. Initially, the still was tested without the solar collector in October to analyse the impact of solar radiation. The researchers observed that decreasing the water level in the basin and increasing solar radiation intensity both resulted in higher freshwater production. Additionally, when the solar collector was combined with the still, the production rate increased by 36%. Almuhanna [44] also designed and tested a single slope solar still, exploring the effect of solar radiation intensity on freshwater production. The study found that as the intensity of solar radiation increased, the rate of freshwater production also increased.

In a study conducted by Subramanian et al. [45], a practical and theoretical analysis was performed on a solar still with a single basin. The still was modified by replacing the glass cover with a pyramid-shaped structure and incorporating a flat plate collector. Several parameters, including solar radiation, wind velocity, ambient temperature, time, inlet temperature (flat plate collector), inlet water temperature (still) and freshwater distillate, were recorded during testing between 9 am and 5 pm. It was observed that solar radiation was directly proportional to the production of freshwater on the solar still.

Solar stills operate on two processes, condensation and evaporation. The processes are an important part of the production of stills, hence, continuously improving these processes is vital. Condensation plays a huge role in the freshwater yield of solar stills [20]. Sebaii [46] investigated using computer simulation to determine the effect of wind speed on certain designs on basin type and vertical solar stills in Tanta. Calculations were made on typical summer and winter days to link the still production to wind speed for varying levels of saline water. It was found that the production of distillate is directly proportional to the wind speed on these stills. The average wind speed was also established to be 8 m/s and 10 m/s on winter and summer days, respectively.

Omara et.al [47] reviewed the performance of conventional solar stills with different types of reflectors. Reflectors are a useful and inexpensive way to boost the solar irradiation delivered to the basin liner or water, as well as the distillation efficiency of the still. The study looked at several stills that were incorporated with either internal (IR) or external reflectors (ER) and some with a combination of both to enhance the output of solar stills. According to the literature reviewed for this study, reflectors are only efficient/necessary in areas where the atmospheric temperature and solar irradiance are very low, thus, indicating that reflectors are more efficient in winter compared to summer. It was also noted that the inclination angle of the ER must be changed according to climatic conditions to achieve maximum results. Table 2.1 below shows the summarized works on the influence of solar radiation intensity to freshwater yield discussed in this section.

Table 2.1: The summarized works on the influence of solar radiation intensity to freshwater yield

Still type	Condensation technique	Country conditions	Results (per day)	References
Single slope	Natural wind and flat plate collector	Jordan	3510 ml/day	[43]
Single slope basin	Natural winds	Saudi Arabia	5941.4 ml/m^2/d	[44]
Single basin pyramid	Flat plate collector	India	800 ml at 1180 W/m^2 (max radiation)	[45]
Double slope single basin	Natural Winds	India	5130 ml/m^2/d	[36]

2.3.2 Temperature difference

The air mass within the solar still circulates more vigorously as the temperature difference between the glass cover and the water basin increases. This practice leads to a notable improvement in the transfer of heat through evaporation and convection from the water in the basin to the glass cover. The condensation process is primarily driven by the difference in temperature between the glass cover and the water [48].

According Boukar and Harmim [41], at a maximum temperature difference, efficiency is maximized; this variance may be accomplished by using a glass with a reduced thickness, a cover tilt angle close to that of the area's latitude where the solar still is tested, a thin solution to be distilled and a high wind speed.

Abu-Arabi et al. [49] conducted a study to model and assess the effectiveness of a single-basin solar still with cooling water flowing through a double-glass cover. The area of the still basin was $1m^2$. This design aimed to maintain low glass temperatures and increase the temperature difference between the glass and water, thus, improving the condensation rate. In the same weather conditions in Muscat, Oman, the DGBSS was compared to the traditional single-glass solar still. The presence of water between the double-glass covers enhanced the output of the still. The study revealed that the amount of insulation used had a significant impact on the efficiency of the still. Properly insulated stills would result in a higher yield for the conventional still, but the double-glass still showed higher output when considering heat losses from the water basin to the environment in the simulation.

The irradiance from the sun is the main parameter affecting the rate of evaporation. It, thus, is important to select or make use of material that has thermal conductivity for the construction of solar stills [50]. The temperature difference between the saline water in the basin and the basin cover greatly affects the evaporation and condensation processes. The higher the temperature difference between the saline water in the basin and the basin cover, the higher the evaporation and condensation rates and, therefore, an enhanced production rate [48].

Khan et al. [51] investigated the performance of a hemispherical solar still with and without cooling on the top cover. The cooling mechanism was implemented to increase the condensation rate by enhancing the temperature difference between the water in the basin and the cover. The distillation unit efficiency was enhanced from 34% to 42% when water was supplied at a flow rate of 0.166 ml/s. The findings indicated that the application of water cooling increased the efficiency of the hemispherical solar still by 1.25 times. Table 2.2 below shows the summarized works on the influence of temperature difference to freshwater yield discussed in this section.

Table 2.2: The summarized works on the influence of temperature difference to freshwater yield

Still type	Condensation technique	Country conditions	Results (per day)	References
Single basin	Water film cooling	Jordan	6% efficiency enhancement	[52]
Single basin	Water film cooling	Jordan	20% efficiency enhancement	[53]
Double-glass cover single basin	Natural Wind (water cooling)	Oman	35% efficiency enhancement	[49]
Hemispherical	Natural Wind (water cooling)	India	1.25 efficiency increase	[51]

2.3.3 Evaporation surface area

The performance of solar stills is significantly influenced by the surface area of the basin and the water levels in it. The efficiency of the solar still is determined by the evaporation area, so enlarging the surface area can enhance its effectiveness. This process can be achieved by incorporating materials such as jute, wick, sponge or similar substances. Studies have shown that the use of such materials can increase the output by 15-46% in solar stills [54].

Kwatra [55] conducted a computer simulation to investigate the relationship between distillation yield and evaporation area in a solar still. The study used a solar still with multiple effect, which included several basins to expand the evaporation area. The still was also equipped with a solar collector and evaporator assembly. By multiplying the evaporation area by four, the study found that the distillation yield increased by approximately 19.6%. This result suggests a strong correlation between the size of the evaporation area and the freshwater yield of the solar still.

In a reviewed study by Chaurasiya et.al [56], passive, hybrid and other solar still designs were assessed to determine the most efficient solar stills for residential and industrial applications. Numerous researchers changed the single-basin single-slope solar still by incorporating distinct design modifications. It was discovered that the solar still integrated with the Fresnel lens was a better arrangement with a 638.02% increase in production for a single-basin single-slope solar still. The double-basin single-slope solar still with reflectors and flat plate collector was found to be a promising design with a freshwater yield boost of 127.31%. The solar still with more than one basin integrated with photovoltaic thermal (PV/T) collectors proved to have a greater enhancement in output. In a single basin solar still with a double slope, the external reflector still seemed to perform better with finned, corrugated, black granite and wick. A semi-circular trough with a black fabric and an external reflector enhanced the production by 676%. It was concluded that wick paired with tube solar still is the most productive design for industrial applications, whereas a passive single-basin single-slope solar still is more suitable for home applications due to its greater efficiency and cost-effectiveness.

Alwan et al. [34] conducted a study to explore an improved version of a solar still by combining it with a solar collector and a rotating hollow cylinder. The primary goal was to enhance the performance of the traditional solar still. A rotating hollow cylinder made of galvanized iron sheet was introduced into the system that increased the surface area of evaporation and reduced the thickness of the boundary layer of untreated water. The experiment involved testing the system at three different rotational speeds (0.5, 1, and 3 rpm). The solar still with a solar collector and the rotating cylinder produced 5.5 l/m^2, while the traditional solar still only produced 1.4 l/m^2. It was then concluded that the system performed better at the lowest rotational speed, attributed to the larger evaporation area. Table 2.3, shown below, provides a summary of the studies discussed in this section that investigated the influence of evaporation surface area on freshwater yield.

Table 2.3: The summarized works on the influence of evaporation surface area to freshwater yield

Still type	Condensation technique	Country conditions	Results (per day)	References
Single basin	Solar collector and evaporator	India	19.6% increase in production	[55]
Single basin	Solar collector	Iraq	5.5 l/m^2 (25% increase)	[34]
Single basin single slope (with pond fibres)	Natural wind	India	29.67% efficiency increase	[57]
Single basin (with trays)	Natural wind	Egypt	3100 $ml/m^2/d$ (1.5 times increase in freshwater water production)	[35]
Stepped double slope (with linen wicks and carbon black nanoparticles)	Natural Wind	Egypt	80.57% increase in production	[58]

2.3.4 Basin water depth

Manokar et al. [40] conducted an experimental study to determine how the water depth and insulation in the basin effect the output of a pyramid still. The system was tested by varying the water level from 1 to 3.5 cm with and without insulation. The yield from the still was found to be larger at the lowest water level of 1 cm in both insulated and uninsulated circumstances.

Elango and Murugavel [59] studied the influence of insulation and basin water depth on the performance of a single and double basin still. The water level was adjusted from 1 to 5 cm in both insulated and uninsulated conditions for these studies. During the heating phase, the single basin produced more distillate than the double basin, whereas during the cooling phase, the double basin produced more. Under both insulated and uninsulated conditions, the efficiency of the double basin double slope still outperformed that of the single basin double slope still. At the lowest water level of 1 centimetre, both stills were more effective, producing 5327 l/ m^2 and 4.401 l/m2 per day on the double basin dual slope and single basin dual slope solar stills, respectively. In both cases, the insulated stills outperformed the uninsulated stills.

Badran and Abu-Khader [42] investigated the thermal efficiency of a single-slope solar still using both experimental and theoretical methods. The effect of exploring different water levels in the basin was examined, ranging from 2 to 3.5 cm. These researchers found that as the water level increased, the daily production of the still decreased. This decrease in output was attributed to the higher heat capacity of the water as the depth increased, leading to a smaller temperature difference between the basin and the water that resulted in a lower evaporation rate.

Several experiments have been set up and tested to investigate the effect of saline water depth on the production of solar stills. Khalifa and Hamood [60] conducted a study to validate/verify the influence of saline water depth on the freshwater yield of solar stills. A basin-type solar still was built from 0.8 mm thick galvanized steel and a 4 mm glass cover. Saline water with a salinity level of 1100 – 1400 ppm was used for testing purposes. The system was run during both day and night times; night production was measured at 7 am the following morning and added to the total daily production.

The system was tested at a saline water depth of 1, 4, 6, 8 and 10cm in April and May at Baghdad in Iraq with a latitude angle of 33.3^{o}N. The system was incorporated with calibrated copper constantan thermocouples that were shaded with reflective shields, a thermometer via a selecting switch to take temperatures of the glass cover, saline water and vapor. The glass cover was positioned at an inclination angle of 35^{o} and a 10cm polystyrene insulation was used on the base to prevent heat loss.

The results obtained from the above experiment were compared to those of a similar nature recorded in the existing literature. It was found that the lowest saline water depth produced the highest amount of distillate during the daytime and had the highest temperature. However, even though the highest saline water depth gave low production, during the day it gave a higher nocturnal production (continuous production after sunshine due to the high temperature absorbed and retained by the water).

Rajamanickam and Ragupathy [61] studied the influence of water level in the basin on internal heat and mass transfer in a single basin dual slope still. The still was made of galvanized iron sheets and a 3 mm thick transparent glass cover. After adjusting the orientation, single-sloped and dual-sloping stills of the same basin size were produced and tested by maintaining the depth of the water in the basin at 0.01 m, 0.025 m, 0.05 m and 0.075 m respectively. The greatest freshwater output was 3.07 l/m^2 per day in the dual slope still with a water level of 0.01 m in the still basin and only 0.69 l/m^2m^2 per day with a water level of 0.075 m. These findings revealed that when basin water levels fall, still output increases. Table 2.4 below shows the summarized works on the influence of basin water depth to freshwater yield discussed in this section.

Table 2.4: The summarized works on the influence of basin water depth to freshwater yield

Still type	Condensation technique	Country conditions	Results (per day)	References
Pyramid	Flat plate collector	Egypt		[40]
Single slope	Natural wind	Jordan	25.7 % increase (2 to 3.5 cm)	[42]
Double basin double slope	Natural wind	India	5327 $l/m^2/d$	[59]
Double slope	Natural wind	India	3.07 $l/m^2/d$	[61]
Inverted Absorber Solar Still	Natural wind	Oman	3.41 $l/m^2/d$	[62]

2.3.5 Insulation

To increase efficiency, using insulation to reduce heat loss from the sidewalls and base of the solar stills is another viable option. Various insulation materials including gypsum, sawdust, styrofoam, polyurethane, thermocol and wood have been tested to prevent energy losses from solar stills. The thermal conductivity of the insulation material is a critical factor in determining the material thickness to achieve maximum efficiency [54].

To enhance a still's efficiency, heat losses must be kept to a minimum by using suitable insulation to conserve thermal energy storage. Khalifa and Hamood [63] conducted a practical evaluation of the effect of insulation thickness on a basin solar still. The experiments were carried out on a still with no insulation and a still with insulation of 30, 60, and 100 mm, all with a cover tilt angle of 35° and a saline water level of 40 mm throughout the testing. The comparison of the stills demonstrated that increasing the thickness of the insulation improved the still's efficiency.

Karaghouli and Alnaser [64] studied the influence of insulation on the performance of a single and double basin still. During the period (February to June), single and dual slope solar stills were tested with and without insulation under the same circumstances and with the same basin area of 0.45 m^2. The results demonstrated that the freshwater yield of insulation-equipped stills increased for both single and dual slope stills.

Arunkumar et al. [65] studied the effect of insulation on solar stills. Four 50 m^2 single basin solar stills were constructed and tested in the same weather circumstances of Chennai, India. Three stills were tested: a single slope solar still (SSSS) with no insulation, one with bubble wrap insulation and one with carbon impregnated foam (CIF - diameter 0.17 m, thickness 0.015 m) and bubble wrap insulation. The results of these tests on the three stills were compared to the results of the traditional solar still with sawdust insulation. Wind speed, ambient temperature, solar radiation and internal temperatures were all observed periodically. The output of the SSSS without insulation, SSSS with bubble wrap insulation, SSSS-CIF with bubble wrap insulation, and CSS with sawdust insulation were found to be 1.9, 2.3, 3.1, and 2.2 $l/m^2/d$, respectively. The results confirmed that incorporating insulation material on a still increases its level of production. The still with CIF had the maximum freshwater production because the CIF in the basin increased the evaporation surface area and therefore more production.

Hashim et al. [66] investigated several types of insulation to determine the optimum insulating material for solar stills. Five double-slope basin-type solar stills were built and tested under the same conditions. The stills all had the same dimensions and cover inclination angle of 15°, the basin area was 0.5 m^2 and they were all covered with a transparent glass of 4mm that was fixed on an iron frame. One still had no insulation while the basins of the other four stills were insulated from the following elements: (i) plywood, (ii) glass wool and plywood, (iii) 5 cm thick hay and plywood and (iv) a still made of glass with a 5cm thick air gap between the basin and the glass bottom. The experimental results were 1308.819, 2385.697, 3015.263, 2954.545 and 2283.187 ml/m^2 respectively. The still with no insulation produced less than the insulated stills which proved that incorporating insulation on a solar still enhances its freshwater yield. Glass wool and hay were deemed the best materials for insulation; however, hay was recommended due to its low cost. Table 2.5 below shows the summarized works on the influence of insulation to freshwater yield discussed in this section.

Table 2.5: The summarized works on the influence of insulation to freshwater yield

Still type	Condensation technique	Country conditions	Results (per day)	References
Single slope basin	Natural wind	India	80% increase in still freshwater yield	[63]
Double basin	Natural wind	Iraq	19.9% increase in still freshwater yield	[64]
Single basin	Natural wind	India	3.1 l/m^2/d production	[65]
Double slope basin-type	Natural wind	Iraq	3015.263 ml/m^2	[66]
Double basin double slope	Natural wind	India	5327 l/m^2/d (17.38% increase in production)	[59]

2.3.6 Glass cover thickness and angle of inclination

Ghoneyeri and Ileri [67] performed research into the effect of glass cover thickness on solar stills by building and testing four basin solar stills. Three stills consisted of glass covers of varied thicknesses of 3, 5 and 6 mm while one had a plastic cover. The still with a 3 mm glass cover generated more distillate. Glass is the preferred material due to its better solar transmittance at all angles of incidence and longer life span, however, plastic covers can be used for short-term applications [48].

The yearly solar still production was maximum when the slope of the condensing glass cover was equal to the geographical latitude, according to Sing and Tiwari [68]. In research conducted by Akash et al. [69] in Jordan, a solar still with cover inclination angles ranging from 15°, 25°, 35°, 45° and 55° was evaluated to determine the effect of cover inclination angle on the still. The results showed that 35° was the optimal angle, and the latitude is 30.5852° N, 36.2384° E. As a result, the above-mentioned research findings were validated.

El-Samadony et al. [70] investigated the radiation heat transfer rate within a stepped solar still (SSS) using a theoretical model. The radiation form factor was computed between hot sea water and glass cover. The effect of incorporating the radiation shape component was quantified and subjectively rated. The effect of glass cover tilt angle (from 10° to 70°) and solar irradiation (from 200 to 1200 W/m^2) on SSS generation was investigated, taking into account the radiation shape factor. The radiation shape factor was shown to have a substantial effect on thermal performance projections. Furthermore, the output of the solar still was determined to be responsive to the radiation shape, particularly at low sun irradiation and when the glass cover tilt angles are high (location's latitude angle) and *vice versa*. When the radiation form factor was considered, the percentage improvement in still output was up to 18.8% with a low solar irradiation of 200 W/m^2 and a glass cover tilt angle of 70°.

Ibrahim and Khalifa [71] investigated the development of a basin type still with internal and exterior reflectors positioned at angles of 0°, 10°, 20° and 30° in winter for still cover angles of 20°, 30° and 40°. A basic still equipped with inner and exterior reflectors was tested in the winter at a latitude angle of 33.3° N. It was observed that a still with a larger cover angle has better daily freshwater yield at any reflector angle, and that the daily production of the still with no reflectors remained essentially constant at any glass cover angle. Furthermore, during the winter season at 33.3° N latitude, the most effective still was revealed to be one with a cover inclined at 20° and an internal and external reflector oriented at 20°, with the output of this still being 2.45 times the typical nominal simple still output. Table 2.6 below shows the summarized works on the influence of the thickness of glass cover to freshwater yield discussed in this section.

Table 2.6: The summarized works on the influence of the thickness of glass cover to freshwater yield

Still type	Condensation technique	Country conditions	Results (per day)	References
Single basin	Natural wind	Turkey	15.5% freshwater yield enhancement	[48]
Single basin	Natural Wind	Jordan	6.7 l/day	[69]
Stepped solar still	Natural Wind	Egypt	18.8% freshwater yield enhancement	[70]
Single slope basin type	Natural wind	Iraq	2.45 times freshwater yield enhancement	[71]
Conical single basin	Flat plate collector	New Delhi	6.79 $kg/m^2/d$	[72]

2.3.7 Summary and future directions

Critical parameters influencing the production of solar stills were discussed during this Literature Review. Below are some discoveries recorded:

- The wind speed, temperature difference of the water and glass cover, evaporation surface area, solar radiation intensity and insulation are directly proportional to the production of distillate.
- The basin water depth and the thickness of the glass cover are inversely proportional to the production of freshwater on solar stills.
- A high solar radiation allows the still to continue operating after sunset, therefore, more distillate is produced during a 24 hour period.
- The condensation process has a considerable influence on efficiency of solar stills and this process depends highly on the temperature difference and wind speed.
- The evaporation surface area and basin water depth are linked factors in the still, reducing the water depth results in an increase of the evaporation surface area and, therefore, increases the still's production.
- Insulating the still improves the efficiency by minimizing the heat losses in the system.
- The angle of inclination of the cover plate however depends on the location of the system, it has been proven through research that the system produces maximum results when the inclination is equal to the latitude angle of that specific area.

2.4 Literature Review Summary

The development and improvement of existing solar stills has been an ongoing project for researchers seeking to advance the existing systems and achieve higher distillate output from solar stills. In the literature reviewed on single-stage solar stills both single and double-sloped stills were built using glass covers for the basin covers. Glass is considered the best material for still basin covers because of its superior transmittance and lower reflectance properties [73]. This system’s basin cover was built using steel that has been made into a cold-water holder, this item improved the temperature difference of the system that eventually resulted in an increase in the condensation rate.

2.4.1 Research Gap

It has been observed from the reviewed literature that most designs are modified to enhance freshwater yield of solar stills during the day. Few works have focused on developing a system that can operate continually. This study will consider the enhancement of freshwater yield during night-time as well. The experiment will take place during both day and night times. The system will be incorporated with thermal storage to store solar energy during daytime.

2.4.2 Novelty

Based on reviewed literature, the systems that were designed operate during daytime. It can be observed that there is a variance in their performance. The performance depends on the location where the system is operational, however, there is no work that analysed the performance of these designs under the Cape Town weather in South Africa. This work presents and analyse the performance of the D5S under the Cape Town weather conditions. It further investigates the performance of the system when there is no sunshine.

Furthermore, a new setup is introduced to sufficiently increase the daily productivity of the double slope solar still. In addition to incorporating an evacuated tube solar collector, the still cover is made of a galvanized steel sheet instead of the usual glass. The design of the cover has a hollow section that was used to keep room temperature water to speed up the condensation process inside the basin.

CHAPTER 3 – METHODOLOGY

The detailed construction of the double slope single-stage solar still (D5S) is covered in this chapter. It comprehensively discusses the processes that were utilized to attain the final product and documents the complete construction procedure. It further outlines the experimental setup and testing procedures of the D5S. This chapter discusses all the testing apparatus used, the testing procedure and all tests performed on both the seawater and distillate produced by the system.

3.1 List of Tools and Materials:

- 1mm galvanized steel sheet
- Evacuated tube solar collector
- 1-litre Duram metal silver paint
- Cistern float valve inlet and a ball float.
- 40x40x1.6 mm square steel tubing
- 25x25x1.6 mm square steel tubing
- 15mm copper tubing
- Mechanical copper fittings (T Piece, elbows, straight connectors, etc.)
- Bending machine
- Angle grinder
- Hand drill machine
- Copper crossover tubes (U-shaped tubes) – 15 mm OD
- 90° elbow with 15 mm external diameter.
- 22 mm ball valve
- LPG gas soldering unit
- 2 mm 60T Resin core Lead wire.

3.2 Construction Process

3.2.1 Water basin

The basin is made up of two parts, the water basin and the water basin cover that are bolted together. This section covers the detailed construction process of these parts.

The basin was made of 1 mm galvanized steel. The steel size purchased came as a 1 X 2450 X 1225 mm sheet. The size of the basin was 1250 mm X 840 mm X 500 mm, however, the bending machine available could only accommodate a minimum of 1200 mm length. The basin was divided into two parts, one part is shown in Figure 3.1 below, and pop rivets were used to join the unit as shown in Figure 3.2 below.

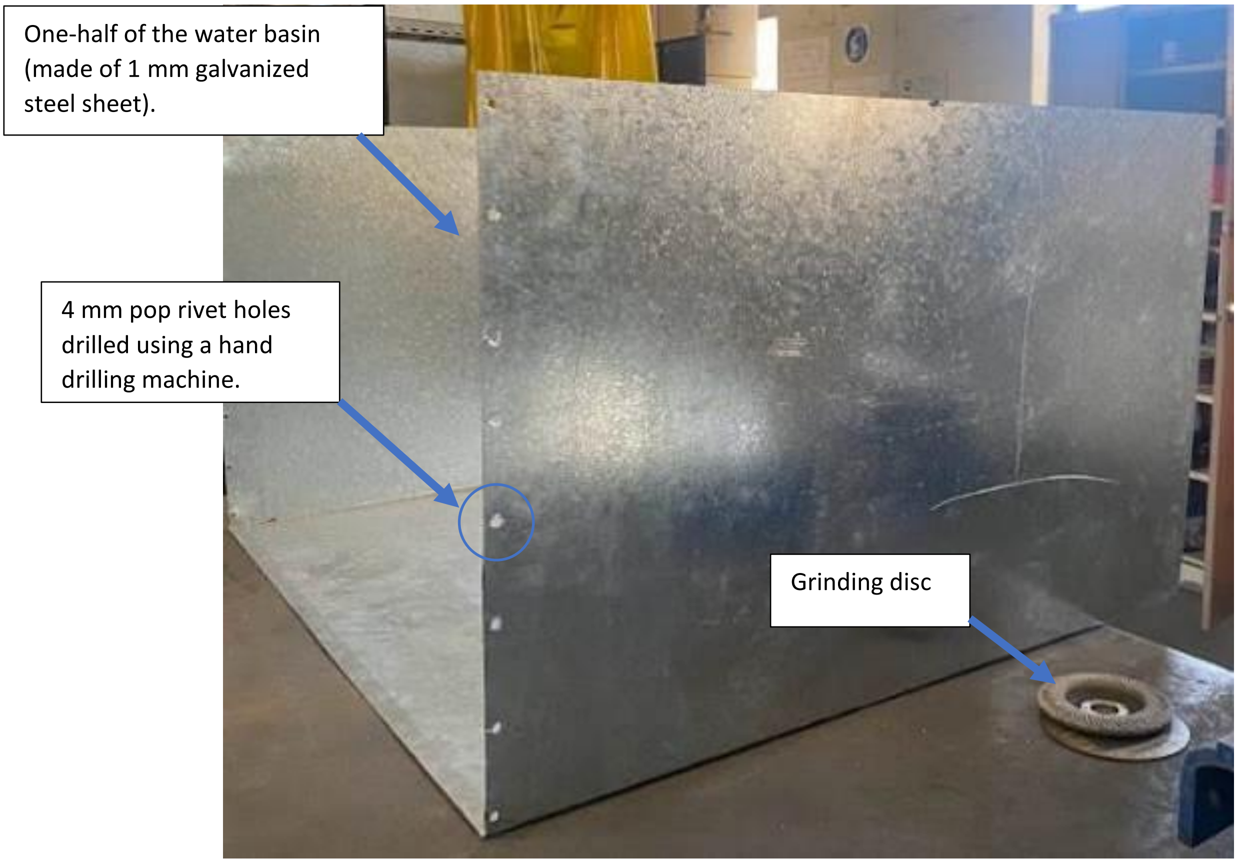

Figure 3.1: Water basin

The material was cut using an angle grinder and tin snip for small cuts and bent using a hydraulic bending machine. To minimize the chances of leaks in the unit, waterproof paint, and silicone were used. Waterproof paint was used with a cloth (membrane). The cloth was cut into strips and paint was applied on both sides of the cloth. The surface of the areas that needed to be sealed was first painted, the painted cloth material was then placed on the surface and another coat of paint was applied. The surface was cleaned and prepped with thinners as shown in Figure 3.2 below before painting to achieve effective results. Silicone was applied before riveting and waterproof paint with membrane was applied afterwards to seal gaps further.

Figure 3.2: Water basin construction

The side panels of the basin with dimensions 840 mm X 500mm shown in Figure 3.3 were also constructed following the same process. They were cut using an angle grinder, tin snip, and bending machine, and pop rivets were used for joining followed by waterproof painting after joining the entire basin unit. The upper section of the side panels was cut at an angle of 120° to accommodate the covers, and the top section was cut separately and joined using brazing as shown in Figure 3.3 below. According to Xiaoqing et al. [74], brazing is a process of putting several metal pieces together by melting and flowing a filler metal into the joint, with the filler metal having a melting point that is lower than the adjoining metal. The pop rivet holes were drilled using a 4 mm drill bit and a drilling machine for 4,8 mm X 8 mm pop rivets.

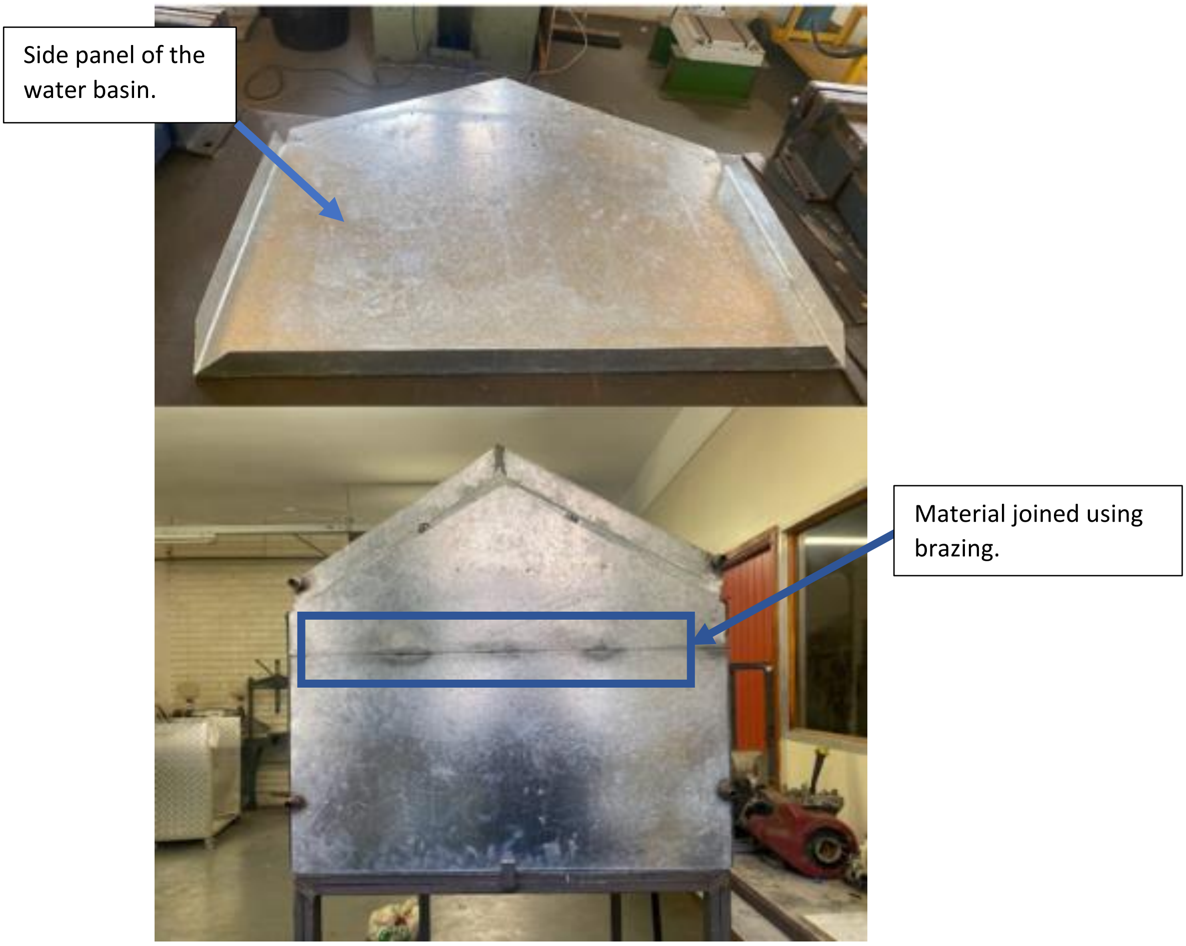

Figure 3.3: Basin side panels

The basin is the most important part of the system, the unit contains seawater that will be received from the saline water tank and circulates between the basin and the solar collector. The evaporation of steam and the condensation processes take place inside the basin resulting in the final production of potable water. Inside the basin, there are collecting trays placed at an angle of 20° delivering the water to the pipe that transports it to the collecting tank outside the unit. The cold-water inlet on the basin is on the one side and the collection tray is on the other side. The basin unit was joined using pop rivets and, therefore, precautions were taken were during the construction process since taking the unit apart would not be an easy task and, more importantly, would damage the unit structure.

3.2.2 Inside collection plates

The water vapour generated inside the basin emerged into condensate on the water basin cover. Due to the slope on the cover, the water droplets slid down. The basin had collection plates pop riveted on both sides to serve as collection plates. The plates were made of the same 1mm galvanized steel sheet as the basin, cut using the angle grinder and bent using the hydraulic bending machine. Silicone and pop rivets were used to attach the plates inside the basin. A hand-drilling machine with a 4mm drill was used to drill holes in the basin and on the plates. A pop rivet gun with 4,8 mm X 8 mm pop rivets was used to attach the plates. Silicone was used as an extra measure to ensure that there were no leaks from the plates to the basin.

Figure 3.4: Collection trays

3.2.3 Basin cover

The cover was made to align with the basin's dimensions of 1250 mm X 840 mm X 500 mm with 100 mm width overlap material that was bent at an angle of 90° using the hydraulic bending machine and joined using brazing to enable the joining of the cover to the basin. The cover consisted of two identical units made of 1 mm galvanized steel that were joined using 4,8 mm X 8 mm pop rivets and brazing to make a hollow cover that held cold water as shown in Figures 3.5 and 3.6 below. The cold water catalysed the condensation process in the system by increasing the temperature difference between the basin and cover.

Figure 3.5: Brazing joint

The material was measured using a tape measure, marked using a scriber, cut using an angle grinder with a cutting disk; the sharp edges were removed using a smooth file and the corners were cut using a tin snip. Silicone was used to seal gaps between the two units. The complete unit was then incorporated with 8mm steel bolts to fit the cover to the basin, bolts were used instead of pop rivets and welding to allow ease of access to the basin.

Figure 3.6: Basin cover

3.2.4 Basin cover cooling water inlet

The cover of the basin had an inlet and outlet for the cooling water. Three holes were drilled using a hand drilling machine with a 4mm drill bit as a pilot drill, followed by a 10mm drill bit. A round file was used to achieve the required diameter, one hole was made for the inlet on one side and two holes on the other side as draining ports.

The inlet was extended using a steel nipple, horizontal copper pipe, 90^{o} copper elbow and vertical copper pipe that were all joined using lead soldering as shown in Figure 3.7 below. The outlet was extended using a steel nipple, horizontal copper pipe and 90^{o} copper elbow on both holes. Both inlets were extended using copper piping and joined with a T piece off-centre to avoid obstruction, a Conex 22mm ball valve was added as an isolation and draining point as shown in Figure 3.8 below. The lead soldering used for joining the copper piping was achieved using an LPG gas cylinder, gas hose, welding nozzle and 2mm 60T resin core lead wire and all the copper piping was cut using the 4-28mm copper pipe cutting tool depicted in Figure 3.16 below.

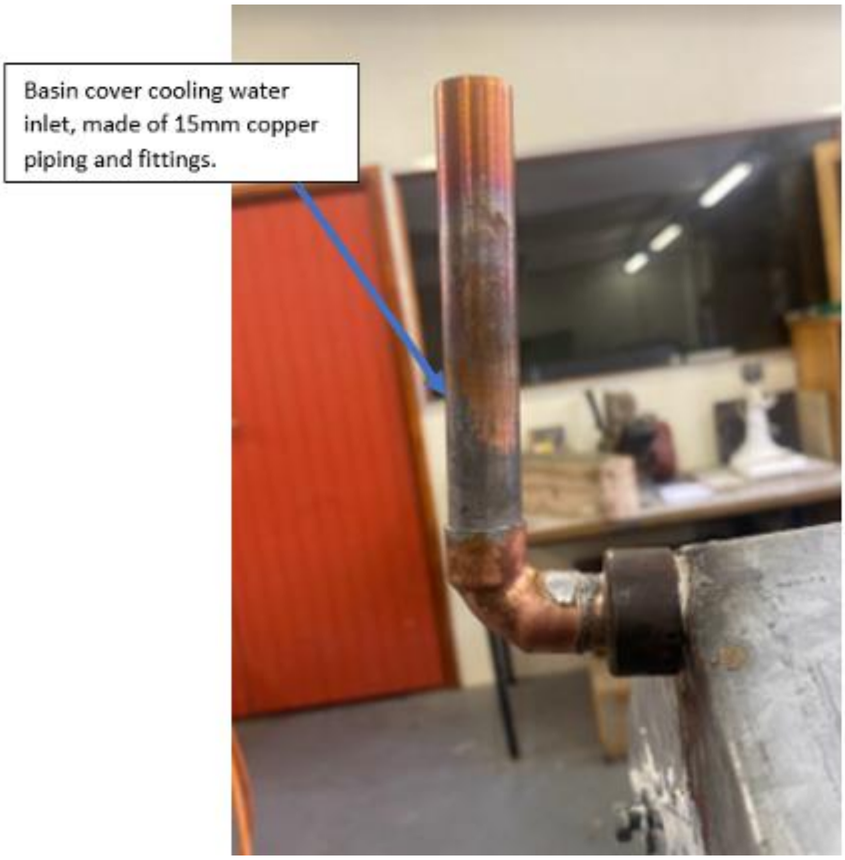

Figure 3.7: Cooling water inlet

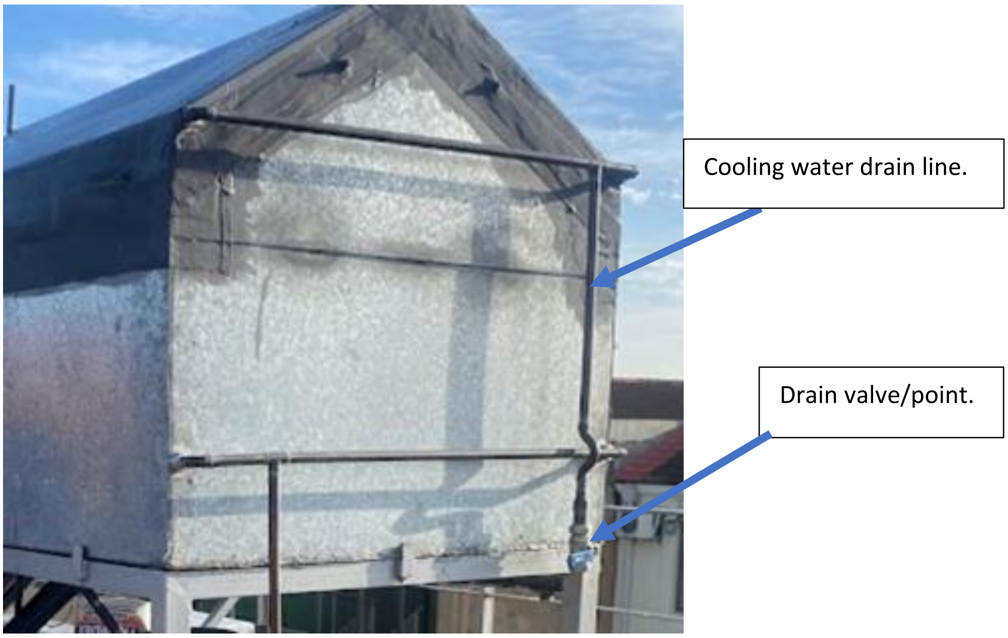

Figure 3.8: Cooling water drain line

3.2.5 Saline water tank

The saline water tank was a 20-litre cylindrical plastic bucket with a diameter of 300 mm and 450 mm in height. The plastic material was selected due to its corrosion resistance. The bucket was placed on an elevated steel frame/stand made of a 25 mm X 25 mm X 2 mm square steel tubing that was attached to the water basin stand using 8mm steel bolts. The frame was elevated to allow saline water to be transported using the force of gravity. The bucket was cut at the bottom with a knife to fit a ¾'' Cobra straight coupler and tied with two 20 mm back nuts as shown in Figure 3.9 below, one inside and one outside the bucket. The outside back nut was joined to the copper piping using lead soldering to ensure no leaks occurred and the inside back nut was screwed in. This action was taken to create a connection for copper piping that was linked to the float valve on the water basin (also serving as the saline water inlet to the basin). The bucket had a lid to keep it closed to prevent foreign objects from entering the tank.

Figure 3.9: Brass back nut

Figure 3.10: Primary tank outlet

A 15mm to ½'' female brass elbow was connected to the float valve facing the direction of the saline tank to fit the 15 mm copper pipe coming from the saline water tank. The 15 mm copper pipe was joined to the brass elbow using lead soldering. The connection from the saline water tank delivered saline water to the basin using the gravitational force. This water was transported to the evacuated solar collector for heating and returned to the basin. As the evaporation and condensation processes took place the condensed droplets were collected through the plates on the side walls and transported to the collecting tank. Figure 3.11 below depicts the elbow-to-copper piping connection.

Figure 3.11: Primary tank to basin connection

3.2.6 Float valve

A float valve was installed on the water basin to control the water level inside the water basin. A hand-drilling machine was used to drill a hole in the valve port. A 4 mm drill bit was used as a pilot drill, followed by a 13 mm drill bit. To achieve a ¾'' (22 mm) port, a round file was used to extend the diameter of the hole by filing in a circular motion ensuring that a circular shape was achieved. Once the correct size was obtained, the float valve was installed from the inside of the water basin and tightened using flat nuts. The float valve was positioned to limit/keep the maximum water depth at 50 mm. This process entails that when the saline water enters the basin and reaches a depth of 50 mm, the float valve will close to stop the flow. Once the water depth decreases to a level lower than 50 mm, the valve will open and allow the saline water to flow into the basin again. The float valve that was used for this system is a 110 mm ball float valve (see Figure 3.12 below).

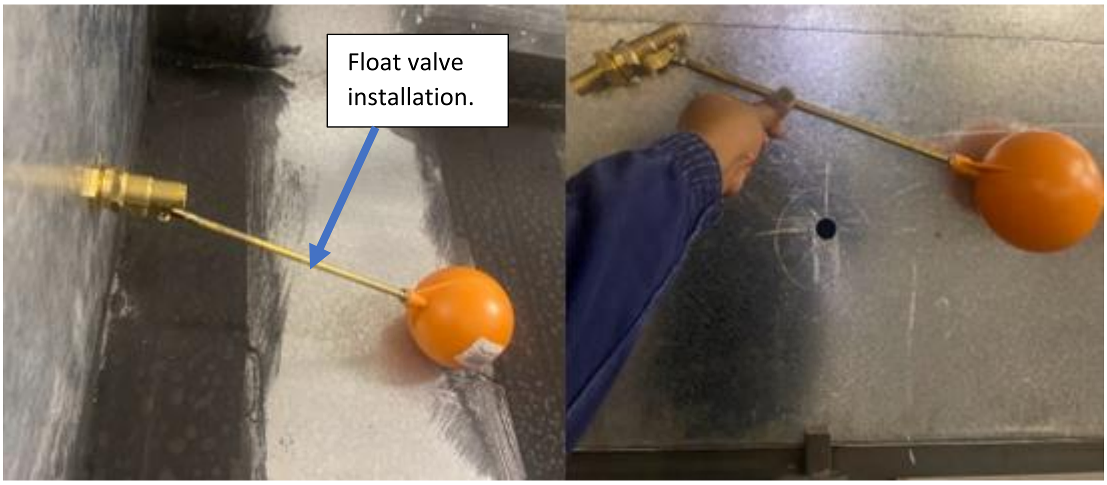

Figure 3.12: Float valve

3.2.7 Saline water tank frame

The saline water frame shown in Figure 3.13 below was used to hold the saline water tank at an elevated position to allow gravity to take its course. The frame was made of 25 mm X 25 mm X 1.6 mm square steel tubing. The tubes were measured using a tape measure, cut using a hacksaw, the sharp edges were removed using an angle grinder with a grinding disc and joined using arc welding. The frame was bolted onto the water basin frame. This process was achieved by drilling 8 mm holes in both frames using a hand-drilling machine. The excess sharp material was removed using a smooth file. The frame was painted using the Duram corrosion-resistant paint (smooth silver).

Figure 3.13: Saline water tank frame (before painting)

3.2.8 Water basin frame

The water basin frame was used to place the seawater basin. The frame was made of 40 mm X 40 mm X 1.6 mm square steel tubing. The tubes were measured using a tape measure, steel ruler and engineering square then cut using a hacksaw. The sharp edges were removed using an angle grinder with a grinding disc and joined using arc welding. All the arc welding joints were cleaned using an angle grinder with a grinding disc. The basin had flat bars welded on all four sides of the frame to support the basin during windy weather conditions. The frame had two extra tubes welded at the top of the frame for the water basin to sit on. The dimensions of the frame were 1200 mm X 850 mm X 500 mm. The frame was painted using Duram corrosion-resistant paint (smooth silver) – Figures 3.14 & 3.15 below show the frame and arc welding joint respectively.

Figure 3.14: Water basin frame


Figure 3.15: Clean arc welding joint

3.3 External Piping

The basin consists of five ports/holes that were used to connect piping for transporting water to different sections of the system. The ports served as the inlet for the saline water from the saline water tank, outlet from the basin to the solar collector, hot water inlet to basin from the solar collector and two outlets for distillate collection. All the ports were drilled using a hand drilling machine with a 4 mm drill bit as a pilot drill followed by a 10 mm drill bit and then a round file was used to achieve the required diameters and round shape. To strengthen the connection points since the basin material is thin, steel nipples were made and joined to the copper piping using lead soldering. All the copper piping was cut using the copper pipe cutter shown in Figure 3.16 below and the copper piping and steel nut connection is depicted in Figure 3.17.

Figure 3.16: Copper Pipe cutter

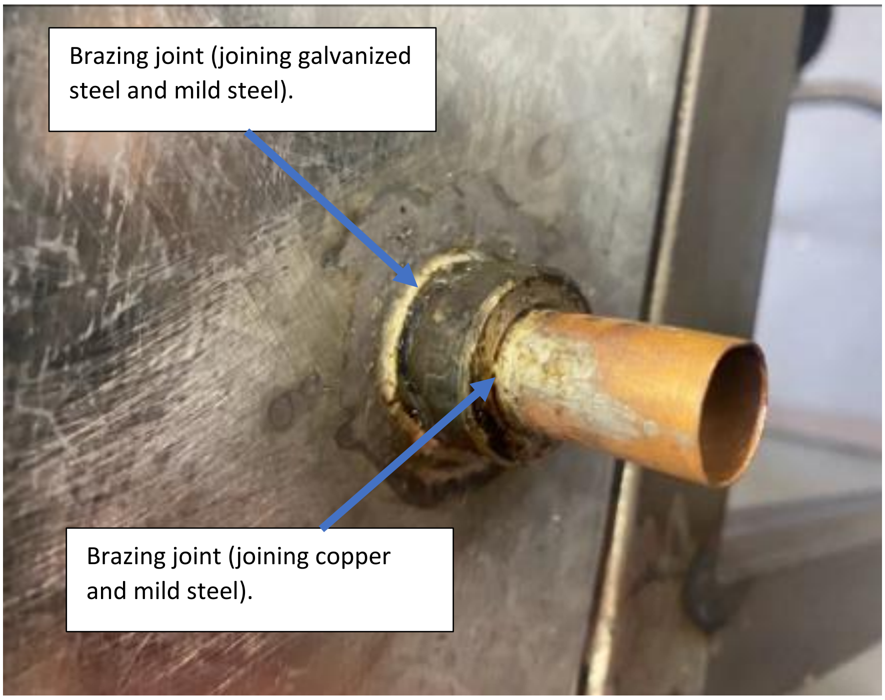

Figure 3.17: Basin pipe connection

3.3.1 Saline water tank to basin connection

The piping connection for delivering saline water from the external tank to the seawater basin was made of 15 mm class 2 copper piping that was connected to mechanical fittings. A ¾'' to 15 mm brass straight coupler, copper elbow and brass ¾'' to 15 mm threaded elbow was connected to the float valve. The joints were achieved by using lead soldering. The pipe was measured, marked and cut using a tape measure, a scriber and a 4 to 28 mm copper pipe cutter, respectively. Figure 3.18 below shows the saline water tank to water basin connection.

Figure 3.18: Saline water tank to basin connection

3.3.2 Water basin to the solar collector

The piping was extended to make a connection to the evacuated tube solar collector. The connection was also made of 15 mm copper piping and the process described in section 3.3.1 above was used to cut and join the copper piping to the fittings. The still basin had two ports on both far ends of the basin on the 1250 mm side.

The connection on the outlet of the water basin to the solar collector comprised a copper pipe welded onto a steel nut/nipple, a 15mm copper straight connector, spool piece, elbow, copper spool piece connected vertically and joined to 15 mm copper elbow that was connected to a copper spool piece horizontally, followed by a T piece that was incorporated to add a drain point as shown in Figure 3.20 below. The T piece connection was then linked to a copper pipe parallel to the basin frame going towards the solar collector inlet, a water circulation pump was later added to the line to increase the water circulation flow. The copper pipe was connected to another elbow with the end connection facing upwards. A copper spool piece was connected vertically that was then connected to a ¾'' to 15 mm brass Conex elbow that was screwed onto the solar collector. The STAG joining compound was applied on the threads, followed by thread tape, before connecting it to the solar collector inlet. Figure 3.19 below shows the basin to solar collector connections.

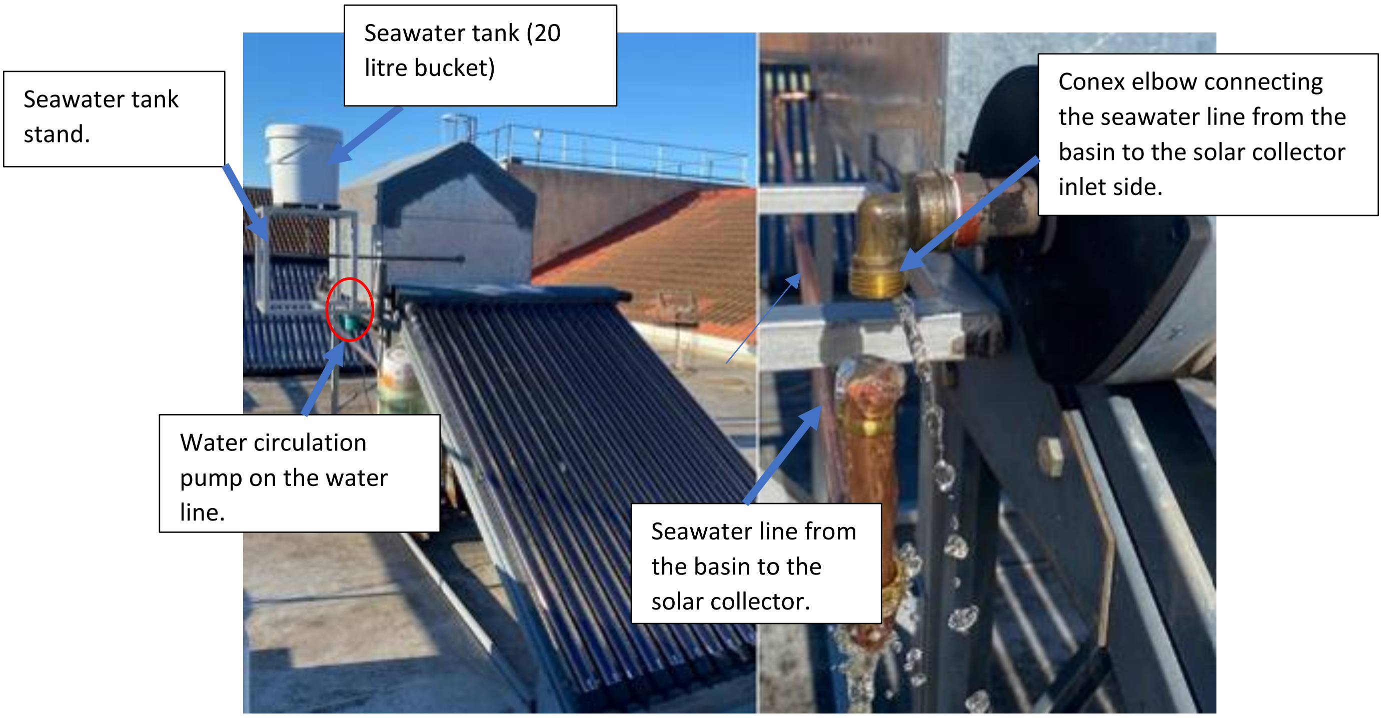

Figure 3.19: Basin to ETSC connection

Figure 3.20: Basin to ETSC connection (drain point)

The connection on the outlet of the solar collector back to the still basin comprised a ¾'' to 15 mm brass Conex elbow that was screwed onto the solar collector and tightened to a 15 mm X 310 mm spool piece. The spool piece was then connected to a copper elbow with the end connection facing towards the basin, followed by a 15 mm X 400 mm spool piece, a straight connector and a spool piece with a steel nipple that was attached to the basin. The STAG joining compound was applied to the threads of the solar collector outlet followed by thread tape before connecting the Conex elbow. The cutting and joining procedure for copper piping was the same as the process described in section 3.3.1 above. Figure 3.21 below shows the line from the solar collector back to the basin.

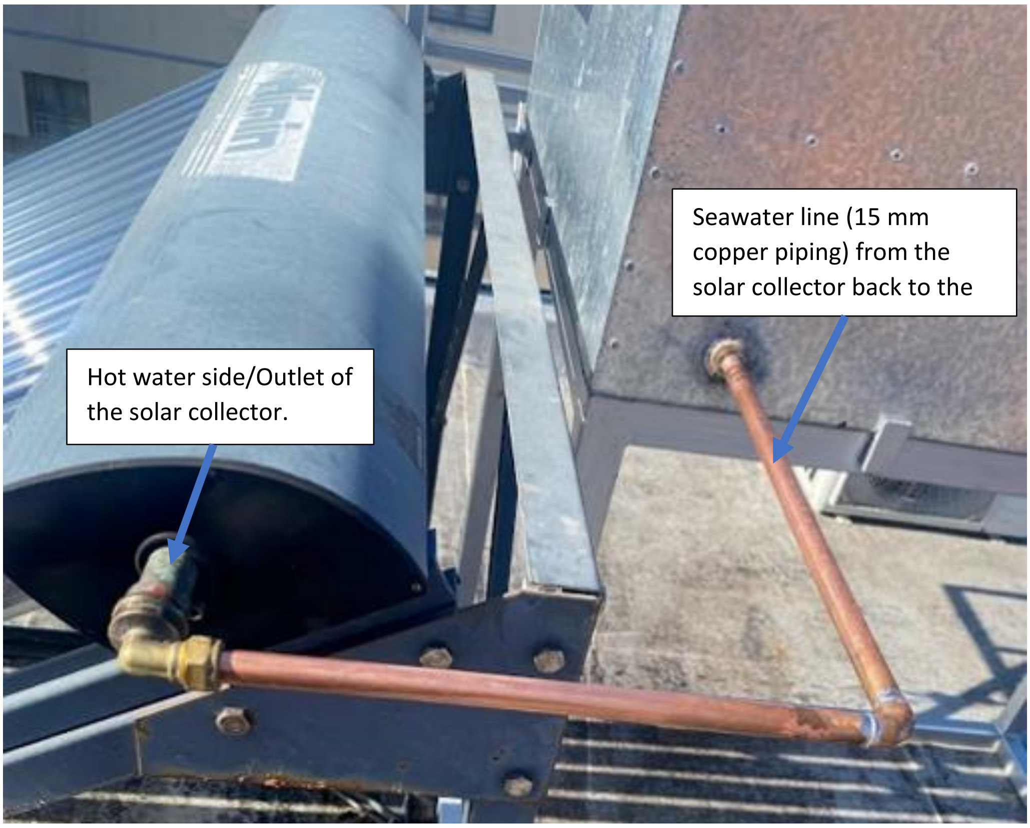

Figure 3.21: ETSC back to basin connection

The piping with the seawater circulation between the water basin and the solar collector was covered with a black form strip for insulation after installing the thermocouples. The foam was tied with cable ties as shown in Figure 3.22 below, to ensure that it held firmly on the piping, this process was undertaken to minimize heat losses, however, since it was only conducted on this piping, heat losses incurred inside the basin.

Figure 3.22: Insulation material

3.3.3 Distillate collection points

There were four collection trays inside the water basin – the construction process was previously discussed in section 3.2.2 above. The collection trays were slightly tilted at an angle of approximately 20° to allow for the collected distillate to flow to the collection ports. The basin had two ports drilled for collection and each incorporated with a copper elbow that was extended using 15mm copper pipe. A T piece was added to join the collection point to create one point, off centre, to avoid obstruction to the system. The T piece was extended by a 580mm copper pipe facing the ground and an elbow was soldered onto it with one end parallel to the ground. A spool piece was added next and an elbow with one end facing down was the last fitting on the distillate collection line as is shown in Figure 3.23 below. The copper pipe was measured, cut and joined using a measuring tape, copper pipe cutter and lead soldering, respectively.

Figure 3.23: Distillate collection point

3.4 Sealing

The water basin was made of 1mm galvanised steel with dimensions 1250 mm X 840 mm X 500 mm (the original steel sheet dimensions were 1 mm X 2450 mm X 1225 mm). The hydraulic bending machine available at CPUT's Mechanical Engineering workshop at its Bellville Campus in Cape Town, could only accommodate a 1.2 m sheet. As a result, the basin material had to be cut into two sections and joined using pop rivets. As the purpose of the basin was to contain water, ensuring that there were no leaks within the system was a crucial part of the construction. This process was achieved by applying silicone between the sheets before riveting and applying waterproof paint with membranes inside the basin on all areas with leaking potential to ensure proper sealing. Silicone was also used between the sheets when joining the basin cover and on the collection plates inside the basin. Figure 3.24 below shows some of the sealing materials that were used on the system.

Figure 3.24: Sealing materials

3.5 Evacuated Tube Solar Collector (ETSC)

The technical specifications of the ETSC are listed in Table 3.1 below and the evacuated solar collector that was used on the D5S to heat the saline water is shown in Figure 3.25 below.

There are mainly two types of solar collectors, a flat plate solar collector (FPSC) and an evacuated tube solar collector (ETSC). The system was energized through an evacuated solar collector, this type of collector was used due to its benefits. According to Zambolin et al. [75], the morning and afternoon collector optical efficiency in FPSC drops due to higher reflecting losses. These efficiency losses in the evacuated tube collector are decreased since the largest portion of the absorbers are exposed to nearly normal radiation for a longer time period due to the shape of the tube. Therefore, in daily testing, the evacuated collector outperforms the flat plate collector across a broader spectrum of operating circumstances. Furthermore, it was stated by Eltaweel et al. [76], that a comparison between FPSCs and ETSCs was conducted and the data analysis indicated that ETSCs had a greater temperature rise than FPSCs. The time required to reach the peak temperature differs between ETSC and FPSC because the conversion factor is larger and the ETSC thermal loss factor is lower. The ESTC for the D5S was positioned at an angle of 33.92° that is equal to the latitude of Cape Town, South Africa.

Table 3.1: Solar collector technical specifications

Item	Specifications
Aperture area	0.6 m^2
Max. Operation pressure	0.6 MPa
Stagnation temperature	240°C
Net weight	62 kg
Fluid content of collector	0.78 L
Dimension	1977 X 1318 X 151 mm
Number of tubes	16

Figure 3.25: Evacuated 16-tube solar collector

3.6 Water Circulation Pump

The system was designed to operate under natural convection, however, during the testing phase, a challenge concerning the continuous flow was experienced. A 220 V water circulation pump was then installed between the outlet of the basin to the solar collector as shown in Figure 3.26 below. The pump speed was set at 1450 rpm. The technical specifications of the pump are included in Appendix B-1.

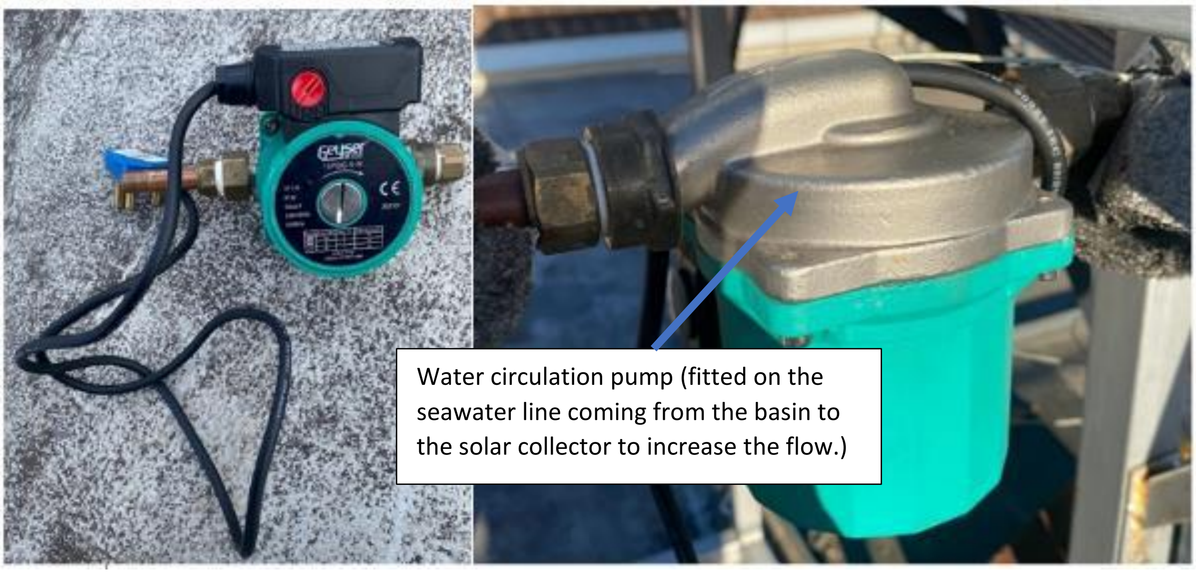

Figure 3.26: Water circulation pump

3.7 Testing Apparatus

i. 1 x temperature data logger 12 channel BTM-4208SD data logger with memory card
ii. 4 x surface temperature probes
iii. HP200 wireless weather station
iv. 1 x weather station display unit
v. 3 x graduated cylinders – 1000 ml, 100 ml and 50 ml measuring capacity
vi. 1 x distillate collecting container
vii. distillate sampling containers
viii. 1 x electrical multi-meter – T235H digital multimeter
ix. 1 x Bante DR900 multi-parameter.

3.7.1 Temperature data logger – 12 channel BTM-4208SD data logger

The temperatures of the inlet and outlet points of the system were monitored during the testing process using a 12-channel BTM-4208SD data logger. The temperature data logger offered multiple sensor types such as J, K, T, E, R and S; the tests were conducted using the K-type sensor setting. The K-type sensor had temperature ranges of -100°C as the lowest limit and 1300°C as the highest limit. The temperature logger could be operated using either 8 X 1.5 V batteries or a direct current (DC) adapter for power. Four K-type thermocouples were used as shown in Figure 3.27 below, the thermocouples were attached to the surfaces of the inlet and outlet points using an insulation tape and then connected to the T1-T4 ports of the data logger. A memory card was used on the temperature data logger to store the temperature data that was then exported to a computer for processing via Excel. For the tests the battery option was used, and this process led to challenges because the logger would switch off and stop recording once the batteries died. Therefore, the process had to be continuously repeated throughout the testing period due to these challenges.

Figure 3.27: Temperature data logger

3.7.2 HP2000 Wireless Weather Station

The operation of a solar still is dependable on climatic conditions. Records of solar radiation, wind speed, wind direction and ambient temperature were collected for the duration of the tests. The HP2000 wireless internet weather station was used for this purpose and installed on the roof of CPUT's Mechanical Engineering Department at its Bellville Campus, as shown in Figure 3.28 below. The weather station consisted of two sensors, the outdoor and indoor sensors. Only the outdoor sensor was used for this experiment, the data was transmitted to the console display unit that was placed indoors and data was collected through a memory card for further processing. The outdoor sensor was solar-powered and transmitted data to the console through a low-power radio, technical specifications of the outdoor sensor are listed in Table 3.2 below.

Table 3.2: Technical specifications of the outdoor sensor

Parameters	**Specifications**
Transmission distance in open field	100 m
Frequency	433 MHz / 868 MHz / 915 MHz
Temperature range	-30˚C--65˚C Accuracy: + / - 1 °C Resolution: 0.1˚C
Measuring range rel. humidity	1%~99% Accuracy: +/- 5%
Rain volume display	0 – 9999 mm (show --- if outside range) Accuracy: + / - 10% Resolution: 0.3 mm (if rain volume < 1000 mm) 1 mm (if rain volume > 1000 mm)
Wind speed	0-50 m/s (0~100 mph) (show --- if outside range) Accuracy: +/- 1m/s (wind speed< 5m/s) +/-10% (wind speed > 5 m/s)
Measuring interval outdoor sensor	16 seconds

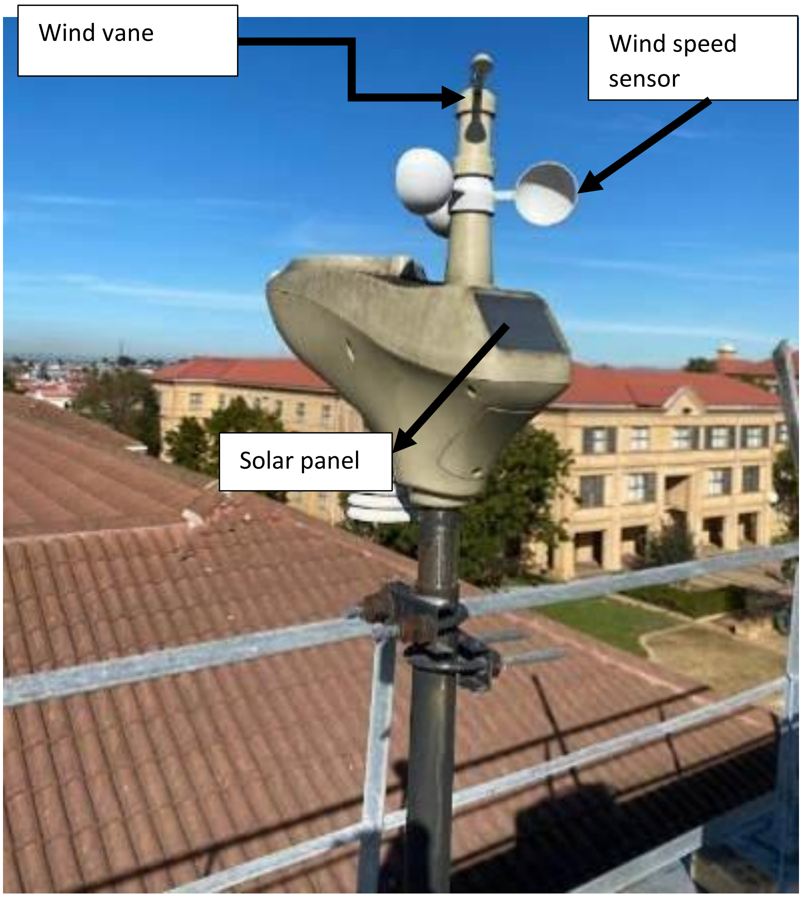

Figure 3.28: HP2000 Weather station

3.7.3 The weather station’s display unit

Figure 3.29: Weather station display unit

3.7.4 Graduated cylinders – 1000 ml, 100 ml, and 50 ml capacity

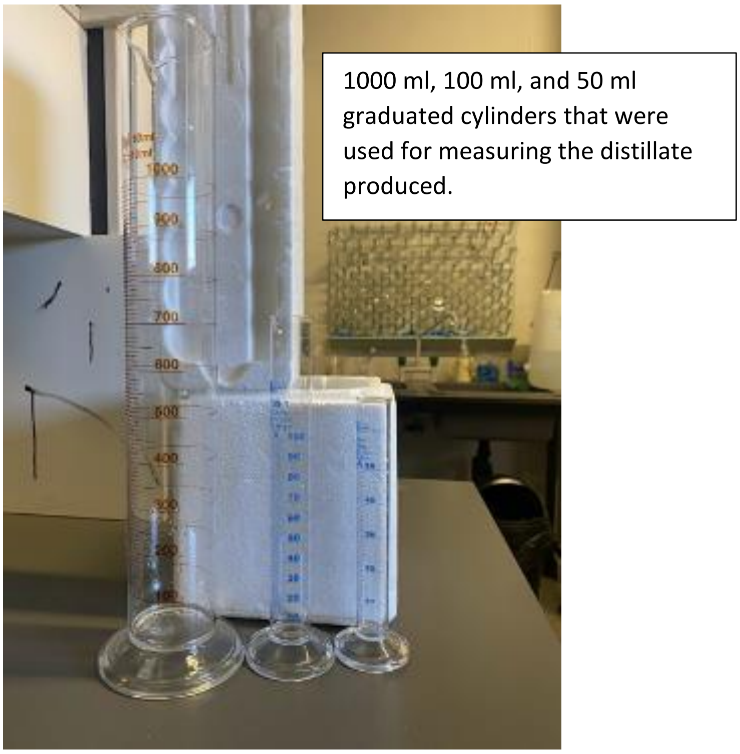

Figure 3.30: Graduated cylinders

3.7.5 Distillate collection

Figure 3.31: Distillate collection container

3.7.6 Sample collection jar

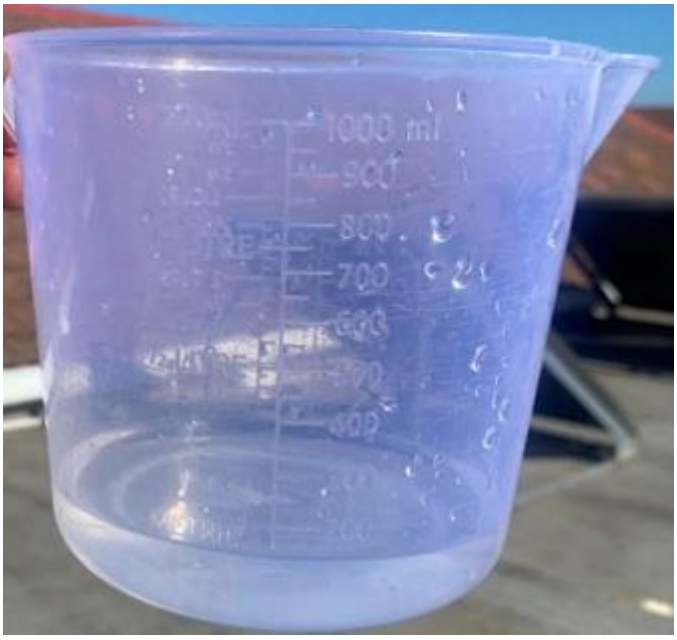

Figure 3.32: Sample collection jar

3.7.7 Distillate sample container

Figure 3.33: Distillate sample container

3.8 Experimental Performance

The main aim of the experiment conducted for this research study was to maximize the distillate production from the system while reducing the losses. The knowledge obtained in the process of completing the literature review relating to factors that affect the production of solar stills was implemented to achieve the best possible results. This experiment was conducted in Cape Town, South Africa (latitude 33.9249° S, 18.4241° E respectively) at CPUT's Bellville Campus. The system design shown in Figure 3.34 below was tested during day and night between 07:00 to 19:00 and 19:00 to 07:00 respectively. It was tested during October to November 2023 (spring season in South Africa). Spring is the second warmest season following summer among the four seasons. Consequently, it was deemed practical to conduct the tests during this period, given the knowledge that solar irradiance significantly impacts the efficiency of solar stills.

Figure 3.34: Double Slope Single Stage Solar Still (D5S)

3.8.1 Testing procedure

After the D5S's construction process was completed, the system was lifted to the roof of CPUT's Mechanical Engineering Department for testing. The assembly of the system was completed on the top of the roof and then placed in position. Prior to placing the cover on the basin, the basin was filled with tap water and monitored for leaks in the piping and water basin. No leaks were detected on the piping, however, minor leaks were detected on the basin. These leaks were sealed using silicone on the outside and waterproof paint with membranes on the inside of the basin. Leak tests again were conducted until no further leaks were detected in the system.

The seawater used for the experiment was collected from the shoreline of Sunset Beach in Milnerton, Cape Town, South Africa. Owing to the saline water having been collected from a sandy and polluted ocean, it was filtered before filling the system using a polyester cross-knit cloth as shown in Figure 3.35 below. This process was completed to prevent sand and other solid particles from causing build-up or blockages in the system. The saline water tank was also cleaned to remove any foreign particles that might have blocked the system and affected the production of the distillate.

Figure 3.35: Seawater filtering

The seawater was then poured into the seawater 20-litre bucket shown in Figure 3.19 above. This bucket was placed at an elevated height to the basin and the seawater was transported to the basin using the force of gravity through 15 mm copper piping. A float valve was installed at the inlet of the basin from the seawater bucket and was positioned to close at a water depth of 50 mm. The seawater was then transported to the solar collector through copper piping with a water circulation pump installed on the line, as shown in Figure 3.19 above, in order to be heated and allow the evaporation and condensation processes to take place inside the basin.

The water circulation occurred during the flow of water between the seawater bucket and the basin, and again between the basin and the solar collector. Once the water heated up, evaporation began and the vapor rose to the basin cover that was positioned at the latitude angle of the testing area where the vapor changed to water droplets (condensation). The water basin was incorporated with four collection trays on the sides as shown in Figure 3.4 above. The water droplets ran down the cover and fell into the collecting trays that were placed at an angle to allow free flow of the distillate water to the copper piping that delivered the distillate to the collecting container as shown in Figure 3.34 above. The distillate produced was then collected every morning and evening at 07:00 and 19:00 respectively to allow for the next cycle to take place. The collection process was completed using the collection jar shown in Figure 3.32 above and kept in sampling containers that were labelled with dates as shown in Figure 3.33 below.

3.8.2 Distillate testing

The distillate produced from the newly designed D5S was taken to CPUT's Chemical Engineering Department for testing. Salinity and conductivity tests were conducted on raw seawater and the distillate produced by the system for both daytime and nighttime samples. The results will be discussed in Chapter 4 of this research report. The tests were carried out using a Bante multi-parameter meter shown in Figure 3.36 below. The Bante DR900 multiparameter water quality meter had multiple measurement parameters, including pH (potential of Hydrogen), mV, relative mV, ion concentration, conductivity, TDS (total dissolved solid), salinity, resistivity, DO (dissolved oxygen) and temperature. This device was only used for testing conductivity and salinity for this experiment.

Water samples were collected and placed in three 40 ml vials to ensure precise measurement. The Bante instrument meter's conductivity electrode underwent calibration using standards of 84 uS/cm, 1413 uS/cm and 12.88 mS/cm. The user manual suggests either conducting a three-point calibration or opting for a standard solution with conductivity closest to the sample for enhanced result accuracy. In this test, the three-point calibration was carried out as recommended. Subsequently, following calibration, the electrode was placed into the distillate samples to gauge their conductivity and salinity and the measurements accurately documented. The specific electrode used for these tests was the CON-1 with a measurement range of 10 μ S/cm to 20 mS/cm and a cell constant (K) of 1. The technical specifications of the unit can be found in Appendix B-2 and the operating manual and calibration settings can be found in Appendix B-3. The results of the water tests were discussed in section 4.5.

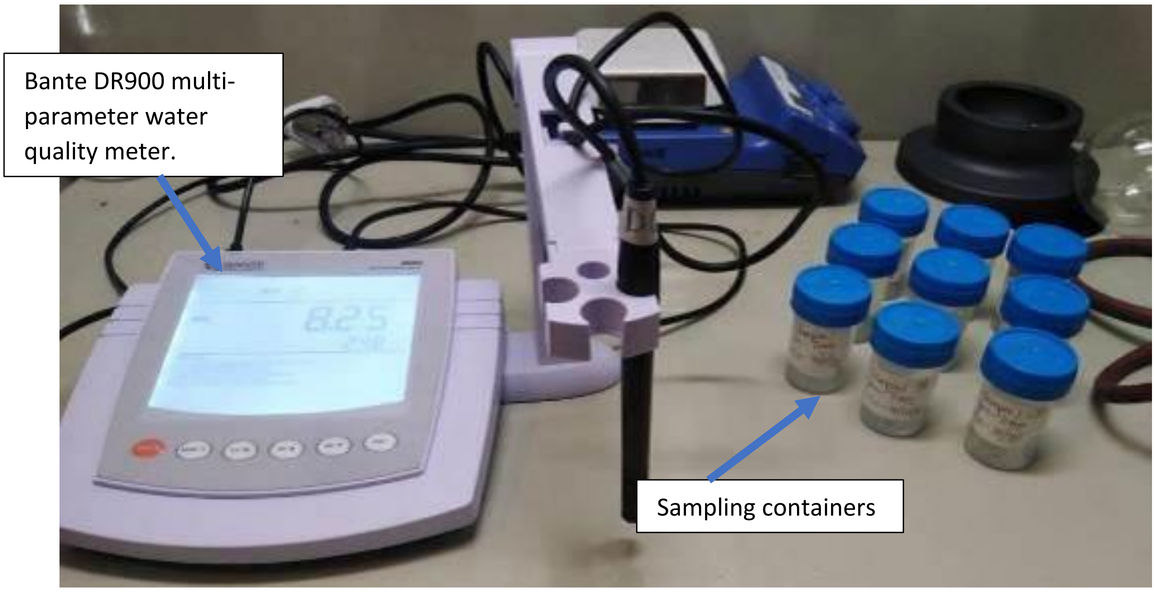

Figure 3.36: Bante DR900 multi-parameter

The resistance tests were conducted in by CPUT's Mechanical Engineering Department upon the raw seawater and day and night distillate samples using an electrical multimeter shown in Figure 3.37 below. The technical specifications of the digital multimeter can be found on Appendix B-6.

Figure 3.37: Electrical multimeter

CHAPTER 4 – RESULTS AND DISCUSSION

This chapter discusses the results obtained from the experiment conducted on the developed double slope single-stage solar still (D5S) that was constructed and tested at CPUT's Bellville Campus in Cape Town, South Africa. The experiment was conducted during the months of October and November 2023 that fall within the spring season in South Africa. The spring season is the second warmest season after summer out of the four seasons, hence testing during this season was considered practical noting that solar irradiance is one of the most important factors that influence the freshwater yield of solar stills. The results discussed in this chapter were collected for 12 days during the previously specified day and night periods. The distillate production, the quality of the distillate and the ambient conditions in which the system was tested will be examined.

4.1 Daily Weather Conditions – Solar Irradiance and Wind Speed

Solar irradiance and windspeed fall are two of the most crucial factors that influence the freshwater yield of solar stills [39]. These parameters were recorded during the experimental process to track the weather for all the testing dates. This section discusses the weather conditions for the testing period, graphs representing the hourly average solar irradiance versus time and the hourly average wind speed versus time were plotted using the Origin software for the twelve-day testing period. The graphs were plotted from 7 am on one day to 7 am the following day to fully represent the weather conditions during the testing period. The discussion on weather conditions was divided into three parts i.e., days with the highest, moderate and lowest solar irradiance. A table recording data pertaining to the distillate produced for day and night times can be found in Appendix A-1 and one presenting data on the average solar irradiance and wind speed for both day and night times can be found in Appendix A-3.

4.1.1 Days with the highest solar irradiance

The first, third, eleventh and twelfth days were the four days with the highest irradiance during the testing cycle with a daily average of 370 W/m^2, 467 W/m^2, 455 W/m^2 and 411 W/m^2 respectively for daytime. The daily solar irradiance average during nighttime ranged between 0 – 9 W/m^2 for the entire testing cycle. The trends depicted in Figure 4.1 to Figure 4.4 below show the average hourly solar irradiance and wind speed versus time (7 am to 7 am) on these days respectively. It can be noted that in the morning the sunlight is still low, it then increases as the day progresses and reaches its peak at noon and shortly afterwards decreases until the sun sets. The highest solar irradiance reached on the testing cycle days was 549 W/m^2, 546 W/m^2, 558 W/m^{2,} and 578 W/m^2 respectively. The peak was reached between 11:00 and 12:00 for all the days during which tests were conducted. It can also be noted that after the sun sets, the irradiance trend stays constant at approximately 0 W/m^2 and the windspeed trend fluctuates during the entire day. The surface temperatures of all the inlets and outlets of the seawater within the system were measured, however, no surface temperatures were recorded for the days with the highest solar irradiance owing to a problem experienced with the data logger batteries.

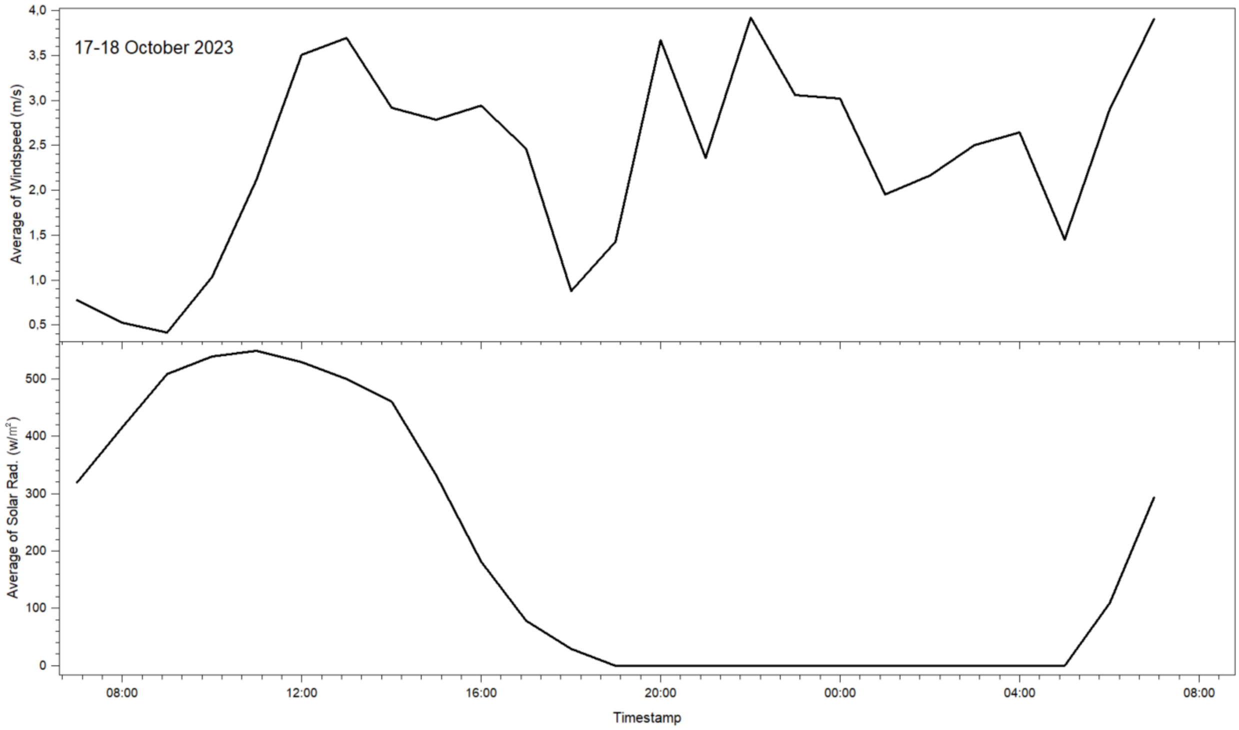

Figure 4.1: Solar irradiance and wind speed vs time graph (day 1)

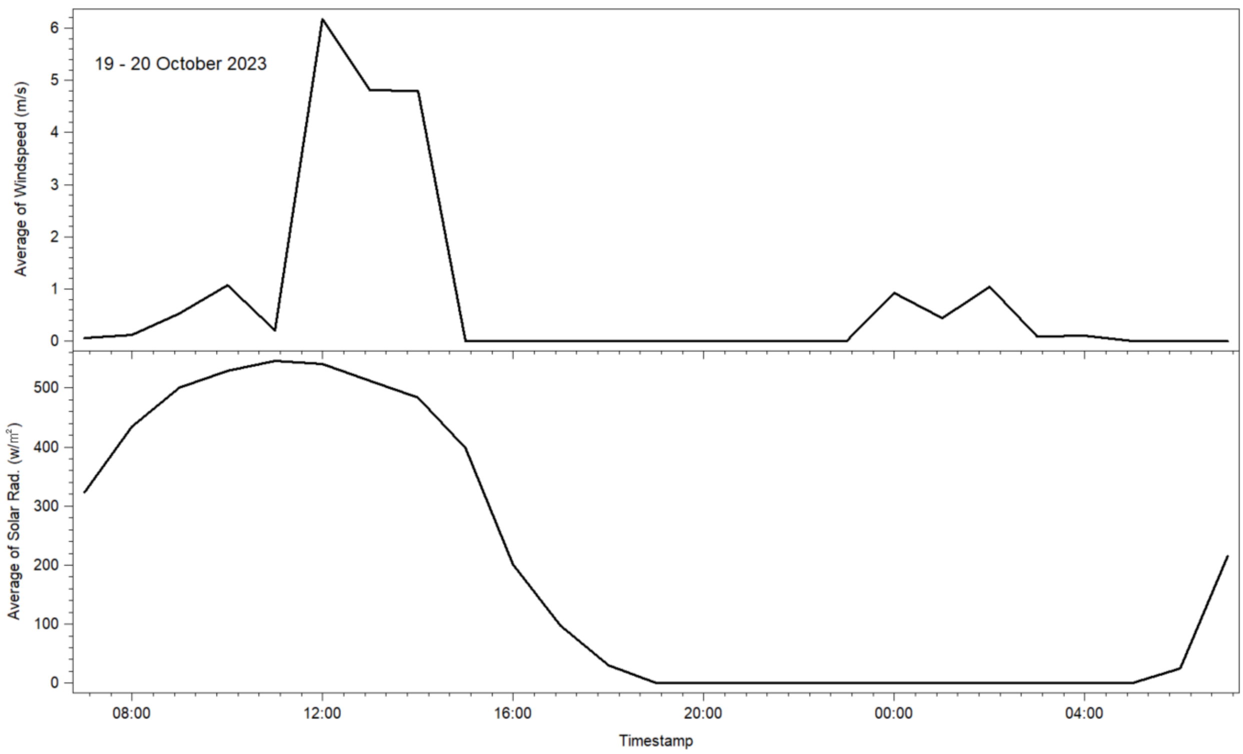

Figure 4.2: Solar irradiance and wind speed vs time graph (day 3)

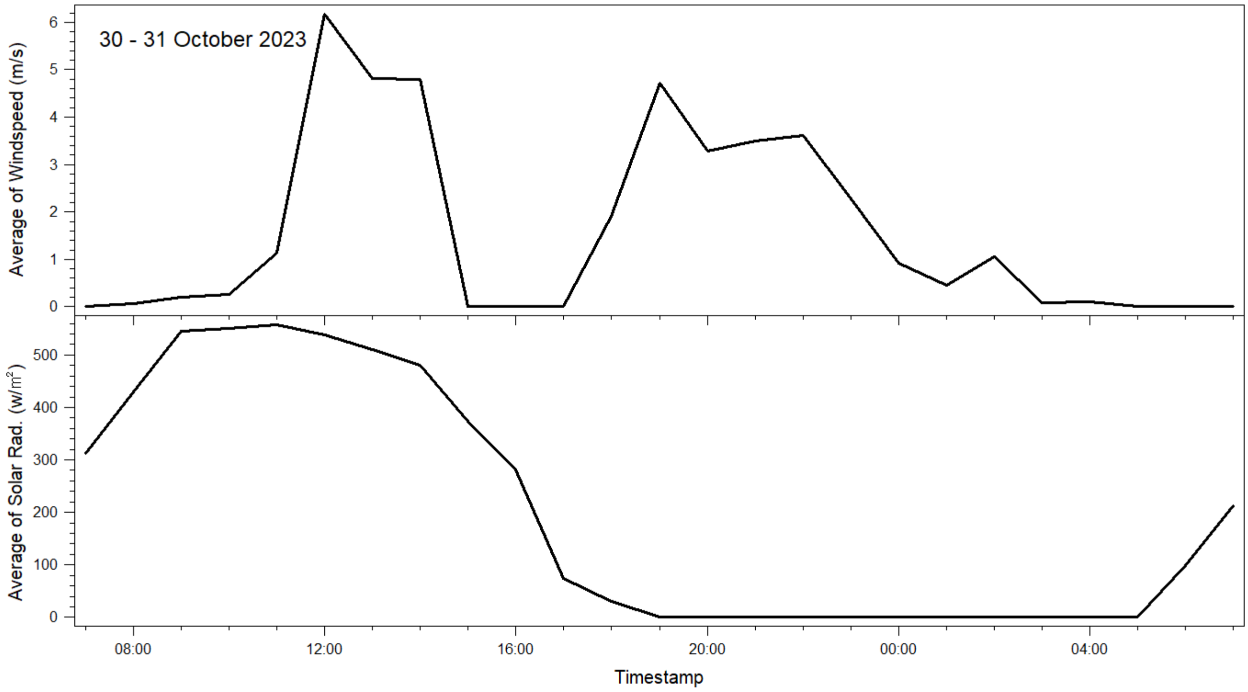

Figure 4.3: Solar irradiance and wind speed vs time graph (day 11)

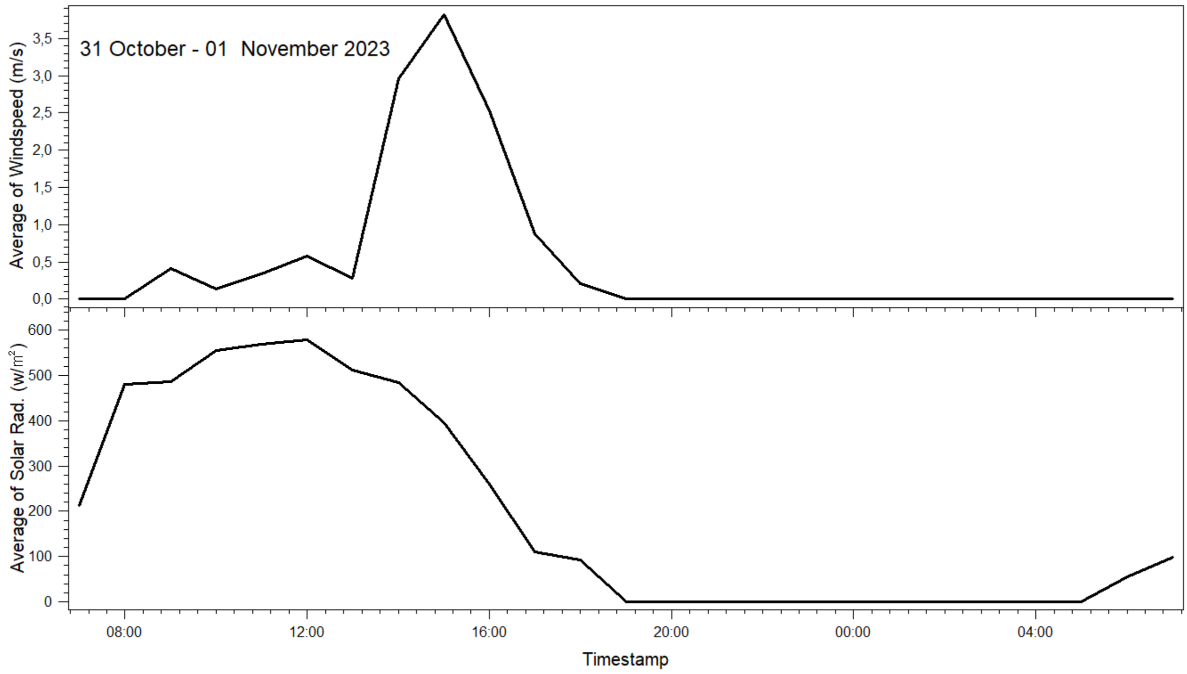

Figure 4.4: Solar irradiance and wind speed vs time graph (day 12)

4.1.2 Days with moderate solar irradiance

The fifth, sixth, seventh and ninth days of the testing cycle were those with moderate solar irradiance with an average of 327 W/m^2, 384 W/m^2, 318 W/m^2 and 335 W/m^2 respectively. The trends in Figures 4.5 to 4.8 below show the average hourly solar irradiance and wind speed versus time (7 am to 7 am) on these days. The irradiance is low in the morning, it increases as the day progresses and reaches its peak at noon and, shortly afterwards decreases until the sun sets. The highest solar irradiances reached on these four days were 489 W/m^2, 544 W/m^2, 501 W/m^2 and 528 W/m^2 respectively. The peak was reached between 11 am and 12 pm on all the days the tests were conducted. The surface temperatures of all the inlets and outlets of the seawater within the system were measured, however, not all the days could be recorded due the already mentioned challenge experienced with the data logger batteries. On day nine, the data logger was operational for the full duration of testing period i.e., 7 am to 7 am the following day. These thermocouple surface temperatures for day nine will be discussed under section 4.1.2.1 below.

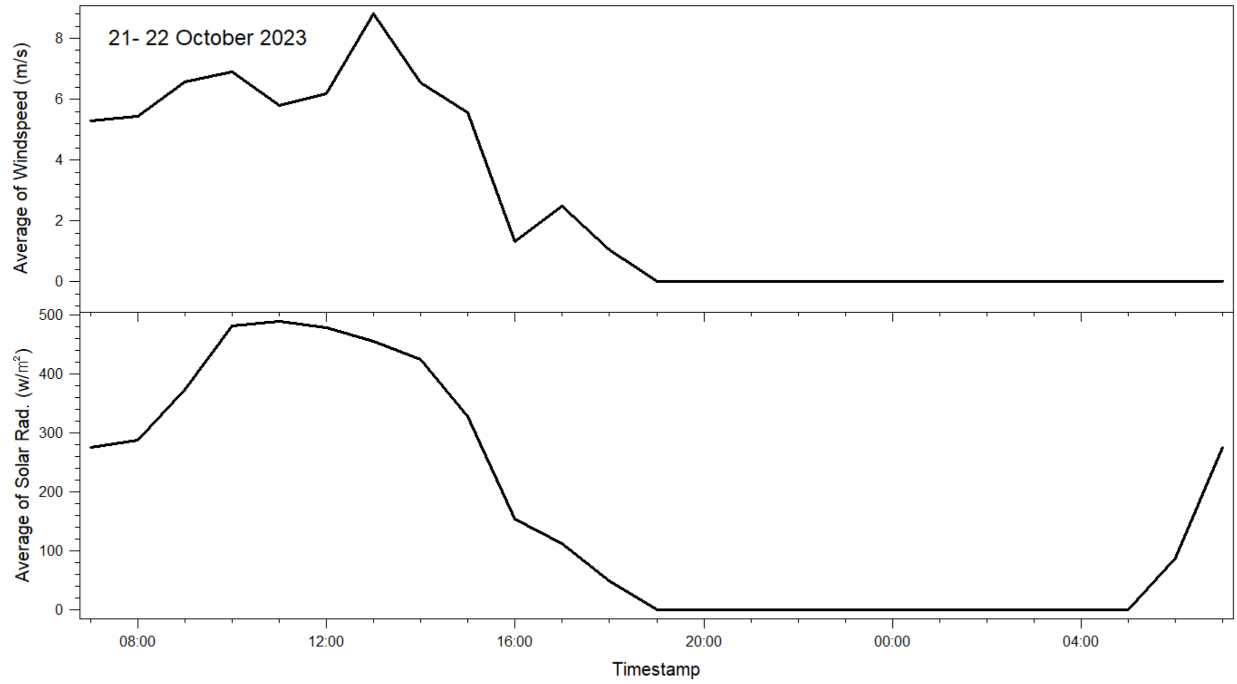

Figure 4.5: Solar irradiance and wind speed vs time graph (day 5)

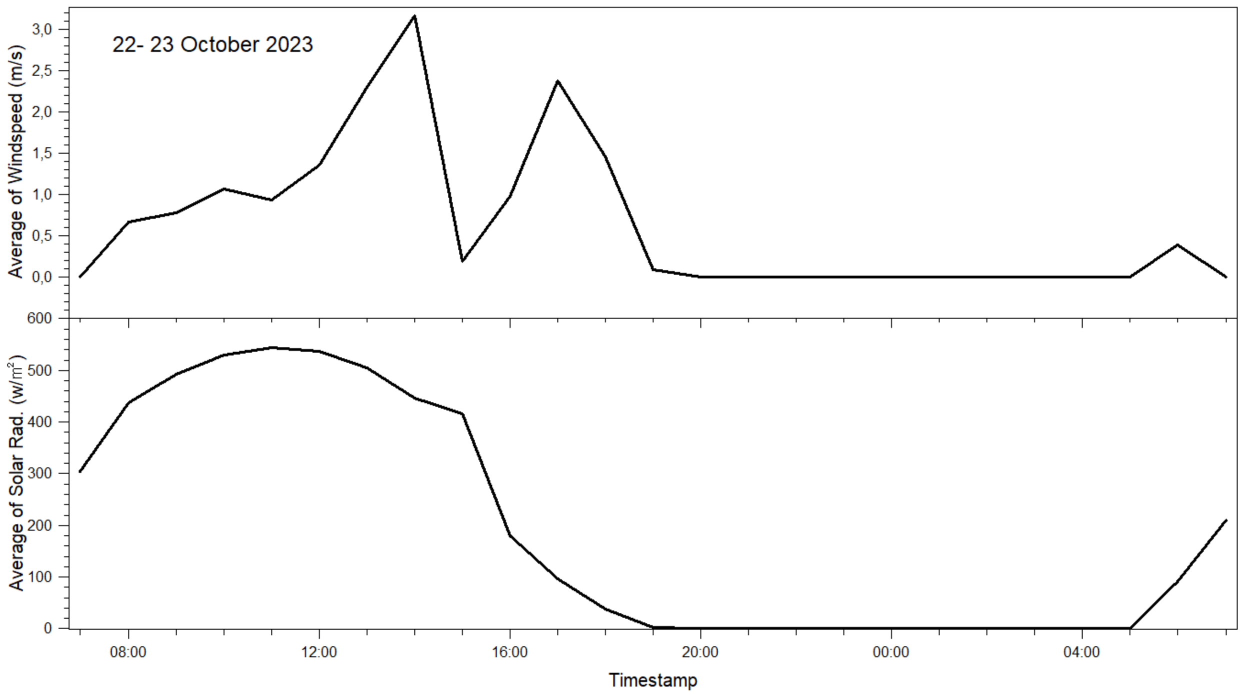

Figure 4.6: Solar irradiance and wind speed vs time graph (day 6)

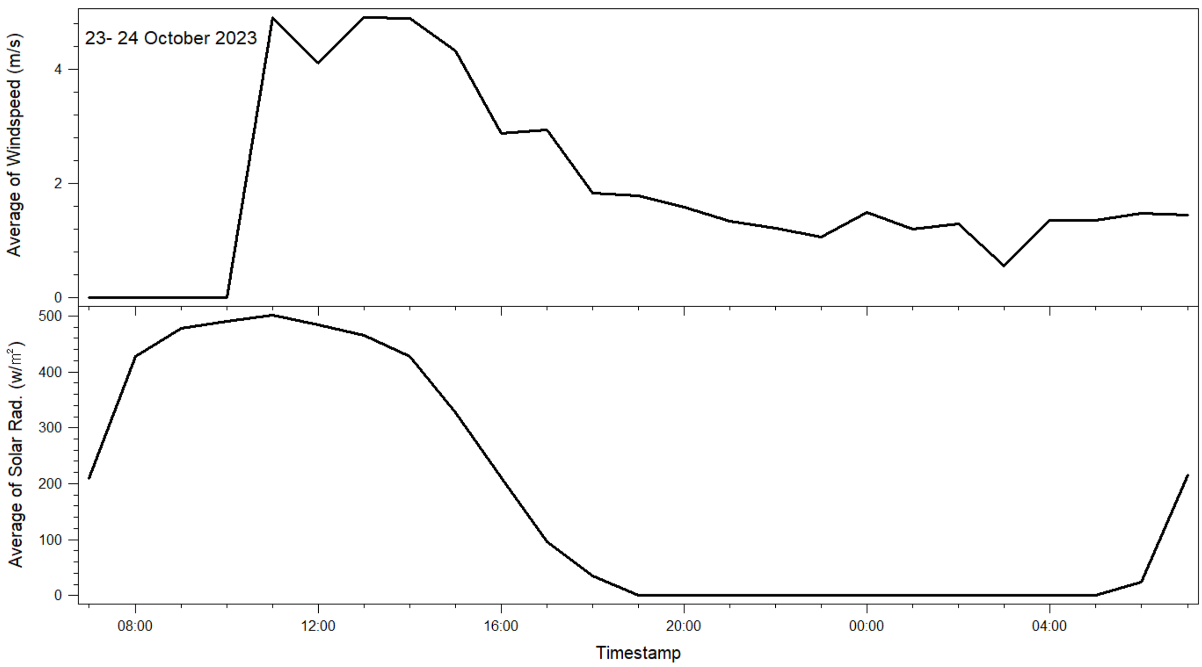

Figure 4.7: Solar irradiance and wind speed vs time graph (day 7)

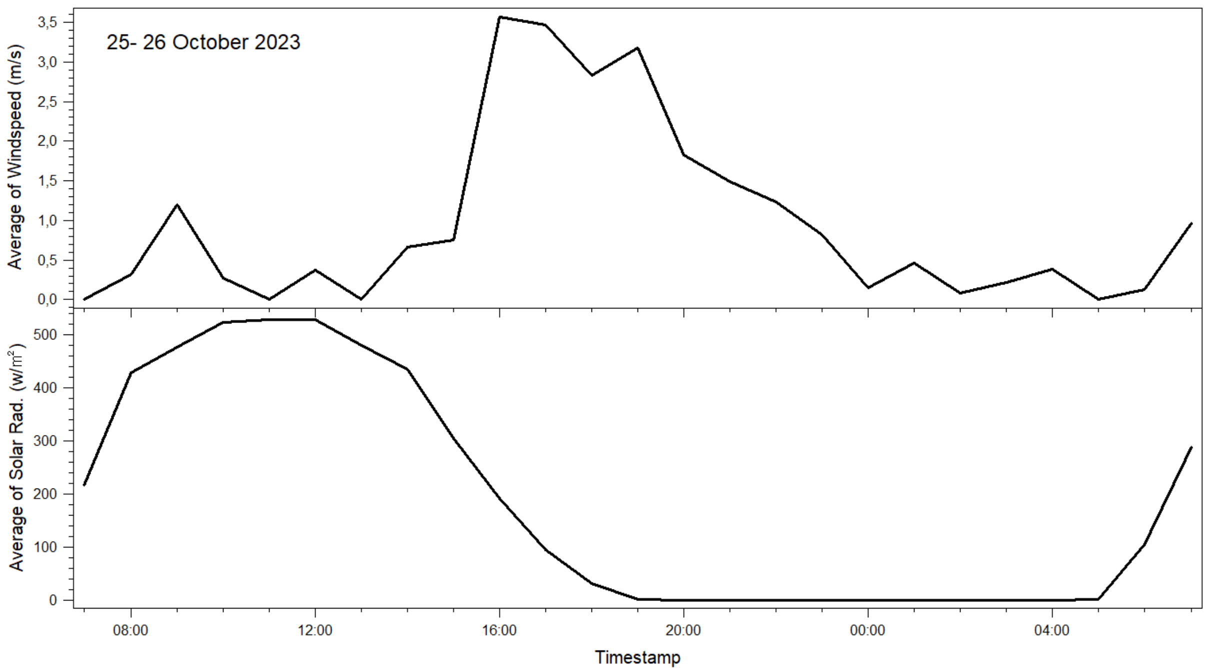

Figure 4.8: Solar irradiance and wind speed vs time graph (day 9)

4.1.2.1 Surface thermocouple temperatures

The newly designed D5S was incorporated with surface thermocouples on the four seawater inlets and outlets to monitor the temperatures in those areas. The thermocouples were used with a 12-channel BTM-4208SD data logger that was discussed in section 3.8.1 above, to read the surface temperatures. The data logger was powered using eight AA 24V batteries, that resulted in multiple disturbances in the data logging process. On 25 October 2023, data was obtained for both day and nighttime testing periods and Figure 4.9 below is a graphical representation of that data. It can be noted that the temperatures increased and reached a peak around noon due to the increase in solar radiation, and a decrease can be noted during the late afternoon. Singh et al. [77] designed, manufactured and tested a hybrid photovoltaic thermal (PVT) double slope active solar still and noted that the temperatures of both the water and cover reached a maximum at around noontime. It can also be noted from the trend in Figure 4.9 below that temperatures started increasing after 5 am owing to the early sunrise. The T1 (outlet from the basin) and T3 (outlet from the solar collector) temperatures were slightly higher compared to that of T2 (inlet to the solar collector) and T4 (inlet to the basin from the solar collector). Although, the piping from the basin to the solar collector and from the solar collector to the basin were covered with insulation material, the graph in Figure 4.9 below clearly shows that heat losses were incurred. Although insulation material minimizes heat losses, the fact that it does not completely prevent them can be clearly noted in this case. The data plotted on Figure 4.9 can be found on Appendix A-2.

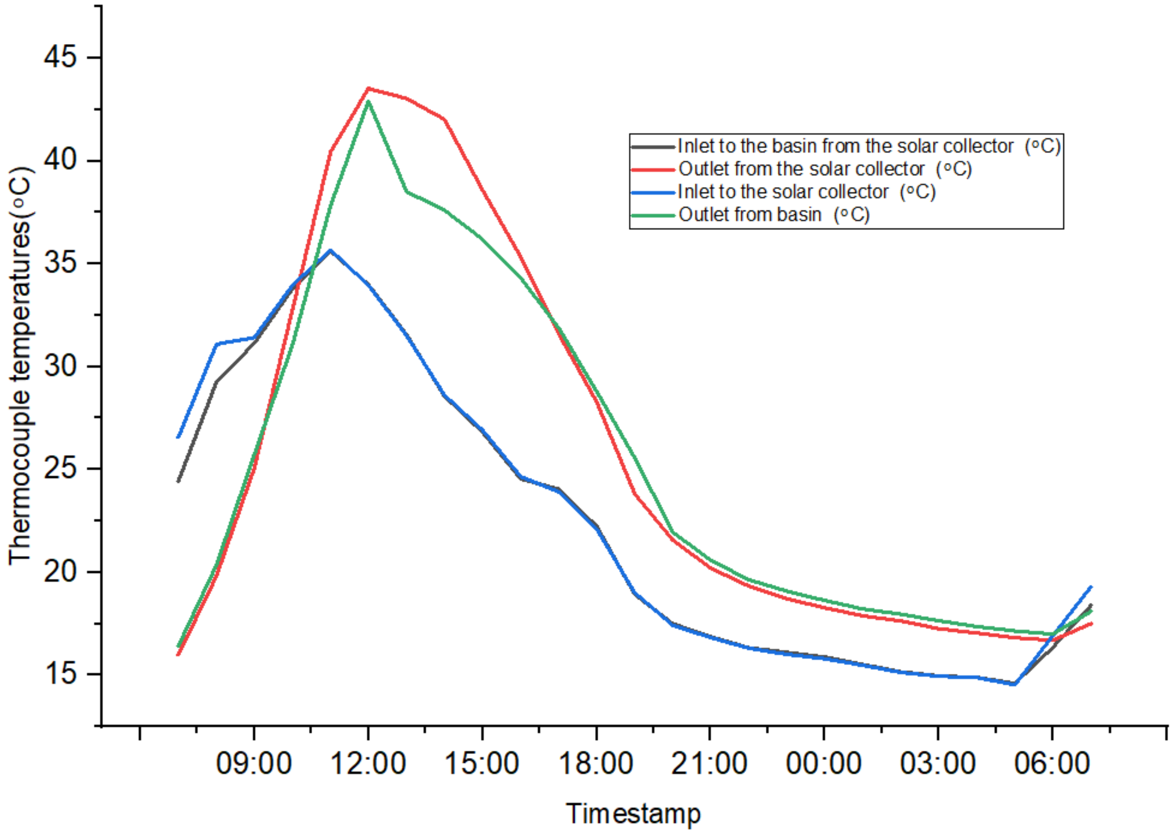

Figure 4.9: Thermocouple temperatures vs timestamp graph

4.1.3 Days with the lowest solar irradiance

The second, fourth, eighth and tenth days of the testing cycle were the days with the lowest solar irradiance with an average of 299 W/m^2, 187 W/m^2, 196 W/m^2 and 308 W/m^2 respectively. The trends depicted in Figure 4.10 to Figure 4.13 show the average hourly solar irradiance and wind speed versus time (7 am to 07 am) on these days. The irradiance is low in the morning, it then increases as the day progresses and reaches its peak at noon and shortly afterwards decreases until the sun sets. The highest solar irradiance reached on these days were 512 W/m^2, 363 W/m^2, 460 W/m^2 and 538 W/m^2 respectively. The peak was reached between 11 am and 12 pm for all the days on which the tests were conducted. The surface temperatures of all the inlets and outlets of the seawater within the system were measured, however, no surface temperature data was recorded for the days with the lowest solar irradiance owing to the previously indicated problem experienced with the data logger batteries.

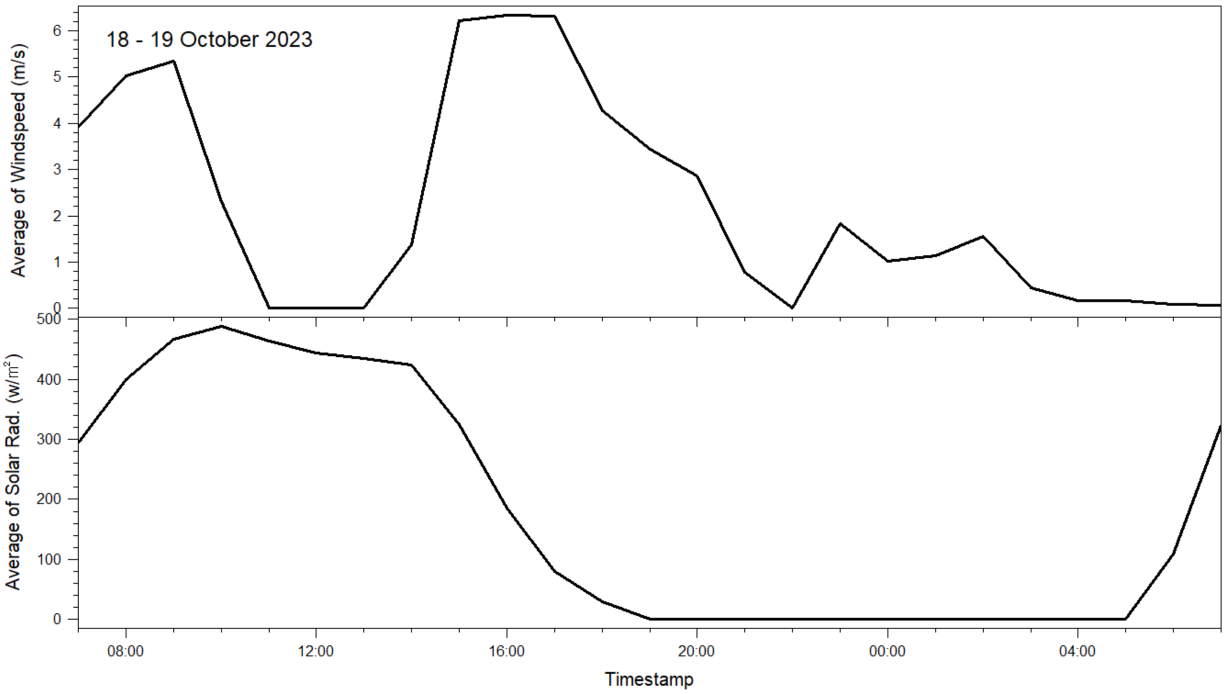

Figure 4.10: Solar irradiance and wind speed vs time graph (day 2)

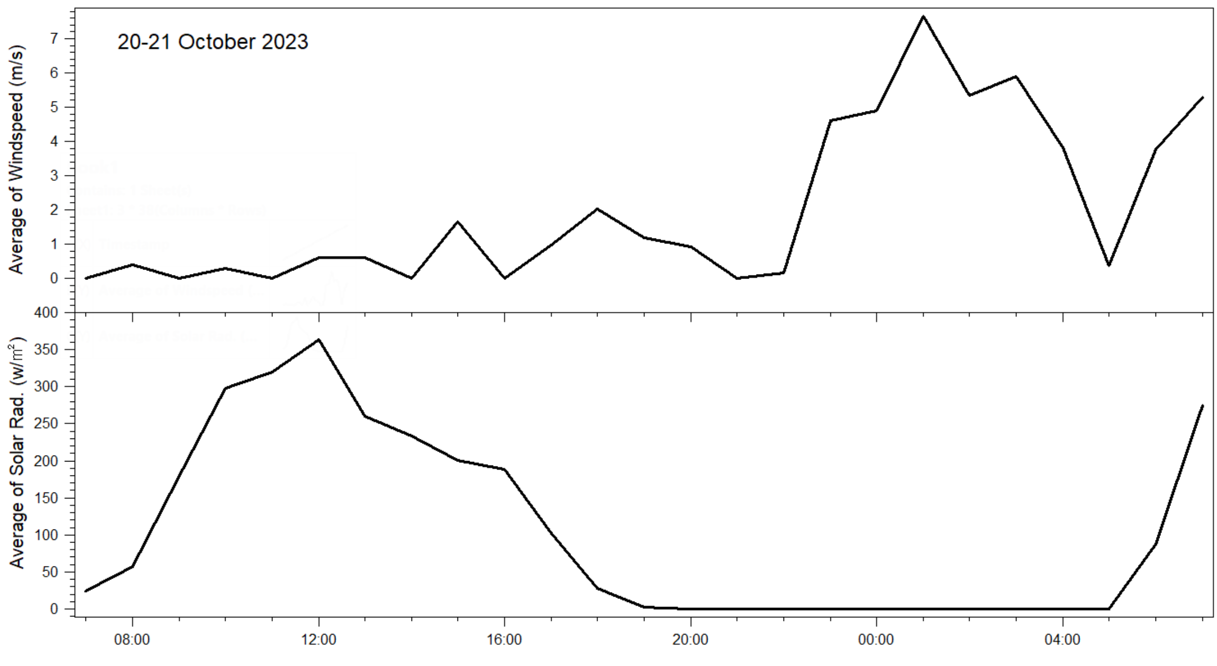

Figure 4.11: Solar irradiance and wind speed vs time graph (day 4)

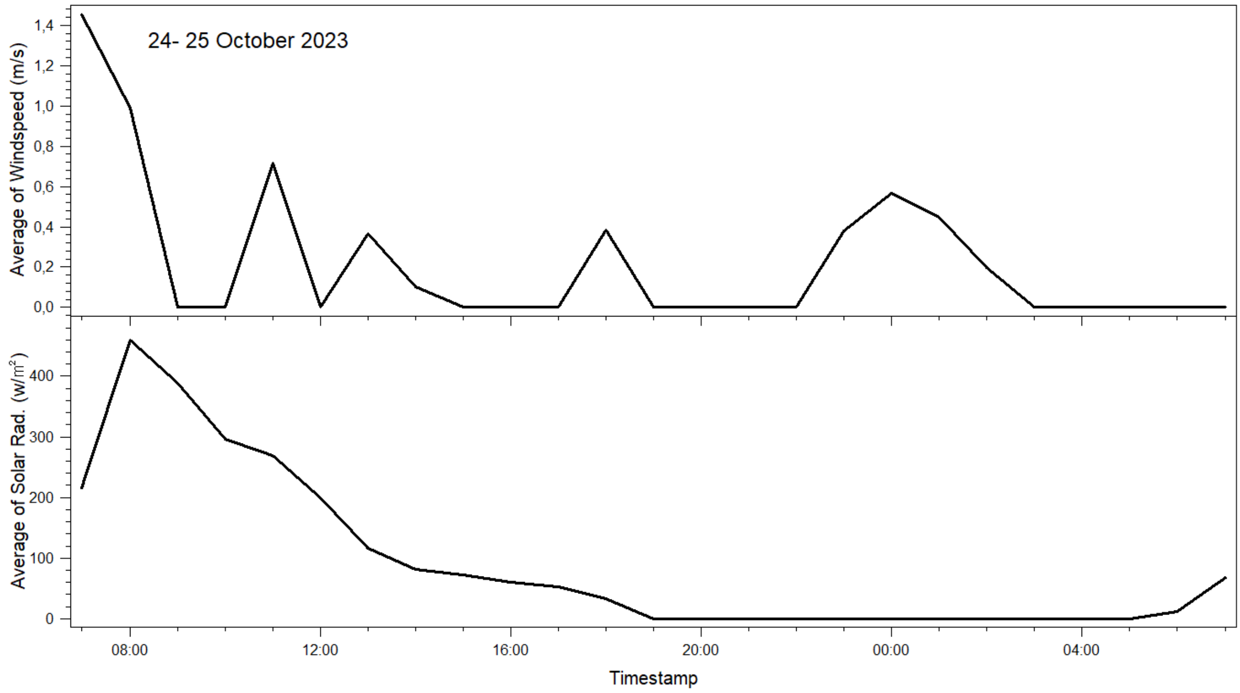

Figure 4.12: Solar irradiance and wind speed vs time graph (day 8)

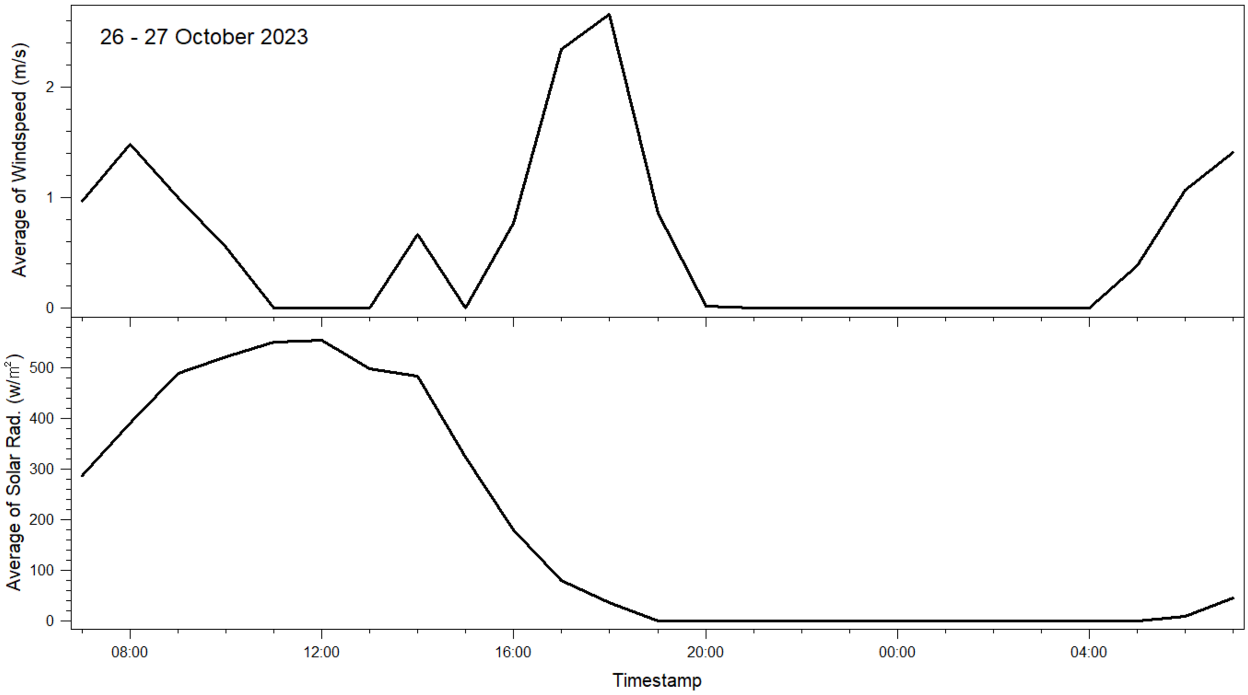

Figure 4.13: Solar irradiance and wind speed vs time graph (day 10)

4.2 Day-Time Experimental Tests

The tests were conducted from 17 October 2023 at 7 am to 31 October 2023 at 7 pm, South African time. Data was collected only for 12 days because from 27 to 29 October the system was not operated due to rainy weather. Figure 4.14 below is a representation of the distillate production collected during the daytime for these 12 days vs the average solar irradiance for these days. The minimum and maximum distillate production for the daytime collection was 53 ml and 325 ml respectively. It can be noted that the maximum production was not achieved on a day with the highest average solar irradiance, even though the minimum production was achieved on a day with the lowest average solar irradiance. The system was made with a steel cover with a hollow area within that held water to cool the hot water in the basin; the cooling water had to be changed by hand, however, the system was not monitored continuously throughout day. It was observed that on extremely hot days, the water's temperature inside the cover quickly increased, which slowed down the cooling effect that the cover was meant to provide. Then, especially on extremely hot days, the condensation rate dropped and the amount of distillate produced decreased. This observation clarifies why the day with the maximum sun irradiation did not yield the most production – the intense heat hindered the production process.

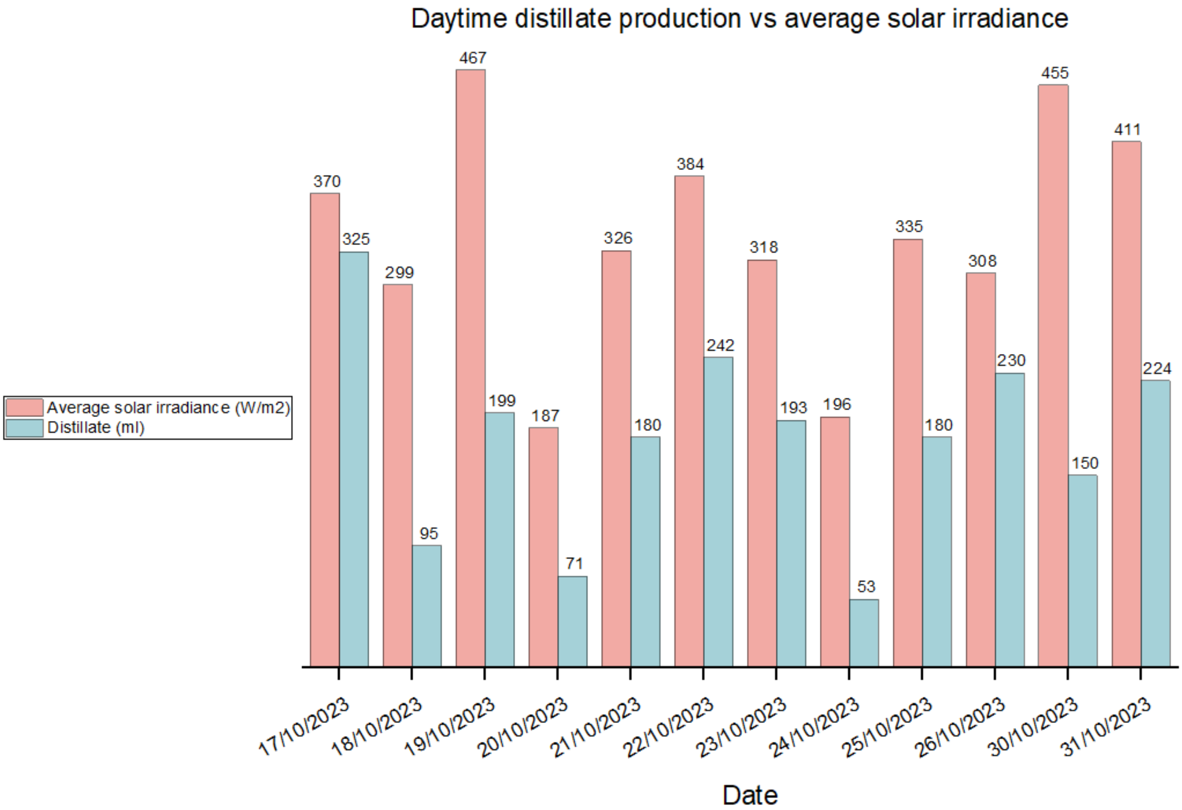

Figure 4.14: Daytime distillate production vs average solar irradiance graph

Figure 4.15 below is a representation of the minimum and maximum temperatures for the 12 days during which tests were conducted. It can be noted from both Figures 4.14 and 4.15 that on high-temperature days the production level was high and *vice versa* for the low-temperature days, as is expected for solar stills.

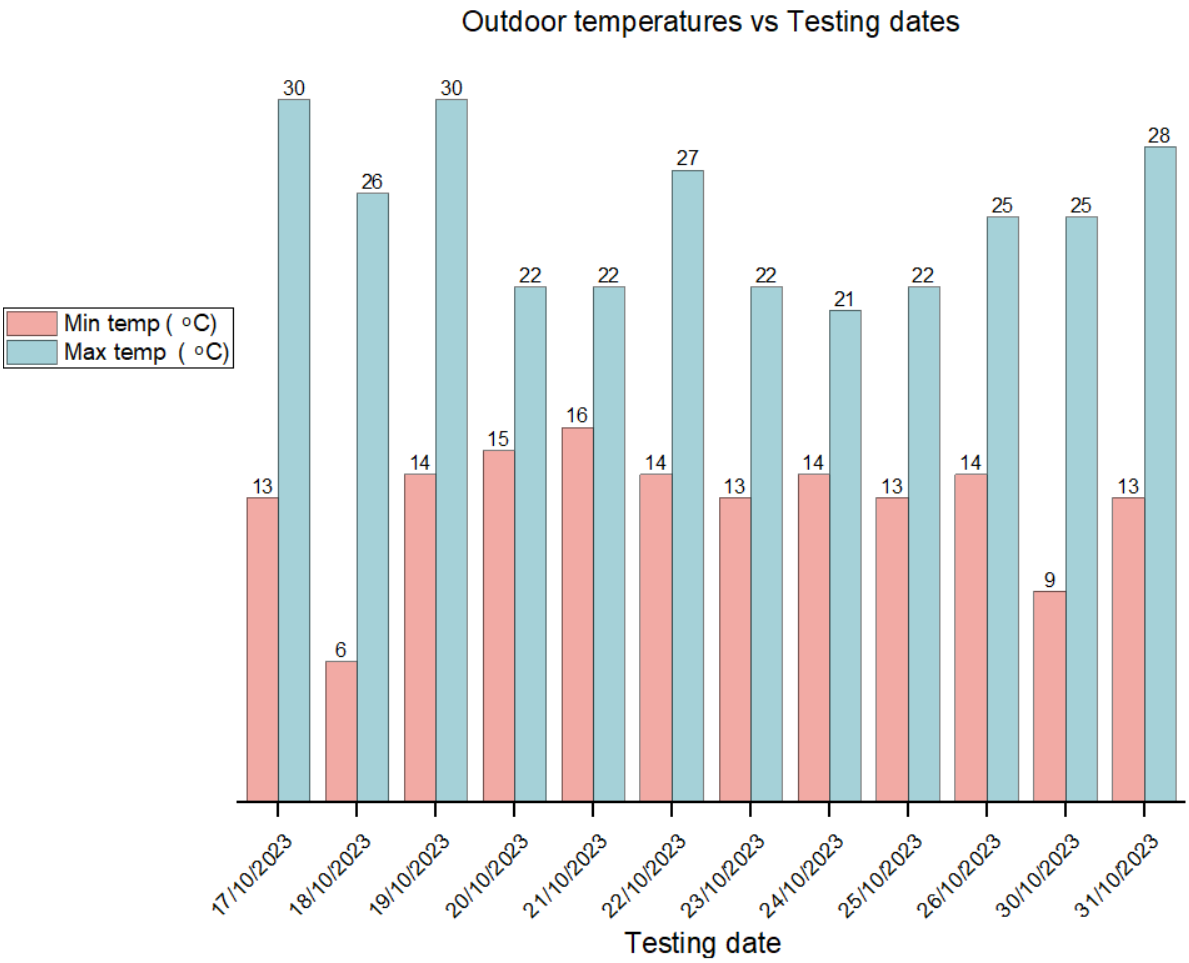

Figure 4.15: Outdoor temperatures vs Testing dates graph

4.3 Nighttime Experimental Tests

As already noted these tests were conducted from 17 October 2023 at 7 pm to 01 November 2023 at 7 am, South African time. Figure 4.16 below is a representation of the distillate production collected during the nighttime periods for the 12 days vs the average solar irradiance for those days. The three lowest production nights were experienced on 20 October (69 ml), 26 October (94 ml) and 25 October (111 ml) respectively, the maximum temperatures for those days were 22°C, 25°C, and 22°C respectively. The three highest production nights were 19 October (219ml), 22 October (218ml) and 17 October (188ml) respectively, the maximum temperatures for those days were 30°C, 27°C and 30°C respectively. It can be noted that minimum and maximum production was achieved on nights that had the lowest temperature and the highest days temperatures respectively. Even though during the night, the temperatures were significantly low, the evacuated tube solar collector kept the water in the system warm for a longer period and, therefore, extended the production hours. ETSC tubes are made from material with a high-temperature resistance and excellent solar irradiation transmittance. The vacuum created within the tubes works as an insulator, reducing heat dissipation to the surroundings [78]. This process is the reason the system continued operating with no solar irradiation available, thus, using ETSCs for nighttime production proved to be a great benefit since heat losses are minimized but still occur at a slower pace after sunset.

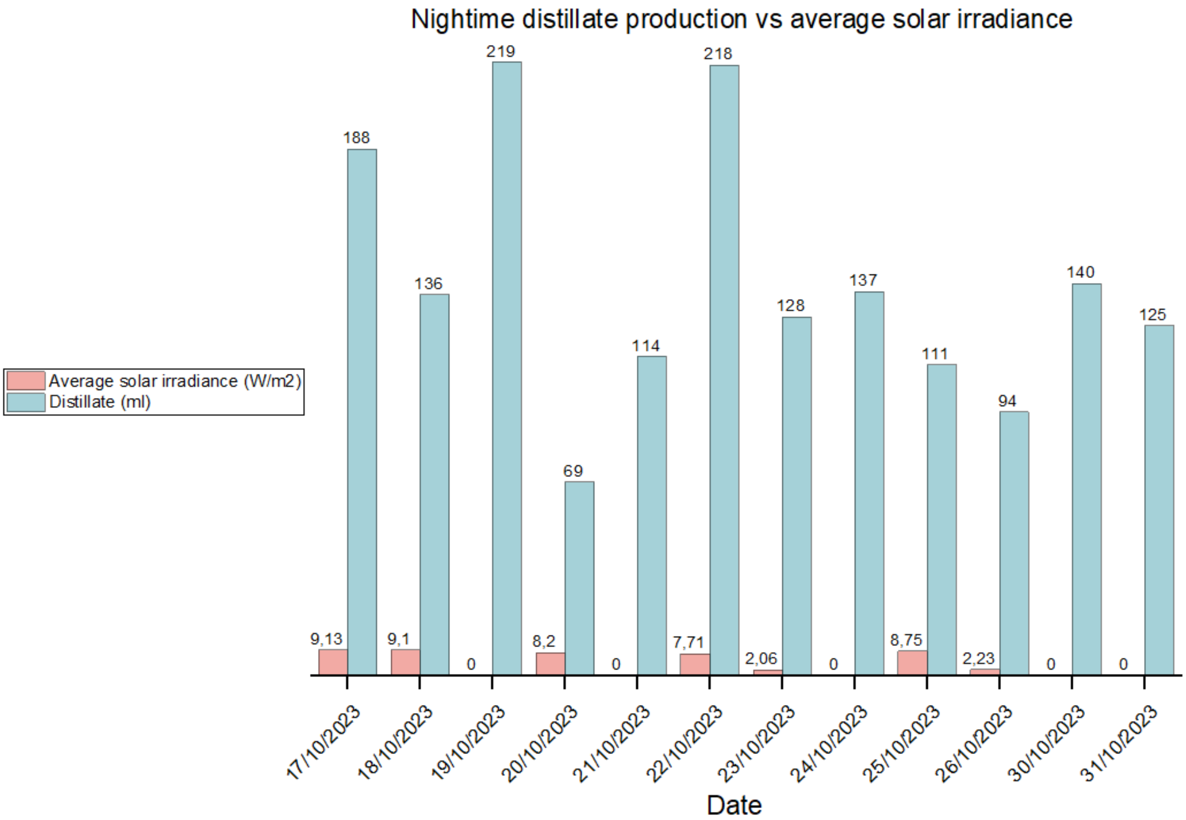

Figure 4.16: Nighttime distillate production vs average solar irradiance

4.4 Daytime vs Nighttime Production

The graph presented in Figure 4.17 below shows the comparison between day and nighttime distillate production collected from the newly designed D5S incorporated with the evacuated tube solar collector (ESTC). There are some differences between night and day time distillate production, the highest and lowest percentage differences were 61.3% on the 24 October 2023 and 2.8% on 20 October 2023 respectively. It was noted that on some days, production was higher during the nighttime compared to daytime. By leveraging ETSC technology, the experiment demonstrated the feasibility and effectiveness of utilizing solar energy for distillation processes, even during non-daylight hours. This finding emphasised the potential of ETSCs to enhance overall freshwater yield and efficiency in solar-powered distillation systems. Additionally, a comparative analysis carried out by Olczak et al. [79] revealed that ETSCs offer distinct advantages, especially during colder seasons, ensuring a more consistent output of thermal energy. This assertion was validated by the experiment's results, wherein nighttime distillate production occasionally surpassed daytime production levels on certain days.

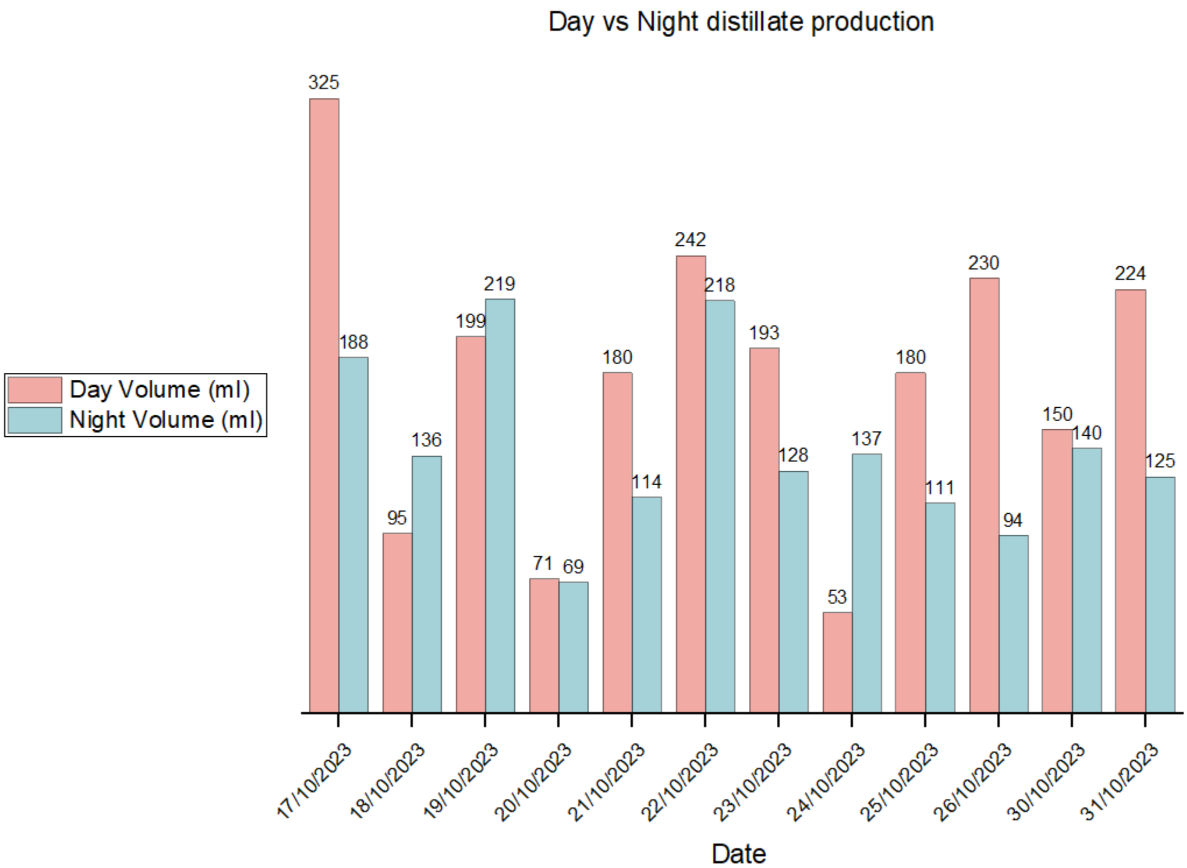

Figure 4.17: Distillate production at day vs night graph

4.5 Practical Salinity and Electrical Conductivity Test Results

Salinity and conductivity tests were conducted on raw seawater and the distillate produced from the D5S. The tests were conducted to check and compare the quality of the water before and after the experiment. These tests were conducted using the Bante DR900 multi-parameter meter at CPUT's Department of Chemistry, Bellville Campus, Cape Town, South Africa. One raw seawater sample, two samples from the distillate produced at nighttime and two samples from the daytime production were tested. Conductivity was measured in mS/cm (milliSiemens/cm) and salinity in psu (practical salinity unit).

Electrical conductivity (EC) is a quick and useful replacement test for TDS concentration in fluids with minimal organic content. It includes determining the electrical conductance of water, it is measured in microsiemens per centimeter (uS/cm) on a scale from 0 to 50,000. This metric indicates the salt concentration in water, with freshwater typically falling between 0 and 1,500 uS/cm, while seawater registers around 50,000 uS/cm [80][81][82]. It is noted in Table 4.1 below that the seawater electrical conductivity measured was 27,14 mS/cm which is equivalent to 27140 uS/cm and the distillate produced by the system ranges between 53.4 – 77.2 uS/cm. According to the World Health Organization 2022 [83], the water produced by the system, thus, can be considered as freshwater

Salinity refers to the total quantity of dissolved salts in water. As these salts dissolve, they break down into ionic particles with positive and negative charges, resulting in improved conductivity. According to the World Health Organization (WHO), drinking water is deemed safe when the total dissolved solids (TDS) level is less than 600 mg/L, or 0.6 psu. However, once TDS levels approach 1000 mg/L (equivalent to 1 psu), water becomes less safe[84][83][54]. The salinity test results obtained from the distillate produced by the newly designed D5S range between 0.03 – 0.05 psu, this result is clear evidence that the water produced by this D5S can be deemed to be within safe limits of salinity for drinking water. Additionally, the resistance of seawater and distilled water were measured and found to be 1.06Mohms and 3.22Mohms (Mega ohms), respectively.

Table 4.1: Conductivity and salinity test results

Sample	Production date	Conductivity (mS/cm)	Salinity (psu)
Raw seawater	-	27,14	13,05
Day sample 1	17 October 2023	0,0772	0,03
Day sample 2	23 October 2023	0,0534	0,03
Night sample 1	17-18 October 2023	0,0607	0,05
Night sample 2	18-19 October 2023	0,0616	0,04

4.6 Uncertainty analysis

Table 4.2 below contains the standard uncertainty of the measuring instruments used for the experiment, calculated according to[85], $U = \frac{a}{\sqrt{3}}$, where a is the accuracy of the measuring instrument and U is the standard uncertainty.

Table 4.2: Standard uncertainty

	Range	Accuracy	Standard uncertainty
Graduated measuring cylinders (1000 ml, 100 ml and 50 ml)	1000 ml: 10 to 1000 ml	1000 ml: ±5 ml	1000 ml: 2,889 ml
	100 ml: 1 to 100 ml	100 ml: ±0.5 ml	100 ml: 0,289 ml
	50 ml: 1 to 50 ml	50 ml: ±0.5 ml	50 ml: 0,289 ml
HP200 weather station (solar radiation and wind speed)	0 to 2000 W/m²	±1 W/m²	Solar radiation: 0.577 W/m²
	0 to 50 m/s	± 1 m/s (wind speed < 5 m/s)	Wind speed (<5 m/s): 0,577 m/s
		± 10% (wind speed> 5 m/s)	Wind speed (>5 m/s): 5,77%
12 channel BTM-4208SD temperature data logger (K type thermocouples)	-30˚C to 65˚C	±1 °C	0,577 °C
Bante DR900 multi-parameter	Conductivity: 0 to 20.00, 200.0, 2000 µS/cm, 20.00, 200.0 mS/cm	Conductivity: ±0.5% F.S.	Conductivity: 0,288%
	Salinity: 0.00 to 42.00 psu	Salinity: ±1% F.S.	Salinity: 0,577%
T235H digital multimeter (Resistance)	200Ω/ 2kΩ/ 20kΩ/ 200kΩ/ 2MΩ/ 20MΩ	0.8% + 5 Digit	0,462%

4.7 Cost analysis

The analysis was done based on the experiment conducted over the 12 days testing period, the freshwater distillate yield used was the average produced over the testing period. It should be noted that this is not entirely accurate as 12 days data is not sufficient to estimate annual operation costs. Number of operational days per year was considered as 350 to accommodate maintenance standing time. The cost analysis was done according to [86].

Annual interest rate (i) = 12%

No. of operational years (N) = 15

Present capital cost (P) = R15 000 (SA Rands)

No. of operational days per year (n) = 350

Freshwater yield/day from the D5S stages (M) = 0.318 (Litres)

Annual freshwater yield = 0.318 x 350 = 111.3 L

Capital Recovery Factor:

$$CRF = \frac{i(i+1)^n}{(i+1)^n - 1}$$

$$= \frac{0.12(0.12+1)^{15}}{(0.12+1)^{15} - 1}$$

= 0.147

Fixed Annual Cost:

$FAC = P$ x CRF

= R15000 x 0.147

= R2202.36

Sinking Fund Factor:

$$SFF = \frac{i}{(i+1)^n - 1}$$

$$= \frac{0,12}{(0.12+1)^{15} - 1}$$

= 0.027

Salvage Cost:

S = 0.2P

= 0.2 x R15000

= R3000

Annual Salvage Cost:

A$SV = SFF \times S$

= 0.027 x R3000

= R81

Annual Maintenance Cost:

AMC = 0.15× FAC

= 0.15 x R2202.36

= R330.35

Annual Cost:

$AC = FAC + AMC - ASV$

= R2202.36 + R330.35 – R81

= R2451.71

Cost per Litre:

$CPL = \frac{AC}{M}$

$= \frac{2451.71}{111.30}$

= R22.08 per litre

CHAPTER 5: CONCLUSION AND RECOMMENDATIONS

5.1 Conclusions

This thesis was based on a study of a new design for a D5S incorporated with the evacuated tube solar collector tested in Cape Town, South Africa. Researchers have conducted multiple experiments on the D5S, however, this proposed design provides a unique approach to improve the production of single-stage solar stills. The system used the force of gravity to transport water from the seawater tank to the basin and a 220 V circulation pump to maintain a continuous flow between the basin and the solar collector. The D5S was incorporated with a cover that contained cooling water to increase the condensation rate of the system.

The above-described experiment on the D5S was run for 12 days from 17 October to 1 November 2023. The system was tested both during the day and nighttime. The total distillate produced during the experiment period was 3821 ml, of which 2142 ml was produced during the daytime and 1679 ml during the nighttime.

The cooling water on the basin cover proved to be more effective in the mornings and evenings. During the day when the outdoor temperature was high, the water within the cover became warmer and, since the D5S was not monitored continuously throughout the day, when the water temperature increased it stopped serving its purpose of cooling, or rather, increasing the temperature difference of the water inside the basin and the cover to speed up the condensation process. However, in the morning when the water was still cold, it served its purpose. In the evenings the water in the cover was still warm after sunset, thus, the heat from the basin cover and the solar collector kept the distillate production going for longer during the night.

From the reviewed literature discussed in Chapter Two of this dissertation, it was noted that the depth of water inside the basin was one of the factors that influenced the production of solar stills. A float valve was installed in the newly designed D5S to ensure that a constant water level was maintained in the system for the duration of the experiment. The float valve was positioned to maintain a water depth of 50 mm.

Incorporating a solar collector (evacuated tube type) proved to be very effective for the D5S, especially during nighttime because it was noted that the system continued to produce distillate even after sunset. It was noted that on 19, 20, 22 and 30 October 2023 the nighttime production almost equaled the day distillate production. The difference was 9,1%, 2,8%, 9.9% and 6.7% respectively. On these days, the system performed at almost the same capacity during daytime and nighttime under completely different weather conditions. This, finding, therefore proved the effectiveness of the role played by the evacuated tube solar collector that was installed on the system for nighttime. The newly designed D5S manufactured and tested for the purpose of this research study performed quite effectively during the day and exceptionally well at night, considering that there was no solar radiation during the nighttime period.

The produced distillate was taken through conductivity and salinity tests, samples of both night and day production were taken and compared. The electrical conductivity and practical salinity measured were between 53.4 – 77.2 uS/cm and 0.03 – 0.05 psu respectively. The safe range of electrical conductivity for freshwater is 0 and 1,500 uS/cm and a practical salinity of less than 0.6 psu [80][82][84]. It can then be concluded that the water produced by the newly designed D5S was within the safe limits of electrical conductivity and practical salinity of drinking water.

5.2 Recommendations for Future Work

The newly designed D5S, however, experienced some challenges and areas for improvement were noted during the testing period. These challenges, together with possible solutions. will be discussed in this section.

This proposed new version of the D5S would greatly benefit from further improvements in common with most, if not all, engineering concepts. Some of the challenges encountered included issues with the cooling design on the basin cover and the low seawater flow rate between the basin and the solar collector. Initially, the system was operated by natural convection; however, the flow was slow. The other challenge was that the surface temperature data logger would switch off while the data logging process was in progress. This practice resulted in some data not being recorded.

The basin cover was filled with cooling water, however, the cooling water became hot during the day, thus, defeating its intended purpose. A possible solution to this problem would be to incorporate insulation material on the cover to minimize heat dissipation into the cover. It would also be beneficial to install a pumping system to keep the cooling water circulating on order to maintain it at room temperature. Another solution would be to install a pump system and a thermostat to detect the water temperature and to start pumping out warm water and pumping in cold water when the water inside the cover reaches a certain temperature. The second and third options, however, would be more expensive because they would require more electrical components being installed within the proposed D5S. Incorporating insulation material would work best for this design and, thus, result in an easy and cheap-to-manufacture system.

The second challenge experienced with the new D5S was with the circulation flow, the solution to which was installing a water circulation pump. To achieve natural convection for future D5S designs, it would be beneficial to design a piping system to allow the gravitational flow of the water. The use of a circulation flow pump is another good but more expensive option.

Another challenge that was experienced during this research study was logging surface temperatures owing to the data logger’s batteries running out of power. It would be useful to utilize a rechargeable data logger and keeping the logger plugged in during the experiment would result in complete data collection. Frequent monitoring of the data logging process would also be advantageous in detecting errors early and minimizing data loss.

To further expand this research study, it would be useful to extend the testing period. This specific experiment was carried out between months with the same season. Therefore, the results obtained are limiting, hence testing during all four seasons would greatly benefit the research and give an overview of the system's efficiency throughout the year.

BIBLIOGRAPHY

[1] S. Dixit, “Solar technologies and their implementations: A review,” *Mater. Today Proc.*, vol. 28, no. xxxx, pp. 2137–2148, 2020, doi: 10.1016/j.matpr.2020.04.134.

[2] M. A. Eltawil, Z. Zhengming, and L. Yuan, “A review of renewable energy technologies integrated with desalination systems,” *Renew. Sustain. Energy Rev.*, vol. 13, no. 9, pp. 2245–2262, 2009, doi: 10.1016/j.rser.2009.06.011.

[3] M. Eltawil, “Renewable Energy Powered Desalination Systems: Technologies and Economics-State of the Art,” *Recommendations*, vol. 12, no. 1, pp. 1–38, 2008, doi: 10.1007/s12045-015-0272-6.

[4] M. Moser, F. Trieb, and T. Fichter, “Potential of Concentrating Solar Power Plants for the Combined Production of Water and Electricity in MENA Countries,” vol. 1, no. 2, pp. 122–141, 2013.

[5] M. Ali *et al.*, “Recent progress in wind energy-powered desalination,” *Therm. Sci. Eng. Prog.*, vol. 47, no. September 2023, p. 102286, 2024, doi: 10.1016/j.tsep.2023.102286.

[6] H. Lu, “Wind energy technologies integrated with desalination systems : Review and,” no. August, 2018, doi: 10.1016/j.desal.2011.04.041.

[7] A. Alkaisi, R. Mossad, and A. Sharifian-Barforoush, “A Review of the Water Desalination Systems Integrated with Renewable Energy,” *Energy Procedia*, vol. 110, no. December 2016, pp. 268–274, 2017, doi: 10.1016/j.egypro.2017.03.138.

[8] D. Khojasteh *et al.*, “A large-scale review of wave and tidal energy research over the last 20 years,” *Ocean Eng.*, vol. 282, no. May, p. 114995, 2023, doi: 10.1016/j.oceaneng.2023.114995.

[9] J. Mi *et al.*, “Experimental investigation of a reverse osmosis desalination system directly powered by wave energy,” *Appl. Energy*, vol. 343, no. May, p. 121194, 2023, doi: 10.1016/j.apenergy.2023.121194.

[10] N. Sharmila, P. J. Ã, A. K. Swamy, and M. Ravindran, “Wave powered desalination system,” vol. 29, pp. 1659–1672, 2004, doi: 10.1016/j.energy.2004.03.099.

[11] F. Alnaimat, M. Ziauddin, and B. Mathew, “A review of recent advances in humidification and dehumidification desalination technologies using solar energy,” *Desalination*, vol. 499, no. August 2020, p. 114860, 2021, doi: 10.1016/j.desal.2020.114860.

[12] E. Jones, M. Qadir, M. T. H. van Vliet, V. Smakhtin, and S. mu Kang, “The state of desalination and brine production: A global outlook,” *Sci. Total Environ.*, vol. 657, pp. 1343–1356, 2019, doi: 10.1016/j.scitotenv.2018.12.076.

[13] U. Caldera and C. Breyer, “Strengthening the global water supply through a decarbonised global desalination sector and improved irrigation systems,” *Energy*, vol. 200, p. 117507, 2020, doi: 10.1016/j.energy.2020.117507.

[14] Y. Zheng and K. B. Hatzell, “Technoeconomic analysis of solar thermal desalination,” *Desalination*, vol. 474, no. July 2019, p. 114168, 2020, doi: 10.1016/j.desal.2019.114168.

[15] M. A. M. Khan, S. Rehman, and F. A. Al-Sulaiman, “A hybrid renewable energy system as a potential energy source for water desalination using reverse osmosis: A

review," *Renew. Sustain. Energy Rev.*, vol. 97, no. June, pp. 456–477, 2018, doi: 10.1016/j.rser.2018.08.049.

[16] L. Huang *et al.*, "Enhanced water yield of solar desalination by thermal concentrated multistage distiller," *Desalination*, vol. 477, no. August 2019, p. 114260, 2020, doi: 10.1016/j.desal.2019.114260.

[17] M. Shatat, M. Worall, and S. Riffat, "Opportunities for solar water desalination worldwide : Review," *Sustain. Cities Soc.*, vol. 9, pp. 67–80, 2013, doi: 10.1016/j.scs.2013.03.004.

[18] T. Yan, G. Xie, L. Sun, M. Du, and H. Liu, "Experimental investigation on a two-effect tubular solar still operating under vacuum conditions," *Desalination*, vol. 468, no. July, p. 114057, 2019, doi: 10.1016/j.desal.2019.06.023.

[19] H. K. Jani and K. V. Modi, "Experimental performance evaluation of single basin dual slope solar still with circular and square cross-sectional hollow fins," *Sol. Energy*, vol. 179, no. December 2018, pp. 186–194, 2019, doi: 10.1016/j.solener.2018.12.054.

[20] P. Zanganeh, A. S. Goharrizi, S. Ayatollahi, M. Feilizadeh, and H. Dashti, "Efficiency improvement of solar stills through wettability alteration of the condensation surface: An experimental study," *Appl. Energy*, vol. 268, no. March, p. 114923, 2020, doi: 10.1016/j.apenergy.2020.114923.

[21] A. Agrawal and R. S. Rana, "Theoretical and experimental performance evaluation of single-slope single-basin solar still with multiple V-shaped floating wicks," *Heliyon*, vol. 5, no. 4, p. e01525, 2019, doi: 10.1016/j.heliyon.2019.e01525.

[22] I. Al-Hayeka and O. O. Badran, "The effect of using different designs of solar stills on water distillation," *Desalination*, vol. 169, no. 2, pp. 121–127, 2004, doi: 10.1016/j.desal.2004.08.013.

[23] T. Arunkumar *et al.*, "A review of efficient high productivity solar stills," *Renew. Sustain. Energy Rev.*, vol. 101, no. May 2018, pp. 197–220, 2019, doi: 10.1016/j.rser.2018.11.013.

[24] H. Hassan, "Comparing the performance of passive and active double and single slope solar stills incorporated with parabolic trough collector via energy, exergy and productivity," *Renew. Energy*, vol. 148, pp. 437–450, 2020, doi: 10.1016/j.renene.2019.10.050.

[25] N. Pangwa and V. Msomi, "Materials Today : Proceedings Progress made in eliminating factors affecting solar stills productivity," *Mater. Today Proc.*, no. xxxx, 2022, doi: 10.1016/j.matpr.2022.03.300.

[26] H. M. Ahmed, F. S. Alshutal, G. Ibrahim, and A. Info, "Impact of Different Configurations on Solar Still Productivity," *J. Adv. Sci. Eng. Res.*, vol. 4, no. 2, pp. 118–126, 2014.

[27] M. Feilizadeh, M. R. K. Estahbanati, M. Khorram, and M. R. Rahimpour, "Experimental investigation of an active thermosyphon solar still with enhanced condenser," *Renew. Energy*, vol. 143, no. October, pp. 328–334, 2019, doi: 10.1016/j.renene.2019.05.013.

[28] R. Sathyamurthy *et al.*, "A Review of integrating solar collectors to solar still," *Renew. Sustain. Energy Rev.*, vol. 77, no. October 2015, pp. 1069–1097, 2017, doi: 10.1016/j.rser.2016.11.223.

[29] D. Dsilva Winfred Rufuss, S. Iniyan, L. Suganthi, and P. A. Davies, "Solar stills: A comprehensive review of designs, performance and material advances," *Renew.*

Sustain. Energy Rev., vol. 63, pp. 464–496, 2016, doi: 10.1016/j.rser.2016.05.068.

[30] V. Sivakumar and E. Ganapathy Sundaram, "Improvement techniques of solar still efficiency: A review," *Renew. Sustain. Energy Rev.*, vol. 28, pp. 246–264, 2013, doi: 10.1016/j.rser.2013.07.037.

[31] M. Mohsenzadeh, L. Aye, and P. Christopher, "A review on various designs for performance improvement of passive solar stills for remote areas," *Sol. Energy*, vol. 228, no. September, pp. 594–611, 2021, doi: 10.1016/j.solener.2021.09.086.

[32] T. Arunkumar, K. Vinothkumar, A. Ahsan, R. Jayaprakash, and S. Kumar, "Experimental Study on Various Solar Still Designs," *ISRN Renew. Energy*, vol. 2012, no. December 2014, pp. 1–10, 2012, doi: 10.5402/2012/569381.

[33] B. Jamil and N. Akhtar, "Effect of specific height on the performance of a single slope solar still: An experimental study," *Desalination*, vol. 414, pp. 73–88, 2017, doi: 10.1016/j.desal.2017.03.036.

[34] N. T. Alwan, S. E. Shcheklein, and O. M. Ali, "Experimental investigation of modified solar still integrated with solar collector," *Case Stud. Therm. Eng.*, vol. 19, no. December 2019, p. 100614, 2020, doi: 10.1016/j.csite.2020.100614.

[35] A. S. Abdullah, M. M. Younes, Z. M. Omara, and F. A. Essa, "New design of trays solar still with enhanced evaporation methods – Comprehensive study," *Sol. Energy*, vol. 203, no. February, pp. 164–174, 2020, doi: 10.1016/j.solener.2020.04.039.

[36] S. J. P. Gnanaraj and V. Velmurugan, "An experimental study on the efficacy of modifications in enhancing the performance of single basin double slope solar still," *Desalination*, vol. 467, no. June, pp. 12–28, 2019, doi: 10.1016/j.desal.2019.05.015.

[37] E. Hedayati-Mehdiabadi, F. Sarhaddi, and F. Sobhnamayan, "Exergy performance evaluation of a basin-type double-slope solar still equipped with phase-change material and PV/T collector," *Renew. Energy*, vol. 145, pp. 2409–2425, 2020, doi: 10.1016/j.renene.2019.07.160.

[38] M. R. Rajamanickam, P. Velmurugan, A. Ragupathy, and E. Sivaraman, "Use of thermal energy storage materials for enhancement in distillate output of double slope solar still," *Mater. Today Proc.*, vol. 34, no. xxxx, pp. 416–419, 2018, doi: 10.1016/j.matpr.2020.02.203.

[39] K. Selvaraj and A. Natarajan, "Factors influencing the performance and productivity of solar stills - A review," *Desalination*, vol. 435, no. October 2017, pp. 181–187, 2018, doi: 10.1016/j.desal.2017.09.031.

[40] A. Muthu Manokar, K. Kalidasa Murugavel, and G. Esakkimuthu, "Different parameters affecting the rate of evaporation and condensation on passive solar still - A review," *Renew. Sustain. Energy Rev.*, vol. 38, pp. 309–322, 2014, doi: 10.1016/j.rser.2014.05.092.

[41] M. Boukar and A. Harmim, "Effect of climatic conditions on the performance of a simple basin solar still.: A comparative study," *Desalination*, vol. 137, no. 1–3, pp. 15–22, 2001, doi: 10.1016/S0011-9164(01)00199-0.

[42] O. O. Badran and M. M. Abu-Khader, "Evaluating thermal performance of a single slope solar still," *Heat Mass Transf. und Stoffuebertragung*, vol. 43, no. 10, pp. 985–995, 2007, doi: 10.1007/s00231-006-0180-0.

[43] O. O. Badran and H. A. Al-Tahaineh, "The effect of coupling a flat-plate collector on the solar still productivity," *Desalination*, vol. 183, no. 1–3, pp. 137–142, 2005, doi: 10.1016/j.desal.2005.02.046.

[44] E. A. Almuhanna, “Evaluation of Single Slop Solar Still Integrated With Evaporative Cooling System for Brackish Water Desalination,” *J. Agric. Sci.*, vol. 6, no. 1, pp. 48–58, 2013, doi: 10.5539/jas.v6n1p48.

[45] R. S. Subramanian, G. Kumaresan, R. Ajith, U. Sabarivasan, K. K. Gowthamaan, and S. Anudeep, “Performance analysis of modified solar still integrated with flat plate collector,” *Mater. Today Proc.*, vol. 45, no. xxxx, pp. 1382–1387, 2021, doi: 10.1016/j.matpr.2020.06.409.

[46] A. A. El-Sebaii, “Effect of wind speed on some designs of solar stills,” *Energy Convers. Manag.*, vol. 41, no. 6, pp. 523–538, 2000, doi: 10.1016/S0196-8904(99)00119-3.

[47] Z. M. Omara, A. E. Kabeel, and A. S. Abdullah, “A review of solar still performance with reflectors,” *Renew. Sustain. Energy Rev.*, vol. 68, no. December 2015, pp. 638–649, 2017, doi: 10.1016/j.rser.2016.10.031.

[48] S. W. Sharshir, N. Yang, G. Peng, and A. E. Kabeel, “Factors affecting solar stills productivity and improvement techniques : A detailed review,” *Appl. Therm. Eng.*, vol. 100, pp. 267–284, 2016, doi: 10.1016/j.applthermaleng.2015.11.041.

[49] M. Abu-Arabi, Y. Zurigat, H. Al-Hinai, and S. Al-Hiddabi, “Modeling and performance analysis of a solar desalination unit with double-glass cover cooling,” *Desalination*, vol. 143, no. 2, pp. 173–182, 2002, doi: 10.1016/S0011-9164(02)00238-2.

[50] A. M. Burbano, “Evaluation of basin and insulating materials in solar still prototype for solar distillation plant at kamusuchiwo community, high guajira,” *Renew. Energy Power Qual. J.*, vol. 1, no. 12, pp. 547–552, 2014, doi: 10.24084/repqj12.395.

[51] M. Z. Khan, I. Nawaz, G. N. Tiwari, and M. Meraj, “Effect of top cover cooling on the performance of hemispherical solar still,” *Mater. Today Proc.*, vol. 38, pp. 384–390, 2020, doi: 10.1016/j.matpr.2020.07.513.

[52] B. A. K. Abu-Hijleh, “Enhanced solar still performance using water film cooling of the glass cover,” *Desalination*, vol. 107, no. 3, pp. 235–244, 1996, doi: 10.1016/S0011-9164(96)00165-8.

[53] B. A. K. Abu-Hijleh and H. A. Mousa, “Water film cooling over the glass cover of a solar still including evaporation effects,” *Energy*, vol. 22, no. 1, pp. 43–48, 1997, doi: 10.1016/S0360-5442(96)00088-6.

[54] S. K. Singh, S. C. Kaushik, V. V. Tyagi, and S. K. Tyagi, “Comparative Performance and parametric study of solar still: A review,” *Sustain. Energy Technol. Assessments*, vol. 47, no. August, p. 101541, 2021, doi: 10.1016/j.seta.2021.101541.

[55] H. S. Kwatra, “Performance of a solar still: Predicted effect of enhanced evaporation area on yield and evaporation temperature,” *Sol. Energy*, vol. 56, no. 3, pp. 261–266, 1996, doi: 10.1016/0038-092X(95)00101-V.

[56] P. K. Chaurasiya *et al.*, “A review of techniques for increasing the productivity of passive solar stills,” *Sustain. Energy Technol. Assessments*, vol. 52, no. PA, p. 102033, 2022, doi: 10.1016/j.seta.2022.102033.

[57] S. K. Suraparaju, R. Dhanusuraman, and S. K. Natarajan, “Performance evaluation of single slope solar still with novel pond fibres,” *Process Saf. Environ. Prot.*, vol. 154, pp. 142–154, 2021, doi: 10.1016/j.psep.2021.08.011.

[58] S. W. Sharshir, M. A. Eltawil, A. M. Algazzar, R. Sathyamurthy, and A. W. Kandeal, “Performance enhancement of stepped double slope solar still by using nanoparticles and linen wicks: Energy, exergy and economic analysis,” *Appl. Therm. Eng.*, vol. 174,

no. October 2019, p. 115278, 2020, doi: 10.1016/j.applthermaleng.2020.115278.

[59] T. Elango and K. Kalidasa Murugavel, “The effect of the water depth on the productivity for single and double basin double slope glass solar stills,” *Desalination*, vol. 359, pp. 82–91, 2015, doi: 10.1016/j.desal.2014.12.036.

[60] A. J. N. Khalifa and A. M. Hamood, “On the verification of the effect of water depth on the performance of basin type solar stills,” *Sol. Energy*, vol. 83, no. 8, pp. 1312–1321, 2009, doi: 10.1016/j.solener.2009.04.006.

[61] M. R. Rajamanickam and A. Ragupathy, “Influence of water depth on internal heat and mass transfer in a double slope solar still,” *Energy Procedia*, vol. 14. pp. 1701–1708, 2012, doi: 10.1016/j.egypro.2011.12.918.

[62] S. A. Abdul-Wahab and Y. Y. Al-Hatmi, “Performance evaluation of an inverted absorber solar still integrated with a refrigeration cycle and an inverted absorber solar still,” *Energy Sustain. Dev.*, vol. 17, no. 6, pp. 642–648, 2013, doi: 10.1016/j.esd.2013.08.006.

[63] A. J. N. Khalifa and A. M. Hamood, “Effect of insulation thickness on the productivity of basin type solar stills: An experimental verification under local climate,” *Energy Convers. Manag.*, vol. 50, no. 9, pp. 2457–2461, 2009, doi: 10.1016/j.enconman.2009.06.007.

[64] A. A. Al-Karaghouli and W. E. Alnaser, “Performances of single and double basin solar-stills,” *Appl. Energy*, vol. 78, no. 3, pp. 347–354, 2004, doi: 10.1016/S0306-2619(03)00005-9.

[65] T. Arunkumar *et al.*, “Productivity enhancement of solar still by using porous absorber with bubble-wrap insulation,” *J. Clean. Prod.*, vol. 195, pp. 1149–1161, 2018, doi: 10.1016/j.jclepro.2018.05.199.

[66] A. Y. Hashim, J. M. Al-asadi, and W. a Taha, “Experimental investigation of symmetrical double slope single basin solar stills productivity with different Insulation,” *J. Kufa – Phys.*, vol. 1, no. 2, pp. 26–32, 2009.

[67] A. Ghoneyem and A. Ileri, “Software to analyze solar stills and an experimental study on the effects of the cover,” *Desalination*, vol. 114, no. 1, pp. 37–44, 1997, doi: 10.1016/S0011-9164(97)00152-5.

[68] H. N. Singh and G. N. Tiwari, “Monthly performance of passive and active solar stills for different Indian climatic conditions,” *Desalination*, vol. 168, no. 1–3, pp. 145–150, 2004, doi: 10.1016/j.desal.2004.06.180.

[69] B. A. Akash, M. S. Mohsen, and W. Nayfeh, “Experimental study of the basin type solar still under local climate conditions,” *Energy Convers. Manag.*, vol. 41, no. 9, pp. 883–890, 2000, doi: 10.1016/S0196-8904(99)00158-2.

[70] Y. A. F. El-Samadony, W. M. El-Maghlany, and A. E. Kabeel, “Influence of glass cover inclination angle on radiation heat transfer rate within stepped solar still,” *Desalination*, vol. 384, pp. 68–77, 2016, doi: 10.1016/j.desal.2016.01.031.

[71] A. J. N. Khalifa and H. A. Ibrahim, “Effect of inclination of the external reflector of simple solar still in winter: An experimental investigation for different cover angles,” *Desalination*, vol. 264, no. 1–2, pp. 129–133, 2010, doi: 10.1016/j.desal.2010.07.016.

[72] A. K. Mishra, M. Meraj, G. N. Tiwari, and A. Ahmad, “Effect of inclination on internal heat and mass transfer of active solar still having conical condensing cover,” *Mater. Today Proc.*, vol. 38, pp. 105–111, 2020, doi: 10.1016/j.matpr.2020.06.105.

[73] H. Panchal, “Performance Investigation on Variations of Glass Cover Thickness on Solar Still: Experimental and Theoretical Analysis,” *Technol. Econ. Smart Grids Sustain. Energy*, vol. 1, no. 1, 2016, doi: 10.1007/s40866-016-0007-0.

[74] X. Si *et al.*, “Brazing of Cr2AlC and 316H stainless steel using BNi-2 filler: Microstructure, properties and joining mechanism,” *Mater. Charact.*, vol. 207, no. October 2023, p. 113573, 2024, doi: 10.1016/j.matchar.2023.113573.

[75] E. Zambolin and D. Del Col, “Experimental analysis of thermal performance of flat plate and evacuated tube solar collectors in stationary standard and daily conditions,” *Sol. Energy*, vol. 84, no. 8, pp. 1382–1396, 2010, doi: 10.1016/j.solener.2010.04.020.

[76] M. Eltaweel, A. A. Abdel-Rehim, and A. A. A. Attia, “A comparison between flat-plate and evacuated tube solar collectors in terms of energy and exergy analysis by using nanofluid,” *Appl. Therm. Eng.*, vol. 186, no. December 2020, p. 116516, 2021, doi: 10.1016/j.applthermaleng.2020.116516.

[77] G. Singh, S. Kumar, and G. . Tiwari, “Design, fabrication and performance evaluation of a hybrid photovoltaic thermal (PVT) double slope active solar still,” *Desalination*, vol. 277, no. 1, pp. 399–406, 2011, doi: 10.1016/j.desal.2011.04.064.

[78] S. Aggarwal, R. Kumar, D. Lee, S. Kumar, and T. Singh, “A comprehensive review of techniques for increasing the efficiency of evacuated tube solar collectors,” *Heliyon*, vol. 9, no. 4, p. e15185, 2023, doi: 10.1016/j.heliyon.2023.e15185.

[79] P. Olczak and D. Matuszewska, “The Comparison of Solar Energy Gaining E ff ectiveness between Flat Plate Collectors and Evacuated Tube Collectors with Heat Pipe : Case Study,” 2020.

[80] “Water quality standards μ S / cm,” p. 500.

[81] W. Affairs, *WATER QUALITY GUIDELINES AQUATIC*, vol. 7. 1996.

[82] DWAF, *South African Water Quality Guidelines : Domestic Use (second edition)*, vol. 1. 1996.

[83] N. Water and Q. Management, *Australian Drinking Water Guidelines 6*, no. September. 2022.

[84] Y. Meride and B. Ayenew, “Drinking water quality assessment and its effects on residents health in Wondo genet campus, Ethiopia,” *Environ. Syst. Res.*, vol. 5, no. 1, pp. 1–7, 2016, doi: 10.1186/s40068-016-0053-6.

[85] R. Safoui *et al.*, “Atmospheric water harvesting using a desiccant-based solar still: experimental investigation and economic analysis,” *Eng. Res. Express*, vol. 6, no. 4, Dec. 2024, doi: 10.1088/2631-8695/ad970a.

[86] A. E. Abu El-Maaty, M. M. Awad, G. I. Sultan, and A. M. Hamed, “Solar powered fog desalination system,” *Desalination*, vol. 472, Dec. 2019, doi: 10.1016/j.desal.2019.114130.

APPENDICES

APPENDIX A

APPENDIX A-1: Daily Distillate Production Volumes

Date	Time range	Volume (ml)
17/10/2023	07:00 – 19:00	325
	19:00 – 07:00	188
18/10/2023	07:00 – 19:00	95
	19:00 – 07:00	136
19/10/2023	07:00 – 19:00	199
	19:00 – 07:00	219
20/10/2023	07:00 – 19:00	71
	19:00 – 07:00	69
21/10/2023	07:00 – 19:00	180
	19:00 – 07:00	114
22/10/2023	07:00 – 19:00	242
	19:00 – 07:00	218
23/10/2023	07:00 – 19:00	193
	19:00 – 07:00	128
24/10/2023	07:00 – 19:00	53
	19:00 – 07:00	137
25/10/2023	07:00 – 19:00	180
	19:00 – 07:00	111
26/10/2023	07:00 – 19:00	230
	19:00 – 07:00	94
30/10/2023	07:00 – 19:00	150
	19:00 – 07:00	140
31/10/2023	07:00 – 19:00	224
	19:00 – 07:00	125

APPENDIX A-2: Thermocouple temperatures (25/10/2023-26/10/2023)

Timestamp	Average of T4	Average of T3	Average of T2	Average of T1
25/10/2023 07:00	24,43	15,98	26,57	16,42
25/10/2023 08:00	29,25	19,82	31,10	20,35
25/10/2023 09:00	31,15	25,07	31,42	25,72
25/10/2023 10:00	33,80	32,78	33,97	31,07
25/10/2023 11:00	35,63	40,45	35,68	37,83
25/10/2023 12:00	34,00	43,53	33,97	42,92
25/10/2023 13:00	31,57	43,05	31,52	38,52
25/10/2023 14:00	28,57	42,03	28,62	37,62
25/10/2023 15:00	26,82	38,60	26,92	36,20
25/10/2023 16:00	24,55	35,35	24,67	34,33
25/10/2023 17:00	24,05	31,62	23,92	31,90
25/10/2023 18:00	22,25	28,28	22,12	28,80
25/10/2023 19:00	18,93	23,82	19,00	25,57
25/10/2023 20:00	17,50	21,58	17,43	21,97
25/10/2023 21:00	16,87	20,20	16,83	20,58
25/10/2023 22:00	16,33	19,33	16,32	19,65
25/10/2023 23:00	16,12	18,72	16,02	19,08
26/10/2023 00:00	15,88	18,28	15,80	18,63
26/10/2023 01:00	15,52	17,88	15,48	18,22
26/10/2023 02:00	15,17	17,63	15,13	17,97
26/10/2023 03:00	14,97	17,27	14,95	17,65
26/10/2023 04:00	14,90	17,05	14,88	17,37
26/10/2023 05:00	14,60	16,82	14,53	17,15
26/10/2023 06:00	16,35	16,70	16,92	17,00
26/10/2023 07:00	18,40	17,50	19,30	18,10

- T4 Inlet to the basin from the solar collector
- T3 Outlet from the solar collector
- T2 Inlet to the solar collector
- T1 Outlet from basin

APPENDIX A-3: Average Solar irradiance and Wind speed

Date	Timeframe	Average solar irradiance (W/m^2)	Average wind speed(m/s)
17/10/2023	Day 1	370,3254107	2,006365741
	Night 1	9,133076389	2,591049383
18/10/2023	Day 2	299,2478796	3,424189815
	Night 2	9,100826389	1,120563272
19/10/2023	Day 3	466,919596	0,167824074
	Night 3	0	0
20/10/2023	Day 4	187,0553878	0,54533179
	Night 4	8,195939394	3,218557099
21/10/2023	Day 5	325,7091919	5,165509259
	Night 5	0	0
22/10/2023	Day 6	383,8300253	1,272183642
	Night 6	46,287	0,038966049
23/10/2023	Day 7	318,4546515	2,56558642
	Night 7	2,060194444	1,313464506
24/10/2023	Day 8	195,8730556	0,334490741
	Night 8	0	0,133101852
25/10/2023	Day 9	334,6940071	1,223274411
	Night 9	8,747251894	0,830439815
26/10/2023	Day 10	308,2515972	0,871527778
	Night 1 0	2,233791667	0,194058642
30/10/2023	Day 11	455,23625	1,611496914
	Night 11	0	1,668595679
31/10/2023	Day 12	411,1335859	1,012731481
	Night 12	0	0

APPENDIX A-4: Conductivity and Salinity test results

Raw seawater sample:

Conductivity: 27,14 mS/cm

Salinity: 13,05 psu

Night Sample 1:

Collection date: 17 October – 18 October 2023

Volume produced: 188 ml.

Conductivity: 0,0607 mS/cm

Salinity: 0,05 psu

Night Sample 2:

Collection date: 18 October – 19 October 2023

Volume produced: 136 ml.

Conductivity: 0,06156 mS/cm

Salinity: 0,04 psu

Day Sample 1:

Collection date: 23 October 2023

Volume produced: 192,5 ml.

Conductivity: 0,05343 mS/cm

Salinity: 0,03 psu

Day Sample 2:

Collection date: 17 October 2023

Volume produced: 325 ml.

Conductivity: 0,07716 mS/cm

Salinity: 0,03 psu

Units:

Salinity: psu: practical salinity unit

Conductivity: mS/cm: milliSiemens/cm

Instrument used: Bante DR900 multi-parameter meter.

APPENDIX B

APPENDIX B-1: Pump technical specifications

220V Hot Water Circulation Pump

About the 220V Hot Water Circulation Pump

Application

GeyserWise 220V Hot Water Circulation Pump is suitable for installation in balanced pressured solar systems or for hot water circulation.

When installing the pump be sure to follow the appropriate instructions of each particular manufacturer for all other components as well:

- Installation of geyser.
- Installation of solar collectors.
- Installation of controllers.
- Follow rules according to SANS10106.

Installation

Installation, maintenance and dismantling may only be performed by trained personnel in accordance with this instruction manual and safety instructions.

Use the pump only after first thoroughly reading and understanding this instruction manual and the safety instructions. In the event of any ambiguities regarding the installation and operation, consult trained personnel or contact our offices.

Technical information

- Maximum Power 100W
- Rated Power 90W
- Minimum Power 46W
- Diameter 25mm
- Voltage 220V
- Frequency 50Hz
- Maximum water temperature 110ºC
- Maximum ambient temperature 40ºC
- Maximum working pressure 10 bar

Speed	Head	Max capacity L/min	Speed (r/min)
III	6	40	2200
II	5	35	1900
1	3	20	1450

Performance curve

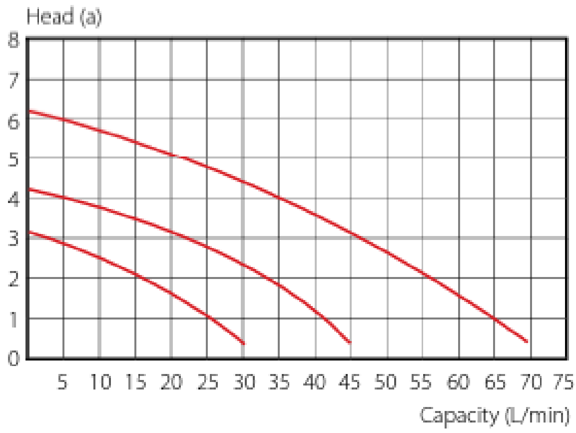

APPENDIX B-2: Bante DR900 multi-parameter meter technical specifications

Specifications

	Model		Bante 900	Bante 901	Bante 902	Bante 903	Bante 904
pH	Range	-2.000–20.000 pH	•	•	•	•	—
	Resolution	0.001, 0.01, 0.1 pH, selectable	•	•	•	•	—
	Accuracy	±0.002 pH	•	•	•	•	—
	Calibration	1 to 5 points	•	•	•	•	—
	pH Buffer Options	USA, NIST, DIN, 2 custom buffers	•	•	•	•	—
ORP	Range	±1999.9 mV	•	•	•	•	—
	Resolution	0.1, 1 mV, selectable	•	•	•	•	—
	Accuracy	±0.2 mV	•	•	•	•	—
	Calibration	1 point	•	—	•	•	—
Ion	Range	0.001–19999 (depending on the range of ISE)	•	—	—	—	—
	Resolution	0.001, 0.01, 0.1, 1	•	—	—	—	—
	Accuracy	±0.5% F.S. (monovalent), ±1% F.S. (divalent)	•	—	—	—	—
	Measurement Units	ppm, mg/L, mol/L, mmol/L	•	—	—	—	—
	Calibration	2 to 5 points (0.001, 0.01, 0.1, 1, 10, 100, 1000, 10000)	•	—	—	—	—
Conductivity	Range	0.01–20.00, 200.0, 2000 µS/cm, 20.00, 200.0 mS/cm	•	•	•	—	•
	Resolution	0.001, 0.01, 0.1, 1	•	•	•	—	•
	Accuracy	±0.5% F.S.	•	•	•	—	•
	Calibration	1 to 5 points	•	•	•	—	•
	Calibration Solutions	10 µS/cm, 84 µS/cm, 1413 µS/cm, 12.88 mS/cm, 111.8 mS/cm	•	•	•	—	•
	Temperature Coefficient	Linear (0.0–10.0%/°C), pure water	•	•	•	—	•
	Reference Temperature	20/25°C	•	•	•	—	•
	Cell Constant	K=0.1, 1, 10 or custom	•	•	•	—	•
TDS	Range	0–10.00, 100.0, 1000 ppm, 10.00, 200.0 ppt	•	•	•	—	•
	Resolution	0.01, 0.1, 1	•	•	•	—	•
	Accuracy	±1% F.S.	•	•	•	—	•
	TDS Factor	0.1–1.0 (default 0.5)	•	•	•	—	•
Salinity	Range	0.00–42.00 psu, 0.00–80.00 ppt	•	—	•	—	•
	Resolution	0.01	•	—	•	—	•
	Accuracy	±1% F.S.	•	—	•	—	•
Resistivity	Range	0.00–20.00 MΩ	•	—	•	—	•
	Resolution	0.01, 0.1	•	—	•	—	•
	Accuracy	±1% F.S.	•	—	•	—	•
DO	Range	0.00–20.00 mg/L, 0.0–200.0% saturation	•	—	—	•	•
	Resolution	0.01 mg/L, 0.1%	•	—	—	•	•
	Accuracy	±0.2 mg/L, ±2.0%	•	—	—	•	•
	Calibration	1 or 2 points	•	—	—	•	•
	Barometric Pressure Correction	60.0–112.5 kPa/450–850 mmHg, manual	•	—	—	•	•
	Salinity Correction	0.0–50.0 ppt, manual	•	—	—	•	•
General Spec.	Temperature Compensation	0–100°C/32–212°F, manual or automatic	•	•	•	•	•
	Memory	500 data sets, USB communication interface	•	•	•	•	•
	Power Requirements	5V DC power adapter	•	•	•	•	•
	Dimensions and Weight	210(L)×188(W)×60(H) mm, 1.5 kg	•	•	•	•	•

APPENDIX B-3: Bante DR900 multi-parameter meter operating manual and calibration settings

Conductivity/TDS/Salinity/ Resistivity

Calibration and Measurement

This section is applicable to model

- 950
- 900/901/902/904

Prior to Use

1. Connect the conductivity electrode to the meter (refer to the *Connection* section on page 6).
2. Soak the electrode for about 10 minutes in tap water to remove dirt and oil stains on the sensor surface.

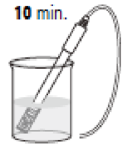

Selecting the Measurement Mode

Press the **Mode** key, the meter will show the conductivity (COND), TDS, salinity (SAL) and resistivity (RES) icons. Select a desired mode.

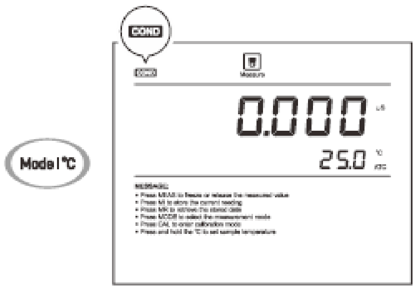

Conductivity/TDS/Salinity Settings

The meter contains 7 conductivity/TDS settings and 7 general settings in the setup menu.

Menu Item	Option and Description	
CELL	**Cell Constant** Set the cell constant to match connected conductivity electrode.	
	0.1	K = 0.1
	1	K = 1 (default)
	10	K = 10
	USEr	Custom
COE	**Temperature Coefficient** Set the temperature coefficient for linear temperature compensation.	
	2.10	0.00 to 10.00%/°C (default 2.10)

CAL	**Calibration Points** Set the number of calibration points.	
	...5	1 to 5 points (default 1 point)
PUrE	**Pure Water Compensation** If enabled, the pure water compensation coefficient will be applied automatically for ultra-pure water measurements.	
	YES	Enable
	nO	Disable (default)
Std	**Reference Temperature** Set the normalization temperature for measurement, the readings will automatically compensate to the selected temperature during measurement.	
	25℃	25°C (default)
	20℃	20°C
tdS	**TDS Factor** Set the default TDS conversion factor.	
	0.50	0.40 to 1.00 (default 0.50)
UnIt	**Measurement Unit** Set the default temperature unit.	
	°C	Degrees Celsius (default)
	°F	Degrees Fahrenheit

If you want to change the current settings, press and hold the 🖹 key to enter the setup menu. Press the ▲ / ▼ key to select an option and press the **Enter** key to confirm.

Refer to the *Setting a Default Option* section for detailed instructions on page 7.

Temperature Compensation

The temperature compensation has a large effect on the conductivity measurement. If enabled, the meter will use the measured conductivity and temperature readings to calculate the result and automatically compensate to the selected reference temperature. If the temperature coefficient is set to 0, the temperature compensation will be disabled, the meter only shows the actual conductivity at the measured temperature.

Automatic Temperature Compensation

Connect the temperature probe to meter, the ATC icon appears on the display, the meter is now switched to the automatic temperature compensation mode.

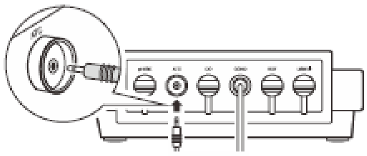

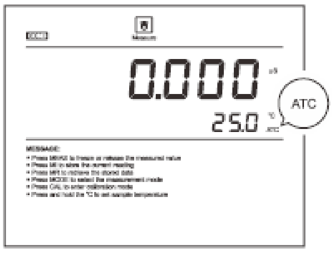

Manual Temperature Compensation

If the meter does not detect a temperature probe, the degrees Celsius icon (°C) will show on the display indicating the meter is switched to the manual temperature compensation mode. To set the temperature value follow the steps below.

1. Press and hold the **°C** key to enter the temperature setting.
2. Press the ▲ / ▼ key to modify the temperature value.
3. Press the **Enter** key to save.

Press and hold the ▲ / ▼ key will make the value change faster.

Selecting a Conductivity Electrode

The 9 series meter is capable of using three types of the conductivity electrodes. Before the calibration and measurement, ensure that you have selected a suitable electrode according to the anticipated sample conductivity. The following table lists the selectable electrode and its effective measurement ranges.

Electrode	Measurement Range	Cell Constant
CON-0.1	0.5 to 100 μS/cm	K = 0.1
CON-1	10 μS/cm to 20 mS/cm	K = 1
CON-10	100 μS/cm to 200 mS/cm	K = 10

H

Conductivity Calibration

Automatic Calibration

The 9 series meter allows 1 to 5 points calibration in the conductivity mode. Before calibration, ensure that selected cell constant (K=0.1, 1, 10) matches connected electrode. If you have selected the manual calibration (USEr), the meter will wait to enter a cell constant.

For better accuracy, we recommend to perform 3 points calibration or select a standard solution closest to the sample conductivity you are measuring. The meter will automatically detect the standard solution and prompt the user to perform the calibration. The following table shows the default standard solution for each measurement range.

Measurement Range	Default Standard Solution
0 to 20 µS/cm	10 µS/cm
20 to 200 µS/cm	84 µS/cm
200 to 2000 µS/cm	1413 µS/cm
2 to 20 mS/cm	12.88 mS/cm
20 to 200 mS/cm	111.8 mS/cm

If you have changed the conductivity electrode, the meter must be recalibrated. Every electrode has a different cell constant.

Single Point Calibration

1.1 Press the **Mode** key to enter the conductivity measurement mode and select 1 point calibration in the setup menu.

1.2 Press the **Cal** key, the display shows ----/CAL1, the meter waits for recognizing the standard solution.

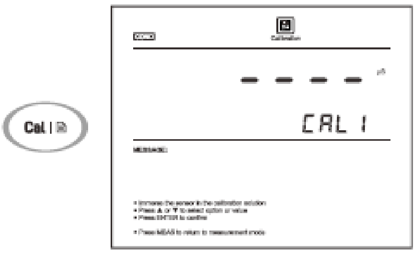

1.3 Rinse the conductivity electrode with distilled water, then rinse with a small amount of standard solution.

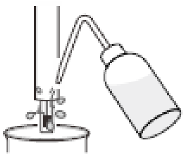

1.4 Place the electrode (and temperature probe) into the standard solution, stir gently to remove air bubbles trapped in the slot of the sensor.

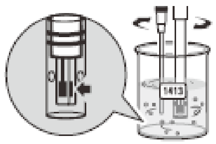

The meter will automatically show the calibration standard (e.g., 1413 µS/cm).

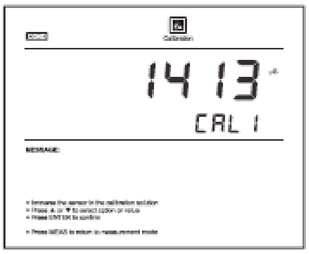

1.5 If necessary, press the ▲ / ▼ key to modify the calibration value. Press the **Enter** key, the Calibration icon begins flashing.

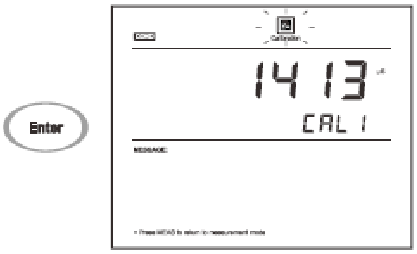

1.6 When the reading has stabilized, the meter will show End and return to the measurement mode.

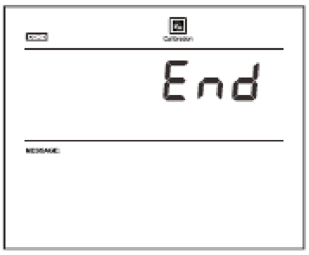

APPENDIX B-4: 12 Channel BTM-4208SD Temperature Data Logger Specifications

2-1 General Specifications

Circuit	Custom one-chip of microprocessor LSI circuit.	
Display	LCD size : 82 mm x 61 mm. ** with green color backlight.*	
Channels	12 channels : T1, T2, T3, T4, T5, T6, T7, T8, T9, T10, T11 and T12.	
Sensor type	Type K thermocouple probe. Type J/T/E/R/S thermocouple probe.	
Resolution	0.1℃/1℃, 0.1°F/1 °F.	
Datalogger Sampling Time Setting range	Auto	1 second to 3600 seconds *@ Sampling time can set to 1 second, but memory data may loss.*
	Manual	Push the data logger button once will save data one time. *@ Set the sampling time to 0 second.*
Data error no.	0.1% of total saved data max.	
Loop Datalogger	The record time can set for the duration every day. *For example the user intend set the record time from the 2:00 to 8:15 every day or record time 8:15 to 14:15.*	
Memory Card	SD memory card. 1 GB to 16 GB.	
Advanced setting	* Set clock time (Year/Month/Date, Hour/Minute/ Second) * Set loop time of recorder * Decimal point of SD card setting * Auto power OFF management * Set beep Sound ON/OFF * Set temperature unit to ℃ or °F * Set sampling time * SD memory card Format	

Temperature Compensation	Automatic temp. compensation for the type K/J/T/E/R/S thermometer.
Linear Compensation	Linear Compensation for the full range.
Offset Adjustment	To adjust the zero temperature deviation value.
Probe Input Socket	2 pin thermocouple socket. 12 sockets for T1 to T12.
Over Indication	Show " - - - - ".
Data Hold	Freeze the display reading.
Memory Recall	Maximum & Minimum value.
Sampling Time of Display	Approx. 1 second.
Data Output	RS 232/USB PC computer interface. * *Connect the optional RS232 cable UPCB-02 will get the RS232 plug.* * *Connect the optional USB cable USB-01 will get the USB plug.*
Power off	Auto shut off saves battery life or manual off by push button, it can select in the inner function.
Operating Temperature	0 to 50 ℃.
Operating Humidity	Less than 85% R.H.
Power Supply	*.Alkaline or heavy duty DC 1.5 V battery (UM3, AA) x 8 PCs, or equivalent.
	*.DC 9V adapter input. (AC/DC power adapter is optional).

Power Current	Normal operation (w/o SD card save data and LCD Backlight is OFF) : *Approx. DC 7.5 mA.*
	When SD card save the data but and LCD Backlight is OFF) : *Approx. DC 25 mA.*
	**.If LCD backlight on, the power consumption will increase approx. 11 mA.*
Weight	Meter : 944 g/2.1 LB.
Dimension	225 X 125 X 64 mm (8.86 X 4.92 X 2.52 inch)
Accessories Included	* Instruction manual........................1 PC * Type K Temp. probe, TP-01...........2 PC * Hard carrying case, CA-08............ 1 PC * SD memory card (2 GB).............. 1 PC
Optional Accessories	* Type K thermocouple probe. TP-01, TP-02A. TP-03, TP-04 * USB cable, USB-01. * RS232 cable, UPCB-02. * Data Acquisition software, SW-U801-WIN. * AC to DC 9V adapter.

2-2 Electrical Specifications (23± 5 ℃)

Sensor Type	Resolution	Range	Accuracy
Type K	0.1 ℃	-50.1 to -100.0 ℃	± (0.4 % + 1 ℃)
		-50.0 to 999.9 ℃	± (0.4 % + 0.5 ℃)
	1 ℃	1000 to 1300 ℃	± (0.4 % + 1 ℃)
	0.1 ℉	-58.1 to -148.0 ℉	± (0.4 % + 1.8 ℉)
		-58.0 to 999.9 ℉	± (0.4 % + 1 ℉)
	1 ℉	1000 to 2372 ℉	± (0.4 % + 2 ℉)
Type J	0.1 ℃	-50.1 to -100.0 ℃	± (0.4 % + 1 ℃)
		-50.0 to 999.9 ℃	± (0.4 % + 0.5 ℃)
	1 ℃	1000 to 1150 ℃	± (0.4 % + 1 ℃)
	0.1 ℉	-58.1 to -148.0 ℉	± (0.4 % + 1.8 ℉)
		-58.0 to 999.9 ℉	± (0.4 % + 1 ℉)
	1 ℉	1000 to 2102 ℉	± (0.4 % + 2 ℉)
Type T	0.1 ℃	-50.1 to -100.0 ℃	± (0.4 % + 1 ℃)
		-50.0 to 400.0 ℃	± (0.4 % + 0.5 ℃)
	0.1 ℉	-58.1 to -148.0 ℉	± (0.4 % + 1.8 ℉)
		-58.0 to 752.0 ℉	± (0.4 % + 1 ℉)
Type E	0.1 ℃	-50.1 to -100.0 ℃	± (0.4 % + 1 ℃)
		-50.0 to 900.0 ℃	± (0.4 % + 0.5 ℃)
	0.1 ℉	-58.1 to -148.0 ℉	± (0.4 % + 1.8 ℉)
		-58.0 to 999.9 ℉	± (0.4 % + 1 ℉)
	1 ℉	1000 to 1652 ℉	± (0.4 % + 2 ℉)
Type R	1 ℃	0 to 600 ℃	± (0.5 % + 1 ℃)
		601 to 1700 ℃	
	1 ℉	32 to 1112 ℉	± (0.5 % + 2 ℉)
		1113 to 3092 ℉	
Type S	1 ℃	0 to 600 ℃	± (0.5 % + 1 ℃)
		601 to 1500 ℃	
	1 ℉	32 to 1112 ℉	± (0.5 % + 2 ℉)
		1113 to 2732 ℉	

Remark :

a. Accuracy value is specified for the meter only.

b. Accuracy is tested under the meter's environment temperature within 23 ± 5℃.

c. Linearity Correction :
Memorize the thermocouple's curve into the intelligent CPU circuit,

@ Above specification tests under the environment RF Field Strength less than 3 V/M & frequency less than 30 MHz only.

APPENDIX B-5: HP2000 Wireless Weather Station Specifications

Specifications

Outdoor data

Transmission distance in open field : 100m(330 feet)
Frequency : 433 MHz / 868 MHz / 915 MHz (option)

Temperature range : -30˚C--65˚C (-22℉ to +149℉)
Accuracy : + / - 1 °C
Resolution : 0.1˚C

Measuring range rel. humidity : 1%~99%
Accuracy : +/- 5%

Rain volume display : 0 – 9999mm (show --- if outside range)
Accuracy : + / - 10%
Resolution : 0.3mm (if rain volume < 1000mm)
1mm (if rain volume > 1000mm)

Wind speed : 0-50m/s (0~100mph) (show --- if outside range)
Accuracy: +/- 1m/s (wind speed< 5m/s)
+/-10% (wind speed > 5m/s)

Light : 0-400k Lux
Accuracy : +/-15%

Measuring interval outdoor sensor: 16 sec
Measuring interval indoor sensor : 64 sec

Indoor data

Indoor temperature range : -10˚C--60˚C (14℉ to + 140℉) (show --- if outside range)

Power consumption

Base station : 5V DC adaptor (included)
Indoor sensor : 2xAAA alkaline batteries (not include
Remote sensor : 3x AA Alkaline batteries(not included

Remark:Be sure to use 1.5V normal Alkaline battery for solar transmitter.

APPENDIX B-6: T235H Digital Multimeter Specifications

Digital Multimeter

T235H

Features

- Diode test
- Continuity test
- Data Hold
- Backlight
- Capacitance test
- Transistor test
- Non-contact EF detection (NCV)
- Torch
- Auto Power off

Technical Overview

Feature	Parameter	Accuracy
DC Voltage (V)	200mV/ 2/ 20/ 200/ 1000V	±0.5% + 3 Digit
AC Voltage (V)	2/ 20/ 750V	±0.8% + 5 Digit
DC Current (A)	200μA/ 2mA/ 20mA/ 200mA/ 20A	±0.8% + 10 Digit
AC Current (A)	200mA/ 20A	±2.0% + 5 Digit
Resistance (Ω)	200Ω/ 2kΩ/ 20kΩ/ 200kΩ/ 2MΩ/ 20MΩ	±0.8% + 5 Digit
AC Frequency Response	40 - 400Hz	
Temperature (°C)	-20 to +1000°C	<400°C ±1.0% + 5 Digit
Input Impedance	10MΩ	
Capacitance (F)	6nF/ 60nF/ 600nF/ 6uF/ 60uF/ 600uF/ 6mF/ 20mF	±3.5 % + 20 Digit
Display	**3½ Digits**	**1 999 Counts**

CAT IV 600V

Model Specification

Power Source	2 x 1.5V AA Batteries
Standard Accessories	K- Type Temperature Probe **TBMTEMPPROBE** (-20°C to 250°C) , Test Leads
Dimensions (mm)	178(L) x 86(W) x 52(H)
Weight (g)	358

APPENDIX B-7: Water quality standards (electrical conductivity)

μS/cm	Use
0 - 800	• Good drinking water for humans (provided there is no organic pollution and not too much suspended clay material) • Generally good for irrigation, though above 300μS/cm some care must be, particularly with overhead sprinklers, which may cause leaf, scorch on some salt sensitive plants. • Suitable for all livestock
800 - 2500	• Can be consumed by humans, although most would prefer water in the lower half of this range if available • When used for irrigation, requires special management including suitable soils, good drainage and consideration of salt tolerance of plants • Suitable for all livestock
2500 -10,000	• Not recommended for human consumption, although water up to 3000 μS/cm can be consumed • Not normally suitable for irrigation, although water up to 6000 μS/cm can be used on very salt tolerant crops with very special management techniques. Over 6000 μS/cm, occasional emergency may be possible with care • When used for drinking water by poultry and pigs, the salinity should be limited to about 6000 μS/cm. Most other livestock can use water up to 10000 μS/cm
Over 10,000	• Not suitable for human consumption or irrigation • Not suitable for poultry, pigs or any lactating animals, but beef cattle can use water to 17000 μS/cm and adult sheep on dry feed can tolerate 23000 μS/cm. However, it is possible that waters below these levels could contain unacceptable concentrations of particular ions. Detailed chemical analysis should therefore be considered before using high salinity water for stock. • Water up to 50000 μS/cm (the salinity of the sea) can be used (i) to flush toilets provided corrosion in the cistern can be controlled and (ii) for making concrete, provided the reinforcement is well covered.